AD-A134 584 LASER EFFECTS AND VULNERABILITY PROGRAM LIQUID PROPELLANT CHARACTERIZATION(U) LOCKHEED MISSILES AND SPACE CO INC PALO ALTO CA PALO ALTO RESEARCH LAB

UNCLASSIFIED JUN 83 LMSC/D878096 DASG60-81-C-0104 F/G 20/5 NL

1/2

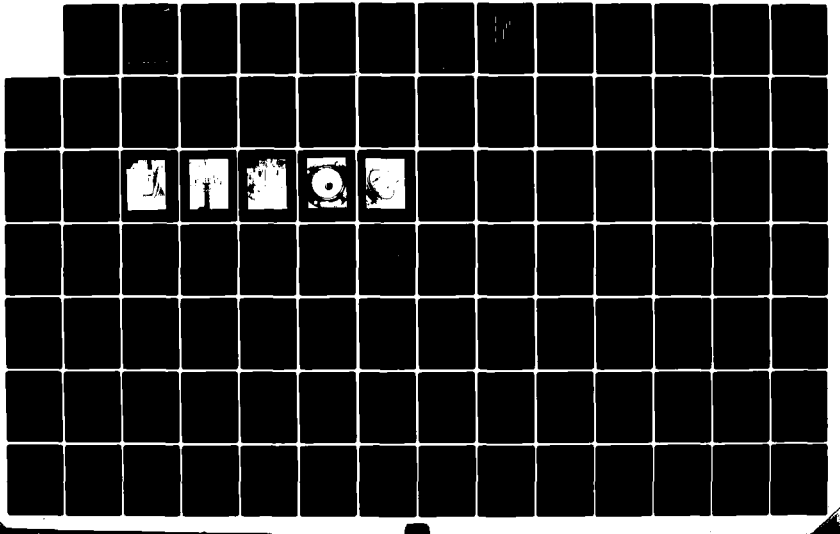

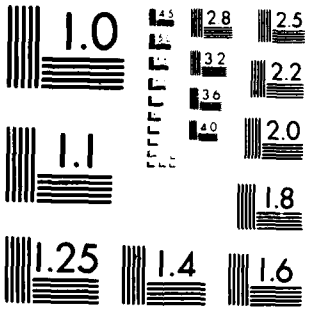

Lockheed Missiles & Space Company, Inc.
SUNNYVALE, CALIFORNIA

FINAL REPORT

LASER EFFECTS AND VULNERABILITY PROGRAM

LIQUID PROPELLANT CHARACTERIZATION

LMSC-D878096 June 1983

Contract Number DASG60-81-C-0104

Prepared for:

Ballistic Missile Defense Advanced Technology Center
Huntsville, Alabama

Lockheed Palo Alto Research Laboratory
Palo Alto, California 94304

TABLE OF CONTENTS

Section 1
INTRODUCTION

(U) This report describes a program which LMSC conducted for the Army BMDATC to resolve a major issue relative to the laser vulnerability of threat liquid propellant ballistic missiles (i.e., the influence of the liquid propellant on the thermal and attendant structural response and failure of missile tanks). LMSC previously has conducted for BMDATC several programs addressing the laser vulnerability of threat liquid propellant missiles, most notably the Laser Vulnerability and Effects Program (LVEP, Ref. 1). LVEP resolved many of the issues of liquid propellant missile laser vulnerability. However, the experimental program only addressed targets without liquids (i.e., "dry-backed" walls). Analytic models have been developed to predict the propellant liquid heat transfer effects, but many uncertainties exist. Thus, this program was conducted to determine the heat transfer characteristics of the liquid propellants of interest. This program only addressed the propellant heat transfer aspects of the problem. Structural response problems were beyond the scope of the program.

(U) This analytic and experimental program was conducted over an 18-month technical period (October 1981 - March 1983). Specific tasks were:

- Development of an analytic model to predict the heat transfer to liquid propellants of interest over the range of laser environments of interest (intensity and spot size).
- Obtain fundamental heat transfer characterization data on the propellants, including surface coefficients, nucleate boiling heat transfer, and critical heat flux.

(U) An analytic heat transfer model was developed for liquid-backed aluminum tanks. The development of the analytic model was initiated in the Novel Kill Mechanisms Program (Ref. 2); those studies indicated that the major uncertainties in the model were associated with the basic heat transfer characteristics of the liquids of interest. These parameters include the Nucleate Boiling

(U) Heat Transfer (NBHT) coefficients and the Critical Heat Flux (CHF). These data are normally obtained (for other liquids) empirically in a standard pool boiling technique. Therefore, a test facility was developed to obtain NBHT and CHF data on two primary liquid propellants of interest, mono methyl hydrazine (MMH) and mixed oxides of nitrogen (MON). The specific objectives of the tests where to: (1) provide CHF data for MMH and MON over the liquid pressure and temperature range of interest, and (2) generate NBHT data for a typical aluminum surface and liquid conditions of interest.

(U) The standard method for obtaining boiling heat transfer data was used in this program; it utilizes an electrically-heated plate. Electrical power is used to provide the heat flux as the controlled, independent variable. The test surface has a calibrated electrical resistance versus temperature dependence. The electrical current is varied incrementally during a test run and the voltage across the metal test specimen is measured. The test surface current and voltage data are reduced to provide a characteristic NBHT curve up to the CHF point for the test liquid. The tests were conducted at the LMSC Santa Cruz Test Base, which has the experience and facilities for handling hazardous fluids.

(U) The test conditions were selected to span the approximate range for appropriate threat vehicle tanks. Liquid temperature and pressure ranges are selected on the same basis. Two test surface materials, aluminum and platinum, were used. Aluminum (the most likely threat vehicle material) was used in most of the test runs to determine surface-fluid combination effects. Platimum is a standard material used in previous tests to obtain data on water. Thus it was used in the initial tests on water, which were performed primarily to establish the validity of the technique. Platimum was also used in a few subsequent tests to obtain a comparison with aluminum. The test procedure employed was based on current technology and techniques developed by liquid heat transfer specialists.

(U) A single test run provides the entire set of empirical data to establish NBHT and CHF for the selected test parameters of pressure, temperature, liquid type, etc. The basic testing approach permits a comfortable, deliberate testing schedule and avoids the high costs, compressed testing schedule, and facility access and scheduling problems usually associated with laser testing.

(U) The schedule for the program is shown in Fig. 1-1. The thermal analysis, which includes the model development, was performed continuously throughout the 18-month technical period. The major effort was the incorporation of the test data. The tests were run in August through October of 1982, paced primarily by facility preparation and checkout.

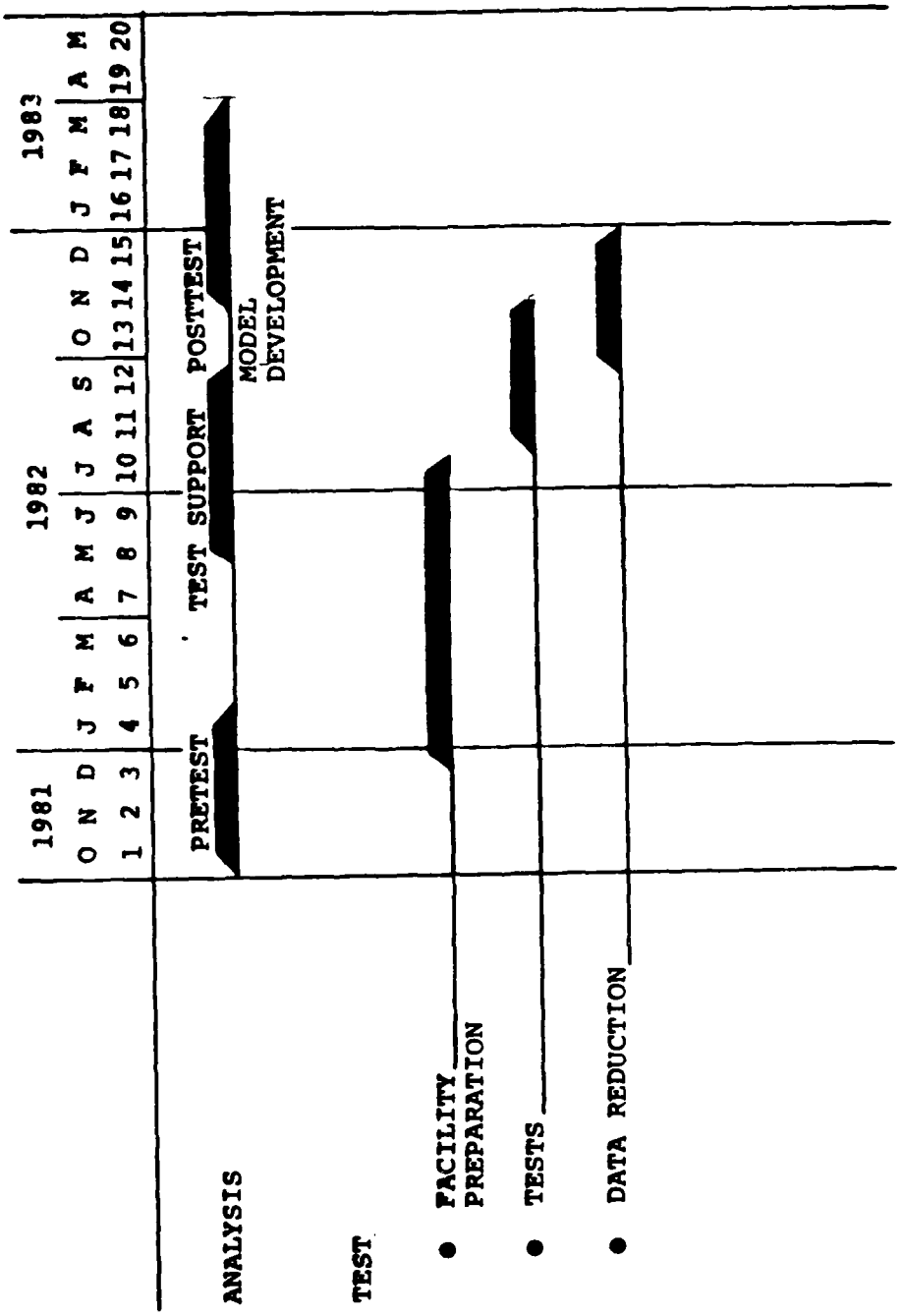

Fig. 1-1 Liquid Propellant Heat Transfer Experiments Schedule

Section 2
LIQUID PROPELLANT HEAT TRANSFER PHENOMENA

(U) One critical issue in laser vulnerability of liquid propellant missiles is not yet satisfactorily quantified. This concerns pressurized liquid propellant booster systems when the tank wall interaction region is in a liquid-backed condition. The unresolved factors principally are based on uncertainties in the fundamental heat transfer properties of pertinent liquid propellants.

(U) The primary heat transfer quantity yet to be accurately established is the critical heat flux (CHF), sometimes called the "burnout" flux. This is the minimum value of laser flux absorbed by the wall which is sufficient to produce an insulating layer of vapor bubbles between wall and liquid. Figure 2-1 illustrates this transition boiling regime and those leading up to it. This burnout flux level is achieved after a dense layer of bubbles forms; when this condition is achieved, the metal wall will be heated promptly to a temperature level required for lethal damage nearly as though the liquid were not present. However, if the absorbed flux is below CHF, heat transfer from wall to fluid remains in the very efficient nucleate boiling regime or below. The large thermal mass of the liquid then acts like a heat sink, and continued laser irradiation at the same absorbed flux level below CHF cannot further heat the wall above the relatively low equilibrium wall temperature corresponding to a continued balance between absorbed laser flux and boiling heat transfer to the large fluid volume. Figure 2-2 quantitatively illustrates the results for absorbed flux above and below CHF. These predictions were obtained using LMSC's liquid heat transfer quantitative models (using pretest predictions of the propellant characteristics).

(U) For aluminum wall and propellants of interest, propellant heat transfer modeling predictions show that an equilibrium wall temperature below that corresponding to CHF is generally inadequate to ensure lethal structural

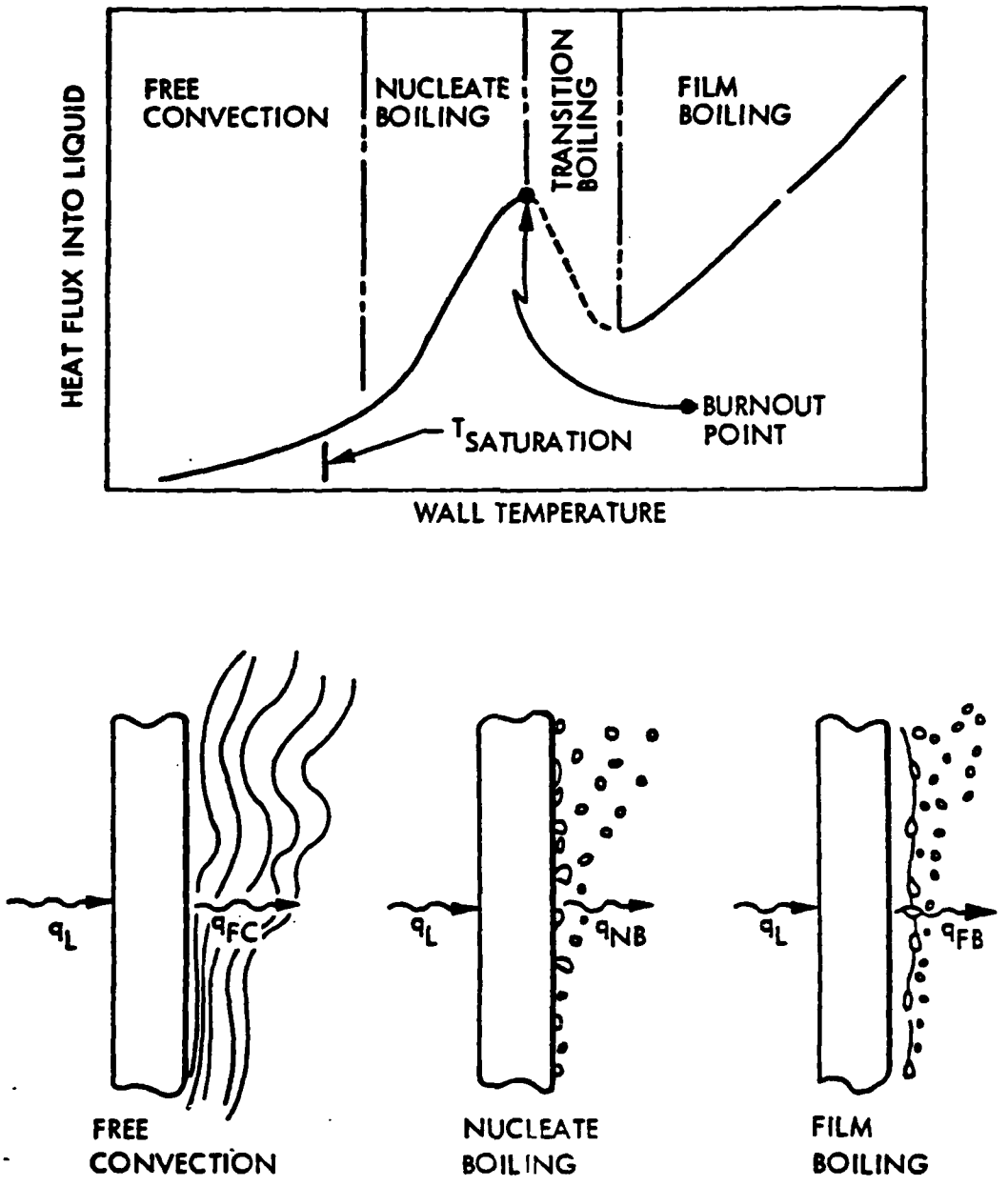

Fig. 2-1 Liquid Cooling Regimes for Laser-Heated Tank Walls

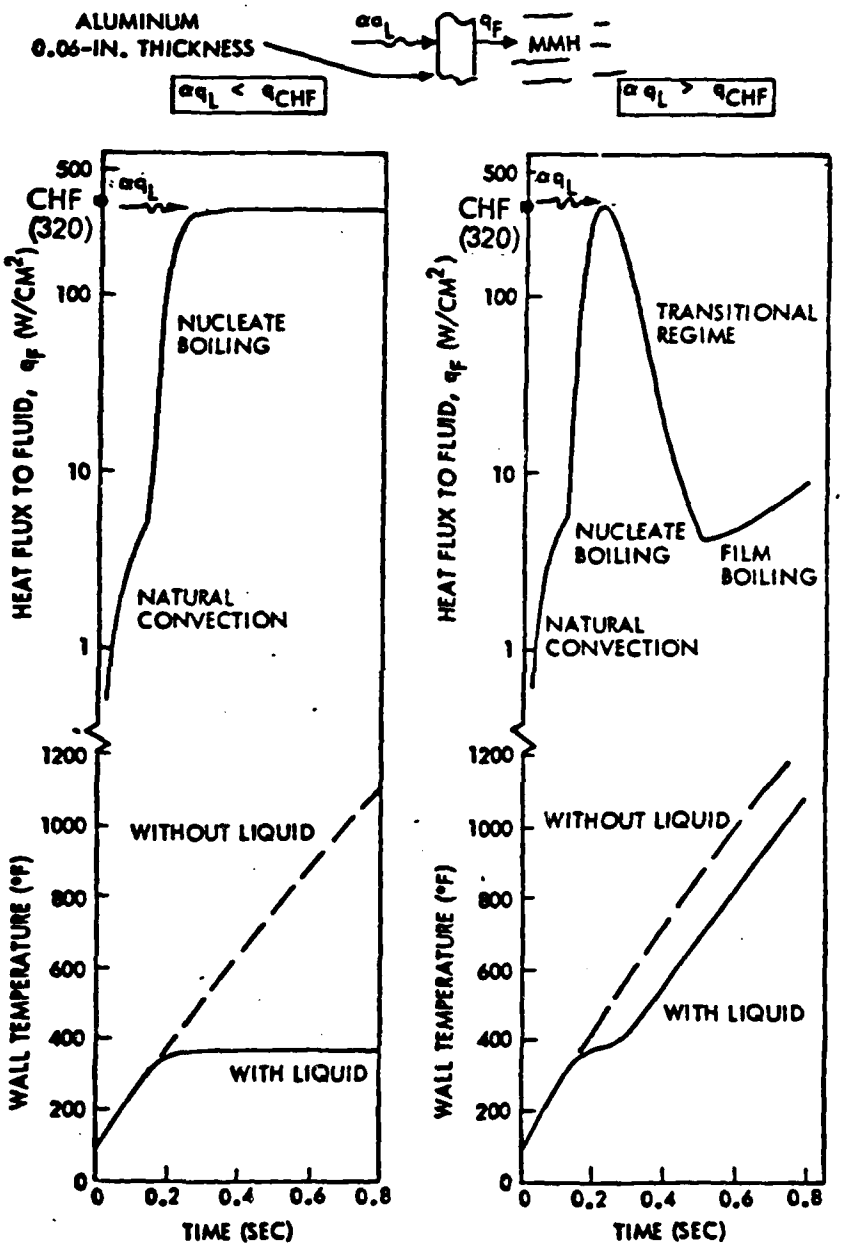

Fig. 2-2 Fuel Tank Temperature Response for Absorbed Flux Below and Above CHF

(U) response. Ensured lethal structural response requires the burnout flux, CHF, to be applied over a spot size dictated by combined liquid propellant heat transfer and structural response criteria.

(U) The quantitative propellant heat transfer data corresponding to the liquid thermal response regime just below, and leading to, the CHF vapor film onset level is the next most important set of propellant heat transfer properties data to be obtained. This regime occurs when the liquid near the wall is heated to its saturation temperature where liquid and vapor can exist together in equilibrium. It is called the nucleate boiling heat transfer regime (NBHT) (Fig. 2-1). The NBHT regime dictates both the irradiation duration required to achieve burnout if the absorbed flux is at or above CHF, and e final equilibrium wall temperature if absorbed flux is below CHF. Th fore, both CHF and NBHT quantitative data must be obtained for the propell in order to adequately establish laser interaction requirements for structu damage for the liquid backed tank wall. The initial, free convection regi gure 2-1) is relatively unimportant because it corresponds to low flux.

(U) A particular liquid booster condition, when the propellant is partially or nearly fully expended also may be identified. In this case, the laser spot is at the liquid level line, encompassing both fluid and gas-backed regions, or is confined to a gas-backed region only. Both of these regimes have been addressed in earlier LMSC studies for BMD with respect to induced structural response. These regimes are not considered to be issues of primary interest for defining lethal structural response. The secondary effects from response of any propellant vapor present in these situations cannot be predicted with the same confidence as that for structural response; they are less important than liquid backed structural response. Therefore, propellant vapor response effects investigations (e.g., deflagration or detonation onset) are much lower in priority that the fully liquid-backed structural response cases addressed here because they cannot be reliably predicted and are beyond the scope and funding level. Postpenetration of liquid-backed wall and subsequent laser interaction with exposed propellant were not addressed for the same reasons.

(U) Once necessary CHF and NBHT data have been obtained experimentally for the liquid propellants, these data must be incorporated into the appropriate heat transfer correlation and modeling relations to give wall temperature as a function of time and laser spot flux distribution as input for structural response predictions. Because of the very nonlinear nature of the liquid heat transfer processes, the wall heating distributions in the laser spot region are expected to be significantly different and rather distorted in comparison with absorbed laser flux spatial distribution. Therefore, besides the basic CHF criterion required over a sizable spot region, structural response (i.e., small spot heating, slow crack growth and propagation, etc.) for the liquid-backed case may be rather different, for the same laser spot spatial flux distribution, than obtained in the dryback cases previously studied by LMSC. Thus, laser spot size effects and distribution are particularly important for the liquid-backed case. Only thermal response effects were addressed in this study (i.e., no structural response analysis or testing was performed).

2.1 KEY ISSUES (U)

(U) Within the framework of the described basic liquid propellant heat transfer problem, there are several important factors which were considered in performing the program to fully resolve the problem in context. These major factors are briefly discussed below.

(U) Available Propellant Data. Because of the hazardous nature of the propellants and the unusually extreme thermal loading conditions of interest, only a modest amount of propellant properties data pertinent to the NBHT and CHF regimes where immediately available. Reference 3 through 6 are a representative set of the existing experimental data base, generally relating to much more mild environmental conditions than those considered here. LMSC performed preliminary analyses on these propellants in earlier BMD-sponsored studies (Ref. 2). These analytic predictions and models provided a first-order bounding of the uncertainty in CHF and NBHT for MMH and MON propellants, and substantially reduced the remaining analysis and testing required for adequate properties determinations and modeling refinements. Analytic modeling is discussed and reviewed in detail in Section 2.2.

(U) Hazardous Propellants. The liquid propellants of interest are very hazardous materials. Special handling and safety procedures are essential in efforts to obtain required basic heat transfer data. Unique testing procedures and techniques must be used to efficiently and cost-effectively obtain the data.

(U) Propellant State Properties. The heat transfer from a metal wall to liquid will depend to some degree on the actual state of the liquid at the time of laser interaction. State conditions such as pressure and initial temperature, as well as other factors such as imposed acceleration vector, surface wettability of the wall material and its roughness condition, all may affect actual heat transfer to some extent. In these tests, nominal initial state conditions of room temperature and 60 psia were assumed. Some variation of initial temperature and pressure were employed in the tests, but this was not a major variable.

(U) The tests were all conducted in a 1-g environment, and no surface roughness variations were made (a modest amount of surface roughness was placed on the ribbons, as will be discussed later).

2.2 ANALYTIC MODELING (U)

(U) A primary goal of this study was to develop high confidence analytic models which can be used to predict the thermal response of liquid propellant backed aluminum tank walls. The accuracy of the existing analytic models will be increased by obtaining the fundamental material properties data that was previously lacking. The refined analytic models could provide confident pretest predictions of liquid heat transfer for subsequent laser tests on structural components. (Neither laser tests nor laser test planning were included in this program.)

(U) Simplified Heat Transfer Models. To help fix ideas regarding heat transfer mechanisms, consider a simple, approximate model for the heat transfer, where the complicating details of any fluid hydrodynamics and phase change effects are ignored initially. The rate of heat transfer from wall to liquid basically depends on the difference between wall temperature T and liquid temperature T_l, where the latter is taken as a constant because of the large fluid volume. Then the rate of heating of a thermally-thin wall depends on a balance between absorbed laser flux and heat transferred to the liquid, or, written as a differential equation,

$$\rho c \delta \frac{dT}{dt} = \alpha q - h(T-T_l)^n \qquad (1)$$

(U) where t is irradiation time; ρ, c, and δ are density, specific heat and thickness of wall; α is wall exterior absorptance to incident laser flux q; h is an empirically obtained heat transfer coefficient for a particular combination of fluid and wall; the exponent n also is an empirically obtained quantity. The initial condition is $T = T_l$ when $t = 0$, at the start of laser irradiation.

(U) If $n = 1$, which corresponds approximately to the free convection regime, the solution to Eq (1) is

$$T = T_l + \frac{\alpha q}{h}\left[1-e^{-\left(\frac{h}{\rho c \delta}\right)t}\right] \qquad (2)$$

(U) The character of this solution is shown in Fig. 2-3. The wall temperature initially slowly increases with time, reaches a nearly linearly increasing intermediate regime, and eventually approaches an asymptotic value of $T = \alpha q/h$ when absorbed laser flux is finally balanced by transfer to the fluid; the wall cannot be further heated under continued laser irradiation. This basic character for wall temperature rise typifies response when αq is below CHF. If αq is above CHF for the liquid, h would eventually abruptly change to a very low value corresponding to onset of a thick layer of vapor bubbles between wall and liquid, and the wall would then heat very rapidly. However, when bubbles first start to form (corresponding to the onset of liquid boiling), the NBHT regime is reached, where n becomes much larger than unity. Heat transfer data for liquids, similar to the volatile propellants of interest here, indicate that n for them ranges from about 3 to 5 in the NBHT regime. A large value for n corresponds to the physical fact that continued vapor bubble generation at, and prompt release from, the wall is an extremely efficient heat transfer process because of the large phase change energy required for vapor formation, the bubble size stability as a function of fluid state, and increased hydrodynamic motion induced by agitation transfer process. For comparison with the foregoing example, consider the case where $n = 2$, qualitatively representing initial transition from free convection to NBHT onset.

(U) With $n = 2$, in Eq. (1), the solution for wall temperature then becomes

$$T = T_1 + \left(\frac{\alpha q}{h}\right)^{\frac{1}{2}} \left[\frac{1-e^{-mt}}{1+e^{-mt}}\right], \quad m = \frac{2(\alpha q h)^{\frac{1}{2}}}{\rho c \delta} \tag{3}$$

(U) The character of this solution also is sketched in Fig. 2-3, where h is assumed to have the same value for $n = 1$ and 2, for simplicity in comparing the two results. The final equilibrium wall temperature in this case is much lower, $T = (\alpha q/h)^{\frac{1}{2}}$. for the same values of absorbed laser flux and heat transfer coefficient. The large relative decrease in equilibrium wall temperature qualitatively corresponds to liquid phase change effects on the heat transfer process. This is a major effect in the NBHT regime.

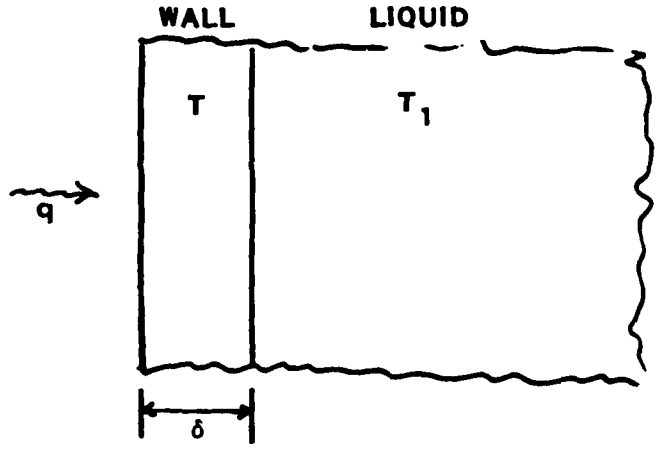

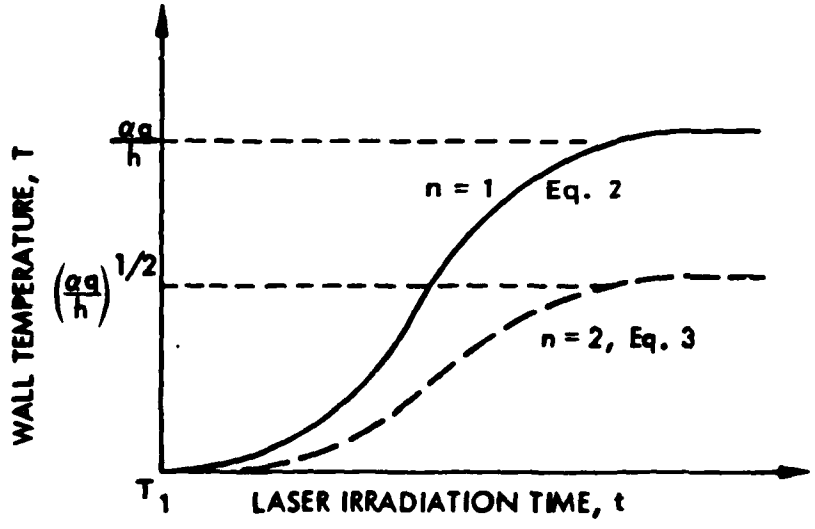

Fig. 2-3 Comparative Fluid/Wall Heat Transfer Solutions

(U) Detailed Analytic Models: Correlation Relations. When the details of liquid phase change, fluid hydrodynamics, acceleration, and other complex effects are all considered together, simplified solutions such as the foregoing can no longer be constructed. One is forced to adopt a modeling approach which combines the dominant features of all the significant effects together, and results in a different modeling relation for each of the several differing heat transfer regimes depicted in Fig. 2-1. The regimes of interest in this study are where NBHT and CHF occur, as discussed earlier. These regimes are typified by boiling heat transfer processes. Their modeling relations are discussed below and include all important factors. Of these factors, the most significant are fluid properties, liquid pressure and temperature, and surface finish. The influence of these factors on prediction uncertainties is discussed later.

(U) Boiling Heat Transfer Prediction Method. As discussed previously, fluid heat transfer in the various convection and boiling regimes must be calculated using semiempirical correlations of data (in the absence of more exact theories). The fact that the heat transfer mechanism differs radically in the various regimes has prevented development of a single correlation equation. However, reasonably successful correlations have been obtained from data within a regime where a particular mechanism prevails.

(U) Nucleate Boiling. In nucleate boiling, the major heat transfer mechanism is convection produced by agitation and vapor/liquid exchange of the bubbles. The solid surface condition also has an important influence. Based on these observations, Rohsenow developed a method for correlating NBHT data which follows the approach used for analyzing turbulent forced convection without boiling (Ref. 7) and accounts for surface effects. The correlation equation is

$$\frac{c_\ell (T_w - T_{sat})}{h_{fg}} = C_{sf} \left\{ \frac{q_F}{\mu_\ell h_{fg}} \sqrt{\frac{\sigma_\ell}{g (\rho_\ell - \rho_v)}} \right\}^r Pr^{1.7} \qquad (4)$$

(NOTE: r = 0.33 for water)

(U) where q_F is the heat flux; $(T_w - T_{sat})$ is the difference between the surface and liquid saturation temperatures; c_ℓ, ρ_ℓ, σ_ℓ, and Pr_ℓ are the specific heat, density, viscosity, surface tension, and Prandtl number of the liquid; ρ_v is the vapor density; h_{fg} is the latent heat of vaporization, and g is gravitational acceleration. The coefficient C_{sf} is an empirical constant that accounts for the effect of the surface-fluid combination; it is determined by plotting experimental NBHT data in terms of the dimensionless groups of Eq. (4).

(U) Critical Heat Flux. The CHF correlation equation is based on a hydrodynamic model which postulates that as increased NBHT produces more and more active nucleation sites, the liquid flow to the surface is restricted sufficiently to produce the onset of unstable vapor blanketing. The CHF occurs at this onset condition. The correlation equation for saturated liquids is: (Ref. 8):

$$\frac{q_{CHF\ (sat)}}{\rho_v\, h_{fg}} = K_1 \left[\frac{\sigma_\ell\,(\rho_\ell - \rho_v)\,g}{\rho_v^2}\right]^{1/4} \left[\frac{\rho_\ell}{\rho_\ell + \rho_v}\right]^{1/2} \tag{5}$$

(U) For subcooled liquids ($T_{liq} < T_{sat}$), the following modification is applied (Ref. 9):

$$\frac{q_{CHF\ (sub)}}{q_{CHF\ (sat)}} = 1 + K_2 \frac{(k_\ell \rho_\ell c_\ell)^{1/2} \left[\dfrac{g(\rho_\ell - \rho_v)}{\sigma_\ell}\right]^{1/4}}{\rho_v\, h_{fg} \left[\dfrac{\sigma_\ell(\rho_\ell - \rho_v)g}{\rho_v^2}\right]^{1/8}} (T_{sat} - T_{liq}) \tag{6}$$

(U) In these equations, ρ_v and ρ_ℓ are the vapor and liquid densities; h_{fg} is the heat of vaporization, σ_ℓ, k_ℓ, and c_ℓ are the liquid surface tension, thermal conductivity, and specific heat, respectively; and g is the

(U) gravitational acceleration. The coefficients K_1 and K_2 are empirical constants that are determined by plotting CHF data in terms of the dimensionless groups of Eqs. (5) and (6).

(U) Computerized Heat Transfer Model. A computer code, FHEAT, has been constructed to provide mechanized, quantitative liquid heat transfer data for the entire set of regimes depicted in Fig. 2-1. FHEAT incorporates the correlation relations for NBHT (Eq. 4) and CHF (Eqs. 5 and 6) of specific interest here. This code also includes prediction capability for the higher wall temperature regimes at and above CHF, corresponding to transition boiling and film boiling regimes. The foregoing models are adapted from those of Ref. 10. The low flux, free convection regime also is modeled in the code so that it can treat the aerodynamic preheating effects on the fluid preceding laser flux application. Variable liquid properties as a function of temperature are included in the code capability, as well as variation in acceleration. This code will be incorporated as a subroutine into the appropriate LMSC structural response predictive codes.

(U) Modeling Uncertainties. At the beginning of the study there was a complete lack of NBHT and CHF data on the MMH and MON liquids of primary interest. Consequently, the use of data correlation equations that employ empirical constants to analyze heat transfer in these liquids imposes some uncertainties on the predictions. These uncertainties, which would be largely resolved with basic experiments such as those performed in this study, are discussed in the following paragraphs.

(U) The NBHT correlation, Eq. (4), accounts for pressure and temperature effects through the fluid properties. The fluid properties for MMH and MON liquids and vapors are known with reasonable accuracy (e.g., Ref. 3). The observed negligible influence of acceleration on NBHT is reflected in the $g^{1/6}$ term of Eq. (4). Therefore, the major source of uncertainty in using Eq. (4) to predict the NBHT of MMH or MON liquids is the effect of surface-fluid coefficient, C_{sf}, which is a function of surface roughness. Because the internal surface roughness of a threat vehicle is unknown and can only be estimated, it is important to bound the uncertainty involved with experiments.

(U) Discussion of the surface finish uncertainty is aided by the sketch of Fig. 2-4. Increasing surface roughness shifts the NBHT curve to the left, improving heat transfer. The lower temperature bound (for all liquids and surface finishes) is the liquid saturation temperature. The upper bound (the maximum temperature attainable for laser environments where $q_L < q_{CHF}$) would be the NBHT curve for propellant/smooth aluminum surface combinations. This bound has some importance in laser/tank lethality analysis. However, without NBHT data for MMH and MON on smooth aluminum, it is undefined. Available data for other fluids on smooth and rough surfaces indicate that the maximum uncertainty in the CHF temperature (the value of T_W when the CHF is reached) is less than 100°F.

(U) In this program relatively smooth aluminum was used as the wall material, resulting in burnout of CHF temperatures which will be on the high band of the expected range.

(U) Since it is a hydrodynamic phenomenon, the CHF level is not very sensitive to the character of the heating surface. Thus, in laser/tank response analysis, surface finish will affect only the wall temperature at which CHF is reached (along the NBHT curve) and not the CHF level itself.

(U) The CHF correlations, Eqs. (5) and (6), account for pressure and temperature effects through the fluid properties. They are not expected to be a source of uncertainty; however, experimental CHF data for MMH and MON are needed to validate the correlation equations for these liquids. In Ref. 8, the value $K_1 = 0.18$ was determined with a ±30 percent associated uncertainty due to the spread of the plotted data (for many different liquids and conditions). This value was used for pretest predictions.

(U) In Eq. (5), the $q_{CHF(sat)}$ is predicted to vary with $g^{\frac{1}{4}}$. This is consistent with the acceleration data presented in Ref. 2. Therefore, the effects of acceleration appear to be fairly well determined, although some uncertainty exists because of the scarcity of data for surface orientations of interest, which are parallel to the acceleration vector. However, relatively recent NBHT

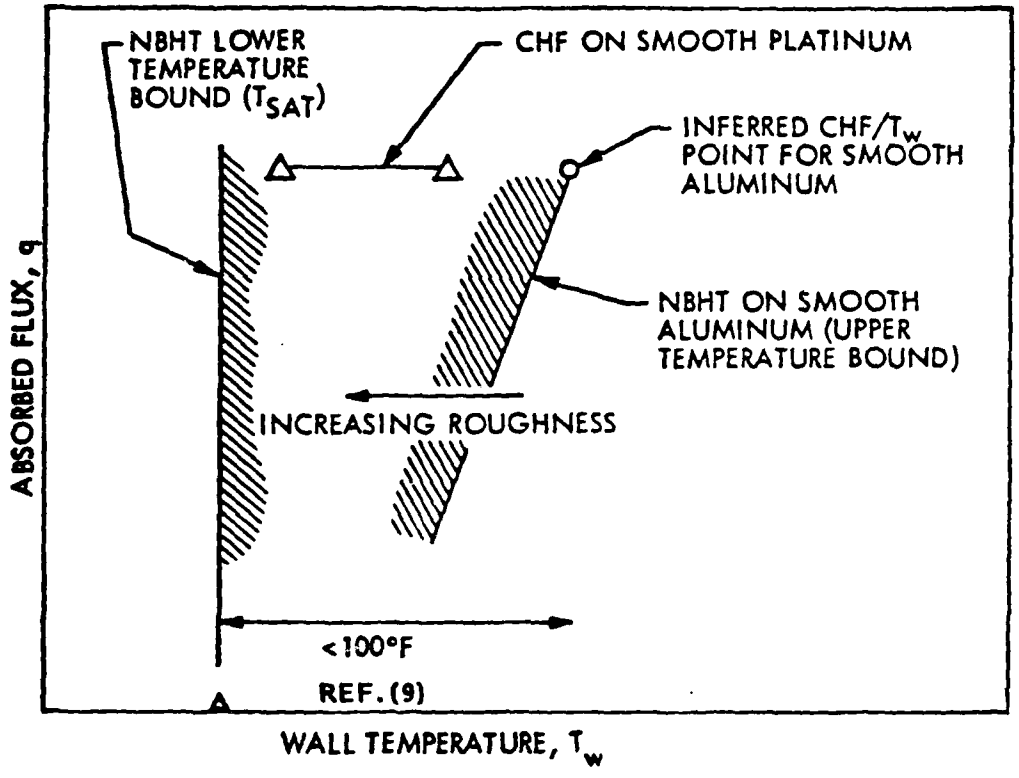

Fig. 2-4 Effect of Wall Surface Condition

(U) data for vertically oriented graphite heater rod surfaces also show an approximately 1/5 to 1/4 power dependence on acceleration when it is parallel to the rod surfaces. Therefore, available empirical data, as well as the correlation relations themselves, all indicate that acceleration has a relatively weak effect on NBHT and CHF. No variations of acceleration were made in this program (all at $g = 1$).

(U) In addition to the uncertainty of the CHF prediction correlations, uncertainties may exist due to variation in threat vehicle tank conditions (propellant properties, pressure, and temperature) assumed in the laser/tank response calculations. Besides the fluid properties, the bulk temperature of the fluid, which depends on the initial temperature at lift-off and aerodynamic heating, has the strongest effect on CHF. Experimentally verified prediction methods are needed to compute estimates of the effect on wall heating due to design and environment variations. Several variations in fluid bulk temperatures were made in this program.

Section 3
TEST PROGRAM

(U) This section describes the basic test program which was performd to obtain nucleate boiling heat transfer (NBHT) and critical heat flux (CHF) data on the primary liquid propellants of interest, MMH and MON. The basic heat transfer data are essential to the development and validation of liquid heat transfer prediction methods for MMH and MON, and the bounding of the associated uncertainties. The test objectives, approach, and test apparatus and procedures for the experiments are presented.

(U) The objectives of the tests were to: (1) provide CHF data for MMH and MON over the liquid pressure and temperature range of interest, and (2) generate NBHT data for a typical aluminum surface and liquid conditions of interest.

3.1 TEST APPROACH

(U) Heat transfer data in the nucleate boiling heat transfer regime for a variety of liquids, most notably and extensively for water, have been obtained experimentally by several investigators over the years. This has led to development of a relatively standard technique for obtaining NBHT which uses an electrically heated metal strip immersed in the liquid in a pressurized container. The technique permits efficient data collection in a straightforward fashion. Unfortunately, as noted earlier, data of this type have not been obtained for the liquid propellants of interest, partly because of their hazardous nature but especially because there was not prior requirement for it. The experimental program used in this study was based on this standard technique.

(U) A schematic of the test apparatus used in this study is shown in Fig. 3-1. Electrical power is used to provide the heat flux as the controlled, independent variable. The test surface has a calibrated electrical resistance versus

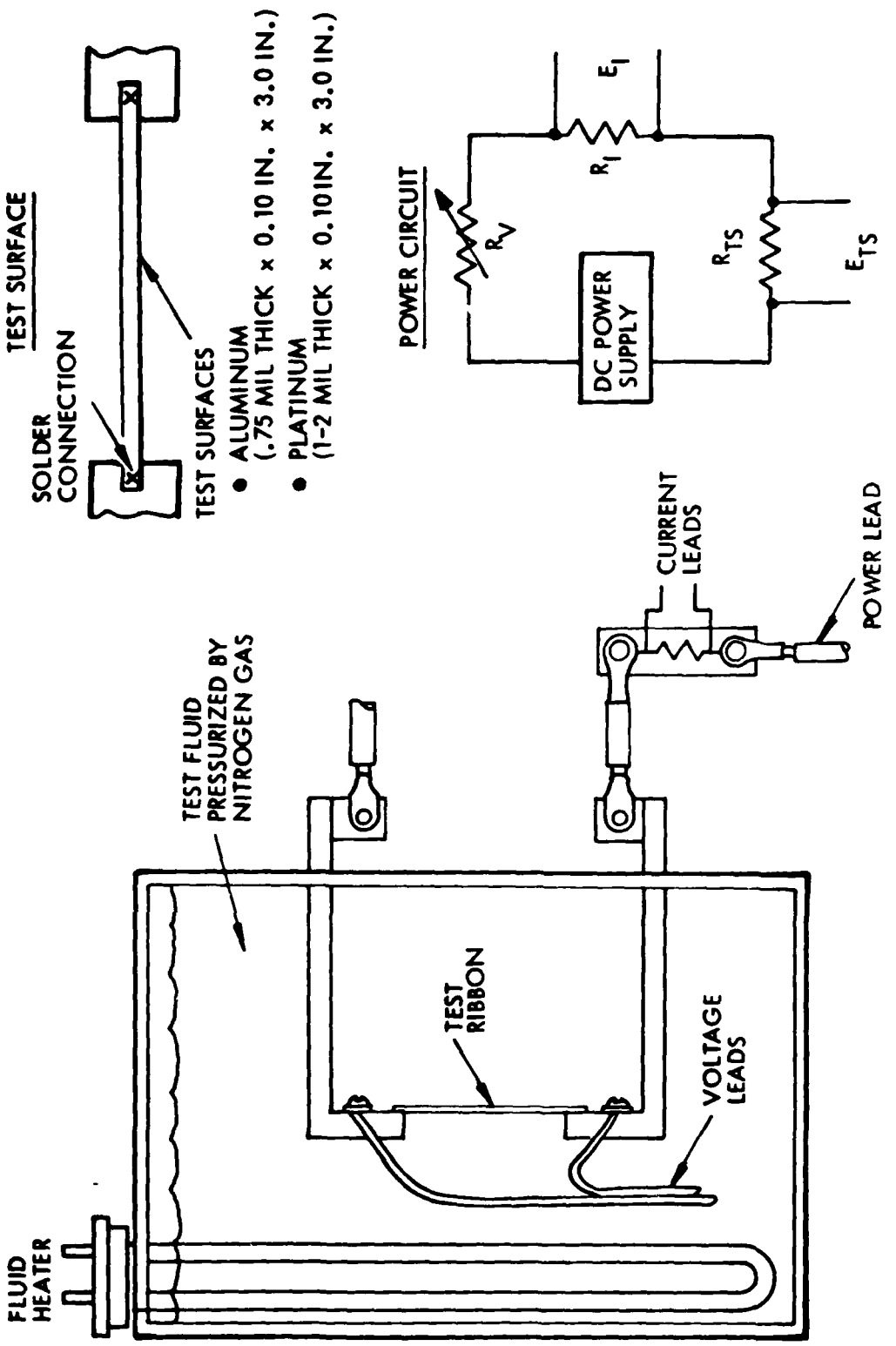

Fig. 3-1 Boiling Heat Transfer Test Apparatus

(U) temperature dependence. The electrical current is varied incrementally during a test run and the voltage across the test metal specimen is measured. The test surface current and voltage data are reduced to provide a characteristic NBHT curve (q_F versus T_w) to the CHF point for the test liquid. The tests were conducted at the LMSC Santa Cruz Test Base, which has the experience and facilities for handling hazardous fluids. Current from a DC power supply was used to heat the test surface. Nitrogen gas was used to pressurize the container. The design of the test ribbon was selected to minimize size effects on the data and simultaneously to satisfy the system electrical current constraints. (Larger surfaces require more current to provide the same heat flux.) The matrix of tests is shown in Table 3-1.

(U) The test conditions were selected to span the approximate range for appropriate threat vehicle tanks. Liquid temperature and pressure ranges are selected on the same basis. Two test surface materials, aluminum and platinum, were used. Aluminum (the most likely threat vehicle material) was used in general. However, tests employing platinum ribbons were also conducted. Platinum is a standard ribbon used in the tests which obtained the existing data. The first tests were run on water (at room temperature and pressure) with platinum ribbons. Their objective was to obtain data with the LMSC facility and compare it to existing data for these standard conditions. The results agreed well with the published data, and thus the technique was validated. The tests on water were followed by tests on isopropyl alcohol with aluminum ribbons. These tests were conducted to gain experience with aluminum ribbons and with a fluid which has a much lower CHF than water (approximately 100 W/cm^2 vs. 600 W/cm^2). These tests were followed by the tests on the actual propellants. The results of the tests are discussed in Section 4.

3.2 TEST FACILITY DESCRIPTION

(U) A schematic of the test facility was shown in Fig. 3-1. This facility was installed at the LMSC Santa Cruz Test Facility (LMSC SCTF). The test tank is

Table 3-1 LIQUID PROPELLANT CHARACTERIZATION TEST MATRIX

Initial Conditions				Comments
Fluid	Specimen	Bulk Temp. (°F)	Pressure (psia)	
Water	Platinum	92	14.7	Technique
↓	Platinum	88	14.7	Verification
Isopropyl Alcohol	Aluminum	68	38	Low Temp.
↓	Aluminum	77	39	Liquid
MMH	Aluminum	80	60	Baseline
↓	Platinum	86	60	Pt vs Al
↓	Platinum	252	56	Sat. Liquid
↓	Aluminum	85	59	One Pass
MON	Aluminum	54	67	Baseline
	Aluminum	50	59	One Pass
	Platinum	52	60	Pt vs Al
	Aluminum	92	63	Higher Bulk T.
	Aluminum	60	58	Rate Effects

(U) 8 inches in diameter by 12 inches in height; it is fabricated of aluminum 6061-T6. The bottom of the tank is a stainless steel burst disc designed to fail at approximately 250 psig (to protect against runaway reactions and over pressure); if failure occurs, the tank will vent through a tube into a safe area. The end flanges contain heaters, propellant fill ports, pressurization ports, and instrumentation ports. The test sample is mounted off the top flange, which includes the power supply leads.

(U) Photographs of the facility are shown in Figs. 3-2 through 3-6. An overview is shown in Fig. 3-2. The vent tube is clearly evident; this tube will vent the tank in case of over-pressure. A close-up of the tank and the associated plumbing and wiring is shown in Fig. 3-3. The set-up includes two separate sets of plumbing: one for fuel and one for oxidizer. This allows switching from one to the other without clean-up (other than the tank), and results in a more straight-forward set-up incorporating the unique details for each type of propellant. A rear view of the plumbing mounting plate is shown in Fig. 3-4 (oxidizer side). Internal views of the tank are shown in Figs. 3-5 and 3-6. The inside of the tank with the top plate removed is shown in Fig. 3-5. The two thermocouple probes can be seen, along with the fill/drain tube in the bottom; the bottom of the tank is the steel burst disc. The top plate is shown in Fig. 3-6, along with the mounting rods and a test specimen in place. The test specimen or ribbon is mounted with a slightly curved or "S" shape to allow for controlled expansion and contraction during and after the test.

(U) Test Specimen ("Ribbon"). The metal test specimen or "ribbon" is shown in Fig. 3-6; the dimensions are shown in Fig. 3-7. The ribbon design requires very thin metal specimens (approximately 1 mil) and very close tolerances (they are essentially foils). Several approaches to fabrication were attempted, including vapor deposition on a ceramic such as aluminum oxide, which was unproven and expensive, and laser cutting techniques, which proved to be unsatisfactory due to edge melting. The approach which was used for both materials

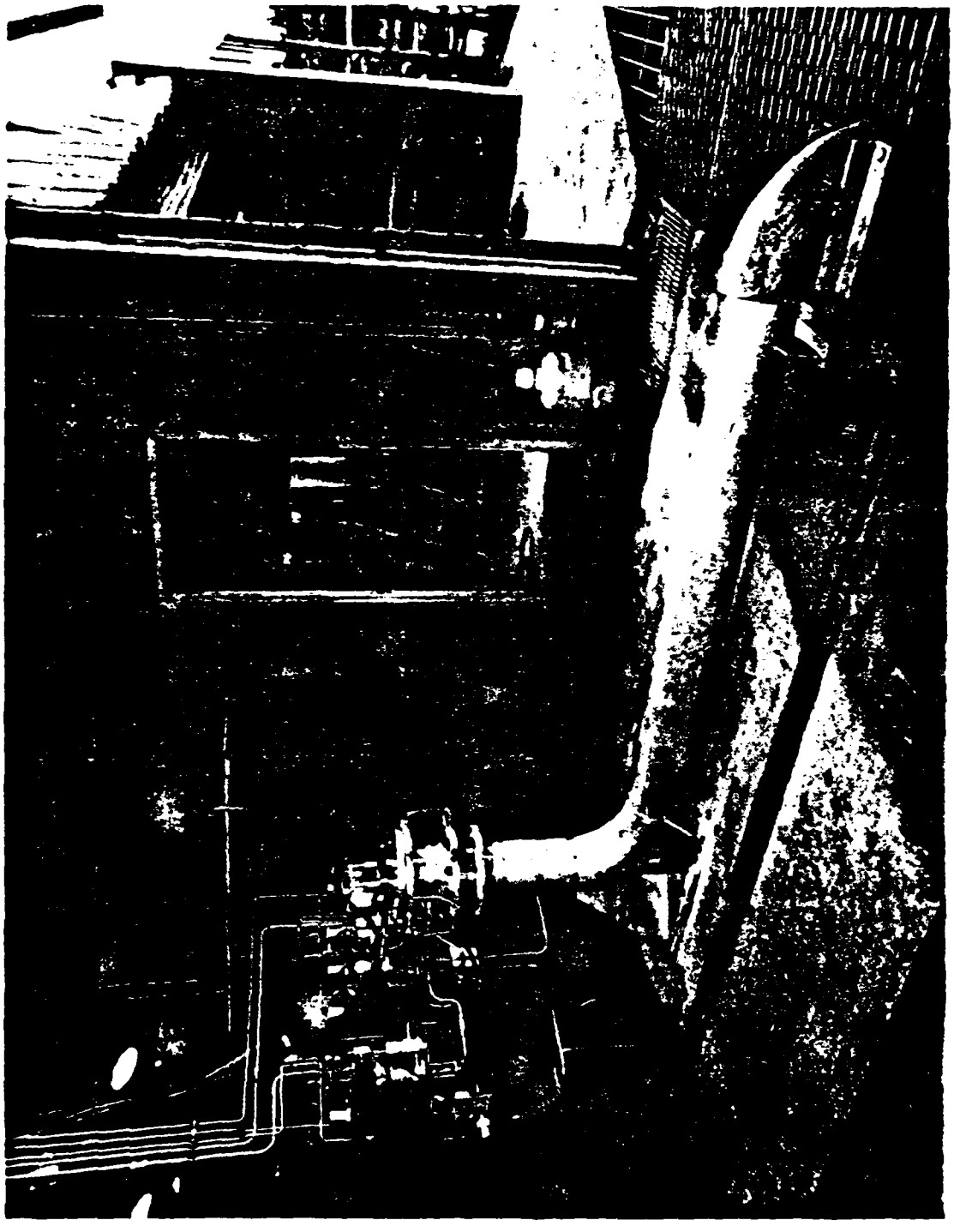

Fig. 3-2 Overview of Liquid Heat Transfer Facility

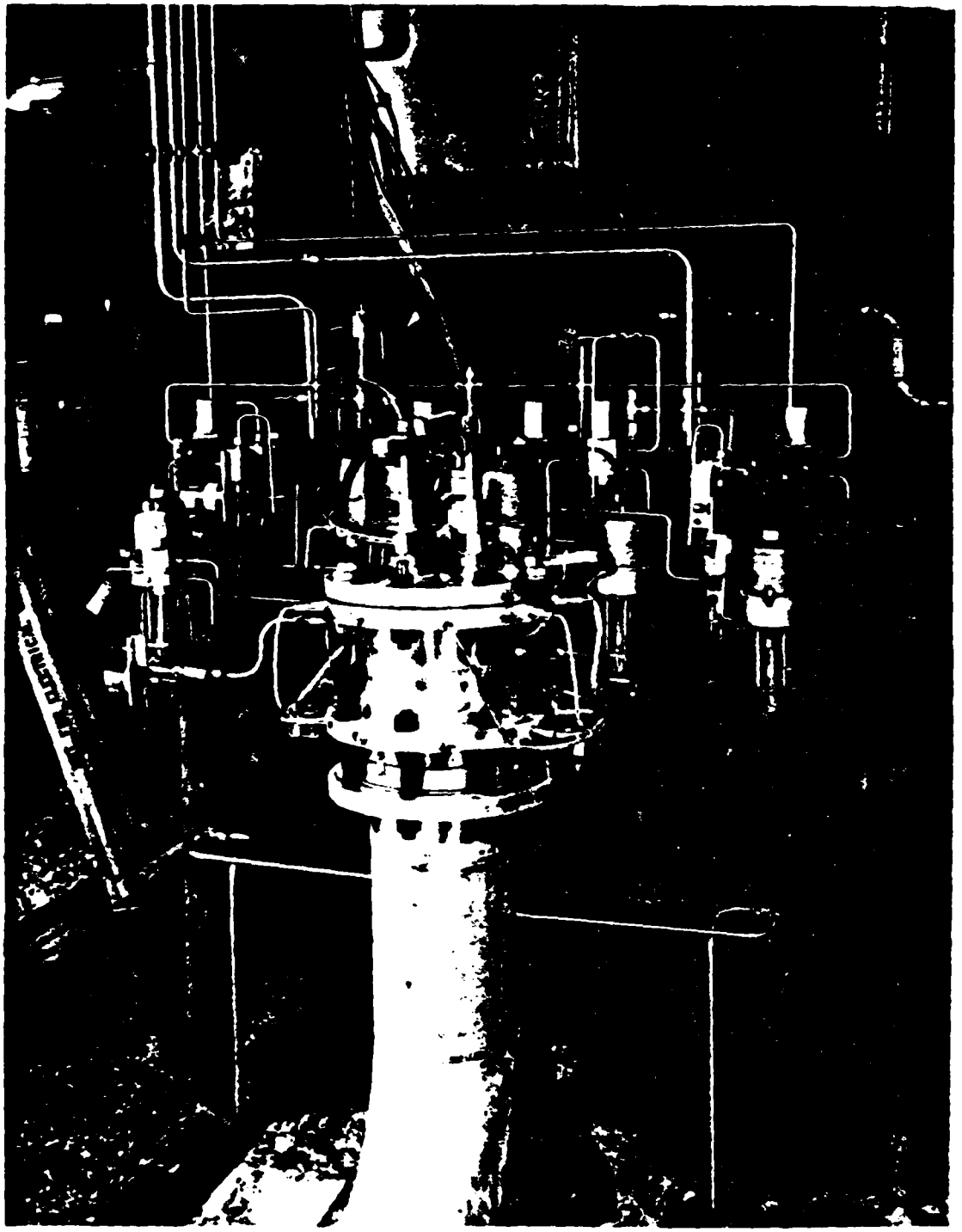

Fig. 3-3 Close-Up of Test Set-Up

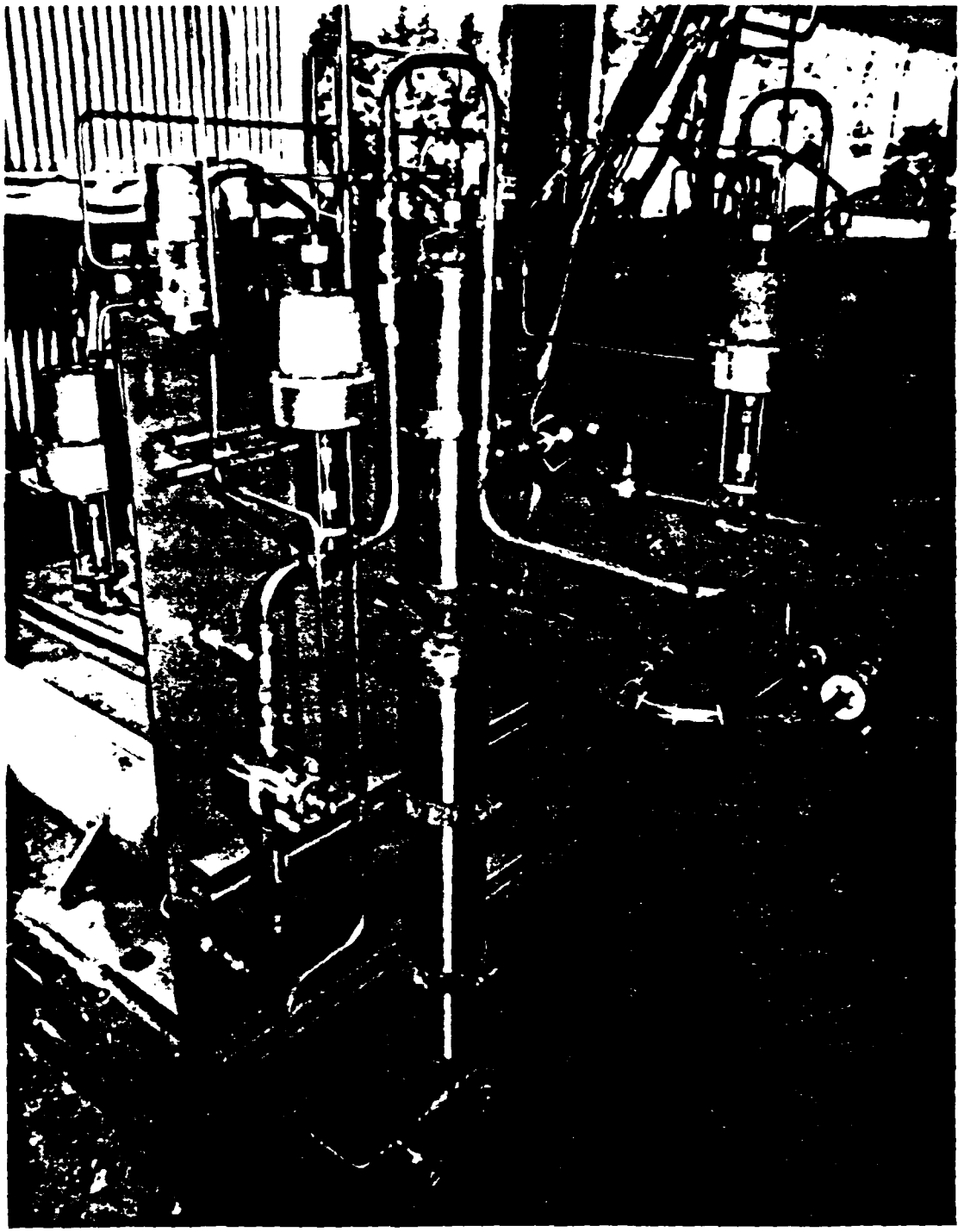

Fig. 3-4 Rear View of Test Set-Up Showing Propellant Feed Tanks and Plumbing

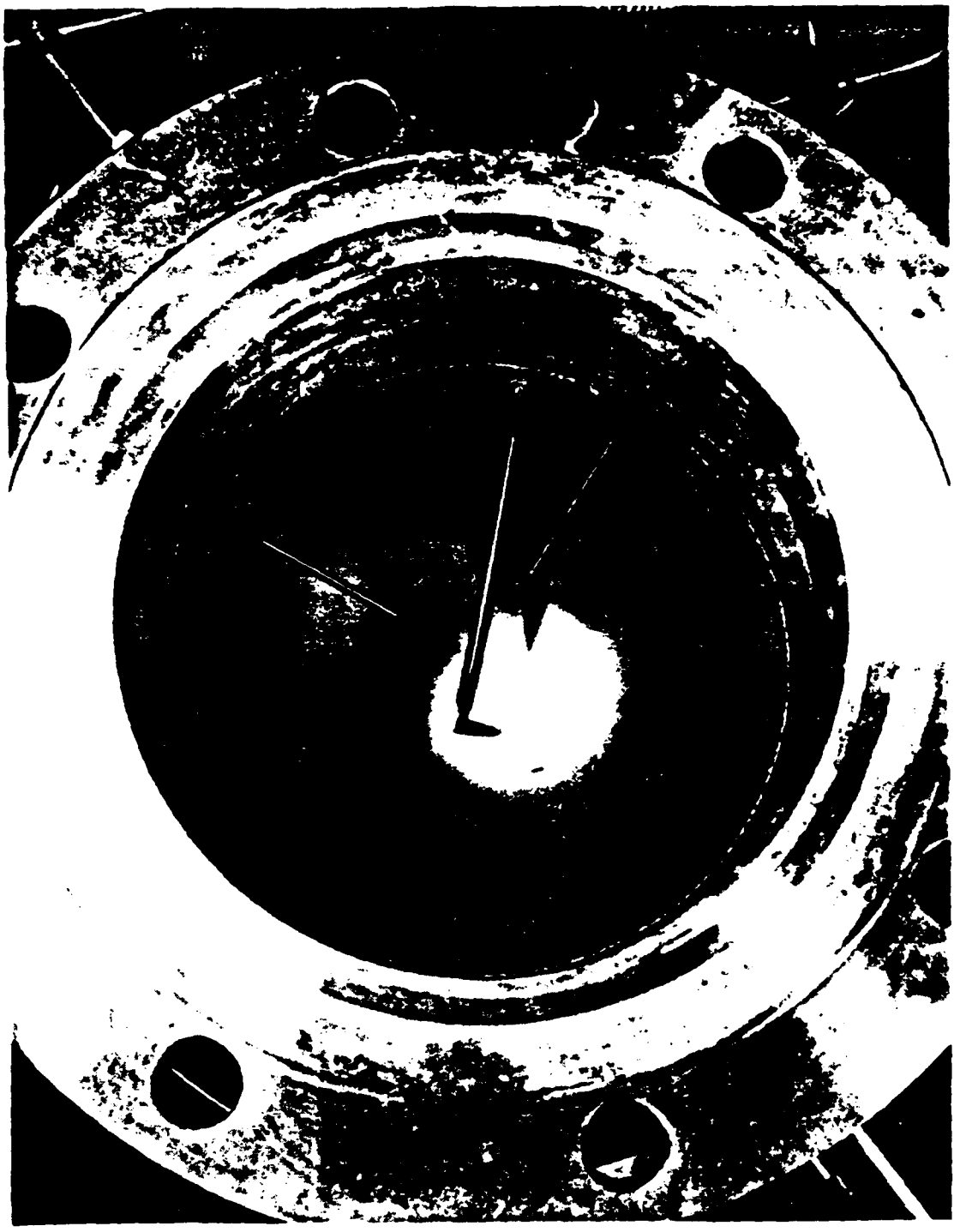

Fig. 3-5 Internal View of Test Tank Bottom

Fig. 3-6 Test Tank Top Plate and Test Specimen

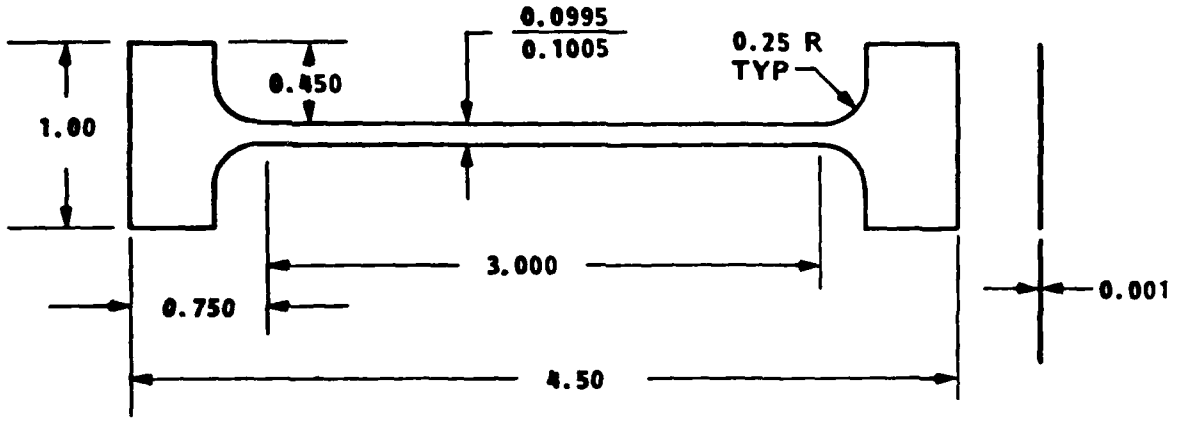

NOTE: ALL DIMENSIONS IN INCHES

MATERIAL: ALFA 00008
ALUMINUM FOIL

Fig. 3-7 Test Specimen (Ribbon) Configuration

(U) was to sandwich the sample foil between thick aluminum backing plates (both sides) and simply machine the samples. This resulted in close tolerances and very smooth edges.

(U) Propellants. The propellants used in the tests were "standard" versions of these particular types. They were obtained from the LMSC facility at Vandenberg Air Force Base, where they were analyzed to determine their specifications before shipment to Santa Cruz. Of major concern for MMH is the water content; several batches were analyzed to find material with a minimum water content. The batch tested had a major content of slightly less than 2 percent, which is within specification. The MON tested was 10 percent NO and 90 percent N_2O_4, which is a common mixture in use today. Other commonly available mixtures are 13 percent NO and 25 percent NO (100 percent N_2O_4 is easily obtained). However, the variation in physical and thermal properties is not a strong function of NO content (see Appendix B); thus the liquid heat transfer characteristics are probably not a strong function of NO content.

3.3 TEST PROCEDURES

(U) The test procedures are outlined in Fig. 3-8. The initial step in a given test is to calibrate the ribbon to determine its electrical resistance as a function of temperature. The aluminum temperature-dependent resistance can be determined in several ways. Calibration in air is very difficult, requiring very small changes in current. Calibration in a heated water bath is much easier. However, there is some concern about reaction between aluminum and water, forming an oxide which changes the ribbon resistance. To check this effect, calibrations were also performed in an oil bath, which allows measurements to higher temperatures (approximately 400°F). The calibrations obtained by these two methods were essentially the same. A typical calibration curve is shown in Fig. 3-9.

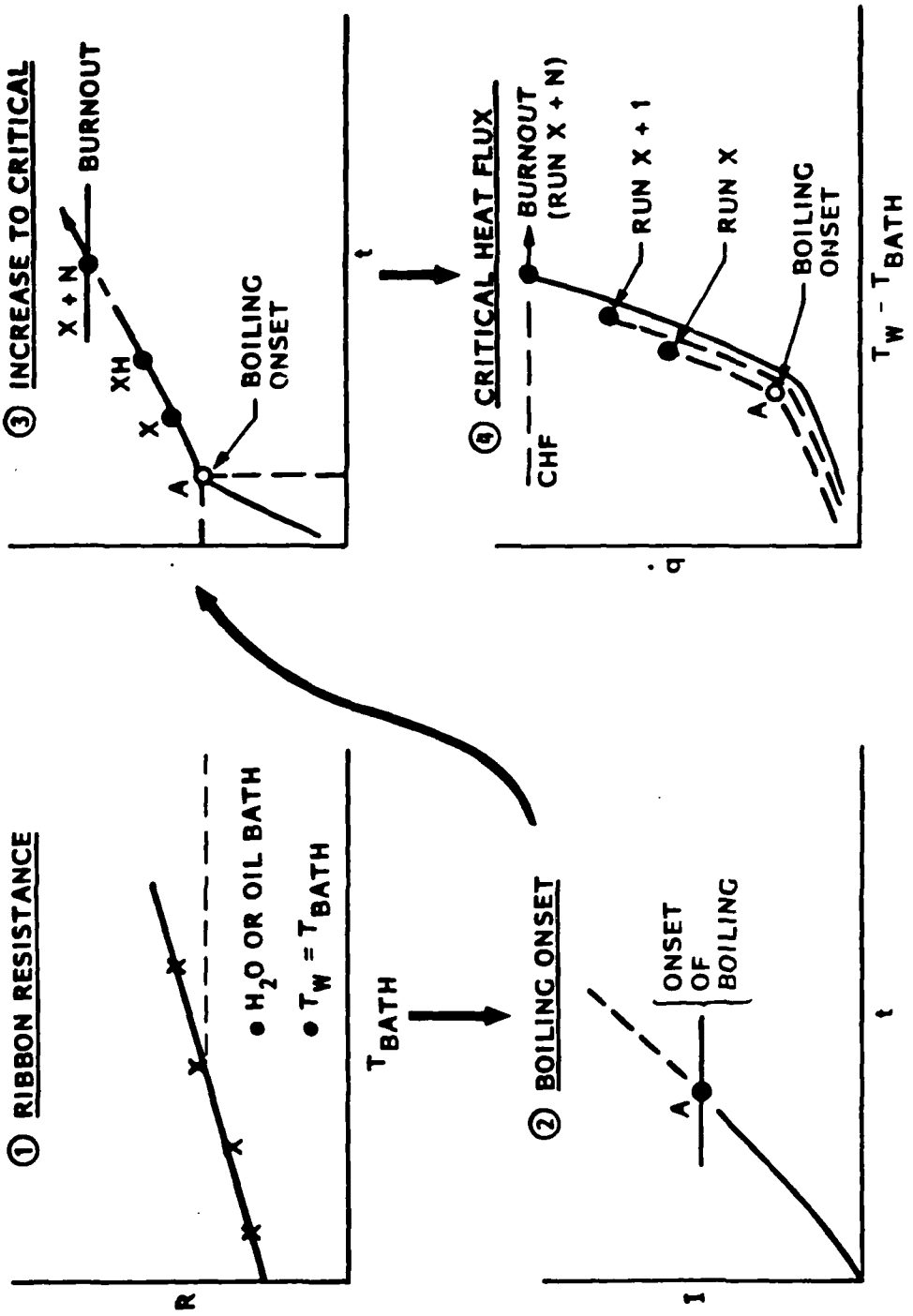

Fig. 3-8 General Test Procedures

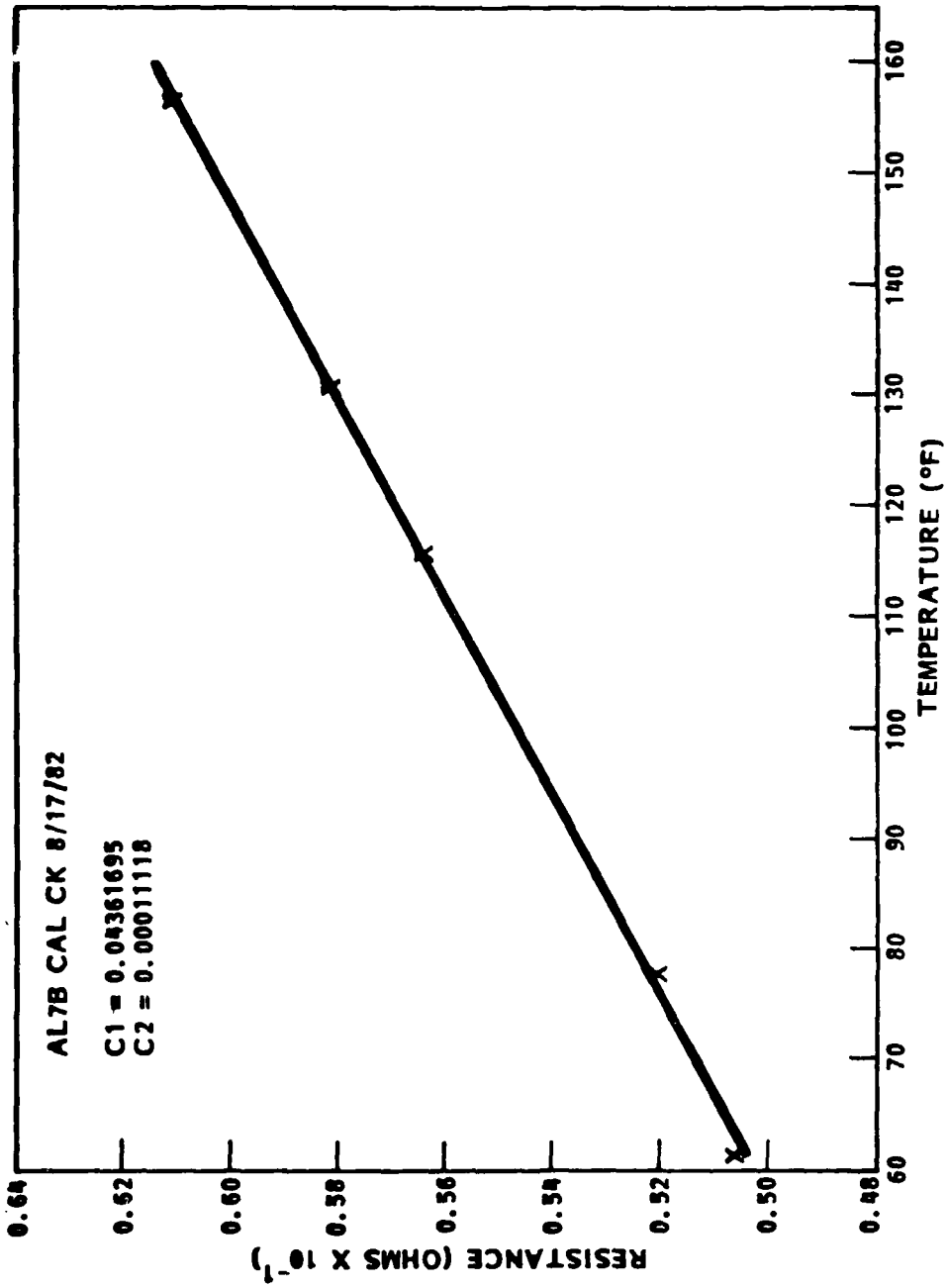

Fig. 3-9 Typical Aluminum Calibration Curve

(U) Once the calibration is completed, the test run is begun. The tank is filled with propellant and brought to the desired initial temperature and pressure conditions. The test specimen is then heated at a predetermined rate by increasing the current at a computer-controlled pressurized rate. The data from the tests is stored directly on the computer; print-outs and plots are available within an hour of the test. A portion of this data is shown in Appendix A).

(U) One of the features of the system is the use of a programmable power supply which allows an accurate and rapid change in delivered power. In the normal test procedure, a predetermined maximum heat rate was set for each run; once reached, the power was shut off and the ribbon cooled back to the initial conditions. The run was then repeated at a higher maximum heat rate until burnout was eventually reached.

(U) This standard cyclic type test procedure allowed some variation in pressure; a very slight increase in the onset of nucleate boiling was observed with increasing pressure (up to 100 psi). This also allows us to "sneak up" on the CHF, the objective being to save the ribbon by shutting down the power very rapidly after burnout is reached (as demonstrated by a very rapid increase in temperature/resistance). However, the rate of temperature increase after burnout was also so rapid that the ribbon failed before the power could be shut off. This cycling approach had the possible draw-back of producing aging effects on the ribbon, such as the build-up of deposits due to possible reactions of the metal with the propellant. To determine if this effect was significant, several runs were made (one for each propellant) wherein the CHF was reached in one pass. The results were within agreement with the normal procedure.

(U) The overall program approach was to first establish the credibility of the experimental technique by obtaining data on water with platinum ribbons and comparing it with existing data. However, several issues arose; probably the

(U) most critical of which is the control of the heat rate (i.e., current control) and the specific heating rate history to be applied. It appears that the previous data was obtained with relatively slow increases in heating rate (i.e., a few to tens-of-seconds at least between increases in heating rate). The actual test procedure employed in the previous tests is not well defined. While this relatively slow procedure is adequate to compare different fluids (and was necessary to correlate the water/Pt data), it creates some issues from both a test technique standpoint and an applicability of data standpoint.

(U) From a test technique standpoint, it would be desirable to increase the heating (in modest steps) in a relatively rapid manner (i.e., 1 second or less), being dictated only by equilibrium considerations for both attainment of ribbon temperature (very short, in the msec range) and fluid dynamic equilibrium (which will be somewhat longer). This not only decreases test time, but also decreases the total heating of the bath. If very long total test times are employed (minutes), an appreciable rise in bath temperature could occur. The heat transfer characteristics can be a strong function of the fluid bulk temperature. Additionally, gross thermal gradients in the fluid could set up abnormal fluid flow fields.

(U) In addition to these test technique considerations, there is a more fundamental concern related to the rate-dependency of the heat transfer. There is no definitive data available on this effect, probably because the previous tests were limited to relatively slow heat rate changes (these limitations have been overcome with the new power supply/controller which permits much more rapid controlled increases in current or voltage). The approach used for the current tests was to use rates which produce total test times the order of 3 to 6 minutes, depending on CHF. This rate allowed a valid comparison of the results on water with previous data, and a direct comparison with the propellants. However, these times/rates, although short compared to previous data, are still one to two orders of magnitude longer than the laser irradiation times of interest. Since it was believed that there may be significant rate

(U) effects for at least some propellants, a preliminary investigation was made on the last run on MON. This result is discussed in Section 4, which follows.

Section 4
DISCUSSION OF RESULTS

(U) This section contains a discussion of the test results and the analytic correlation of those results, including the derivation of the empirical coefficients used in the heat transfer analysis discussed in Section 2.

4.1 TEST RESULTS

(U) The results of the tests are summarized in Table 4-1. The computer plots of all the CHF runs are shown in Appendix A. As discussed in Section 3, and shown in the test matrix in Table 3-1, the test program was initiated with tests on water at standard conditions, the objective of which was to verify the test technique. These were followed by a few tests on isopropyl alcohol to further check out the test technique and to obtain data on a fluid with properties more similar to those of the propellants (especially MON). These tests were then followed by the tests on the actual propellants, first on MMH and finally on MON.

(U) Technique Verification Tests - Water/Platinum. These facility "calibration" tests were performed on water with platinum test specimens at room temperature and pressure, as has been used in previous tests to obtain the existing data. The data indicates that very repeatable results are obtained. Additionally the data, shown in Fig. 4-1, agrees very well with the existing data. Therefore, the test technique and procedures are believed to be valid.

(U) A series of tests were conducted on each of two platinum ribbons. The general procedure was to initially characterize the free convection regime and the transition to boiling. These tests were conducted over a relatively long time (approximately 1 to 3 minutes); the maximum heat rate was increased each time up to levels well above boiling onset, but below burnout. Once the

Table 4-1 LIQUID PROPELLANT CHARACTERIZATION RESULTS

Initial Conditions				Results (At Burnout)			Comments
Fluid	Specimen	Bulk Temp. (°F)	Pressure (psia)	Run Time (s)	Specimen Temp. (°F)	Heat Flux (W/cm^2)	
Water	Platinum	92	14.7	350	310	610	Technique
↓	Platinum	88	14.7	352	335	605	Verification
Isopropyl	Aluminum	68	38	192	273	95	Low Temp.
Alcohol	Aluminum	77	39	200	291	108	Liquid
↓							
MMH	Aluminum	80	60	325	285	280	Baseline
↓	Platinum	86	60	260	286	300	Pt vs Al
↓	Platinum	252	56	196	330	132	Sat. Liquid
↓	Aluminum	85	59	352	331	295	One Pass
MON	Aluminum	54	67	270	157	118	Baseline
↓	Aluminum	50	59	232	150	95	One Pass
↓	Aluminum	92	63	257	132	110	Higher Bulk T
↓	Aluminum	60	58	12	132	49	Rate Effects
MON	Platinum	52	60	168	160	98	Pt vs Al

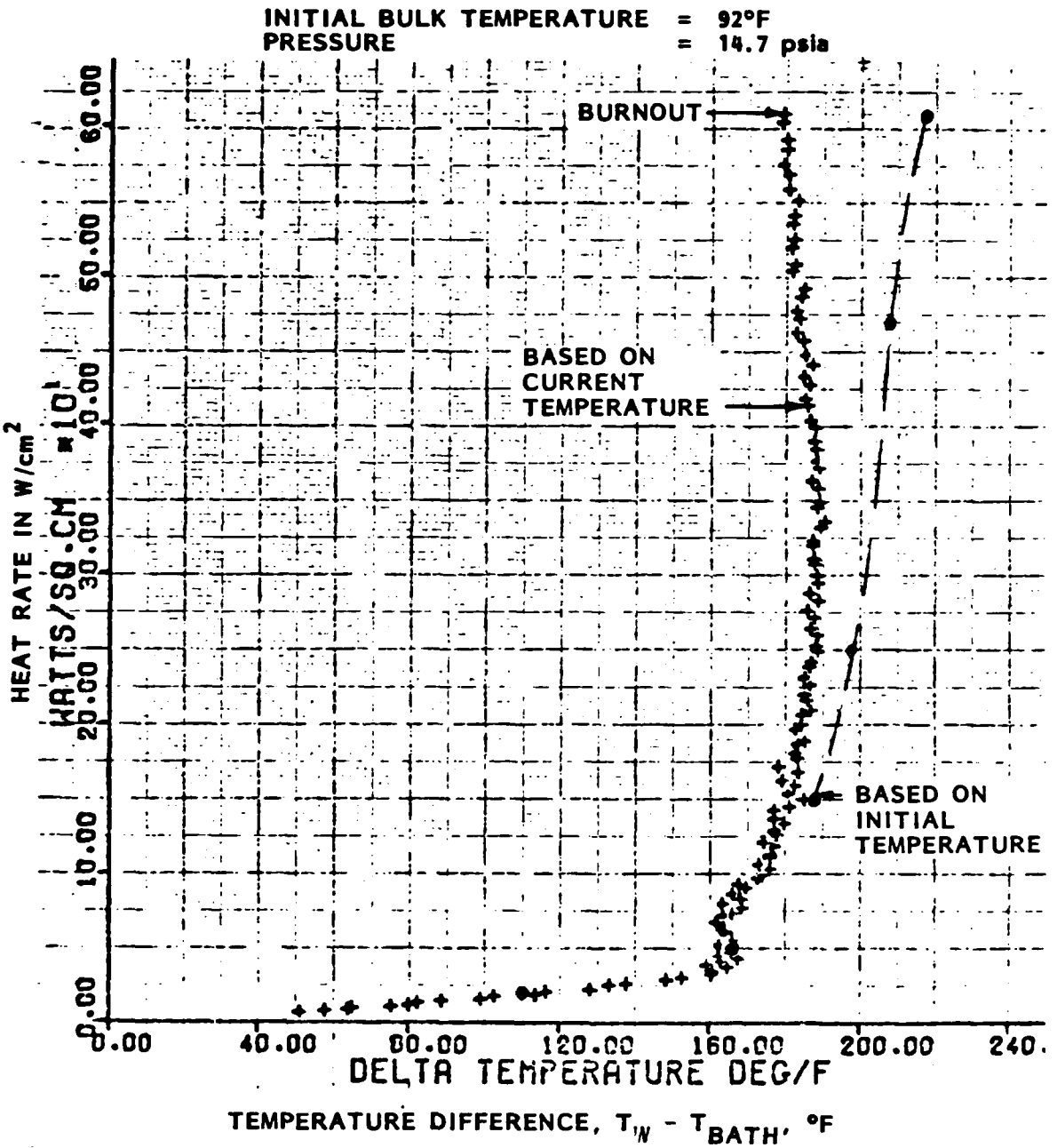

Fig. 4-1 Water at Standard Conditions With Platinum Ribbon

(U) characterization at low heat rates was obtained, the burnout (CHF) tests were conducted. These tests used heat rate increases which typically resulted in about 350 seconds total test time. Again the maximum flux was increased in steps until burnout was reached. The results of the last test for one ribbon are shown in Fig. 4-1. The figure shows the temperature difference between the ribbon and the real time bath temperature as a function of the heating rate to the ribbon. Also shown is the temperature rise relative to the initial bath temperature; the difference in the two curves is due to rise in bath temperature during the test.

(U) The two tests (see Table 4-1) show excellent agreement. Both ribbons failed in about the same time (350 seconds); the final bath temperature rise was about 40°F in each case. The burnout heat fluxes were essentially identical (610 and 605 W/cm^2, respectively). The general character of the curves and the slopes are similar (heat transfer coefficients). The first ribbon underwent transition to boiling at a slightly lower heat flux (40 to 60 vs. 60 to 80 W/cm^2) and temperature rise (160 to 170°F vs. 190 to 200°F). Thus the ribbon temperature during nucleate boiling was typically 20 to 30°F lower for the first ribbon. These differences may be due to slight differences in roughness, or may be just experimental scatter. Based on these results, it was believed that the test technique was valid (i.e., was producing valid, repeatable results). Thus, the program proceeded to the propellant tests.

(U) Isopropyl Alcohol. Before proceeding to the tests on propellants, tests on isopropyl alcohol using aluminum ribbons were conducted as a further check-out of the test technique. Alcohol is predicted to have heat transfer properties such that boiling and burnout should occur at much lower heat fluxes than water; thus the two sets of data should bracket the anticipated response of the propellants.

(U) In addition, two pressure levels were tested (40 and 60 psia) to check out the facility and determine pressure effects. The results of one of the burnout

(U) test on alcohol is shown in Fig. 4-2. This test was run at 38 psia. Burnout occurred at 95 W/cm^2 with a temperature difference of about 200°F. Transition to nucleate boiling occurred at about 12 W/cm^2 ($\Delta T \approx 160°F$). Tests at 60 psi (not shown) indicated boiling onset at slightly higher heat rates (about 15 W/cm^2) and temperature rises (about 160 to 180°F). This trend is as anticipated, since the higher pressure should suppress boiling onset somewhat. However, the dependency does not appear very strong.

(U) Thus the tests on the two well-characterized fluids, water and alcohol, do indeed bracket the CHF results for the propellants (see the following discussion). Although these are somewhat academic, it is interesting that the critical heat flux for alcohol is essentially the same as that for MON, and thus it could be used as a simulation liquid if desired. Only the CHF is simulated, however; the nucleate boiling regime occurs at somewhat higher temperatures for alcohol relative to MON. To simulate both CHF and NBHT for MMH, a mixture of alcohol and water may be possible.

(U) Monomethyl Hydrazine. Four separate test conditions were employed for MMH as shown in Table 4-1. The first three tests were run using the same procedures as used on the previously reported tests. That is, a series of individual tests on the same ribbon were conducted, with the maximum heat flux increased slightly each cycle up to the point of burnout. For the first two test conditions, both with room temperature fluid, the pressure was varied on each succeeding run (i.e., one run at 40 psia, the next at 60 psia). For the other two tests, only 60 psia data was taken. In the third test, the MMH was pre-heated to the saturation point (i.e., just about to boil), which is about 275°F at 60 psia. In the last test, the ribbon was not cycled through incremental heat fluxes, but rather was taken to burnout on one run.

(U) The results of the burnout test for the first set of conditions (i.e., aluminum, room temperature, 60 psia), are shown in Fig. 4-3. The burnout heat flux was about 280 W/cm^2; the ribbon temperature was 275°F (or a rise of 196°F

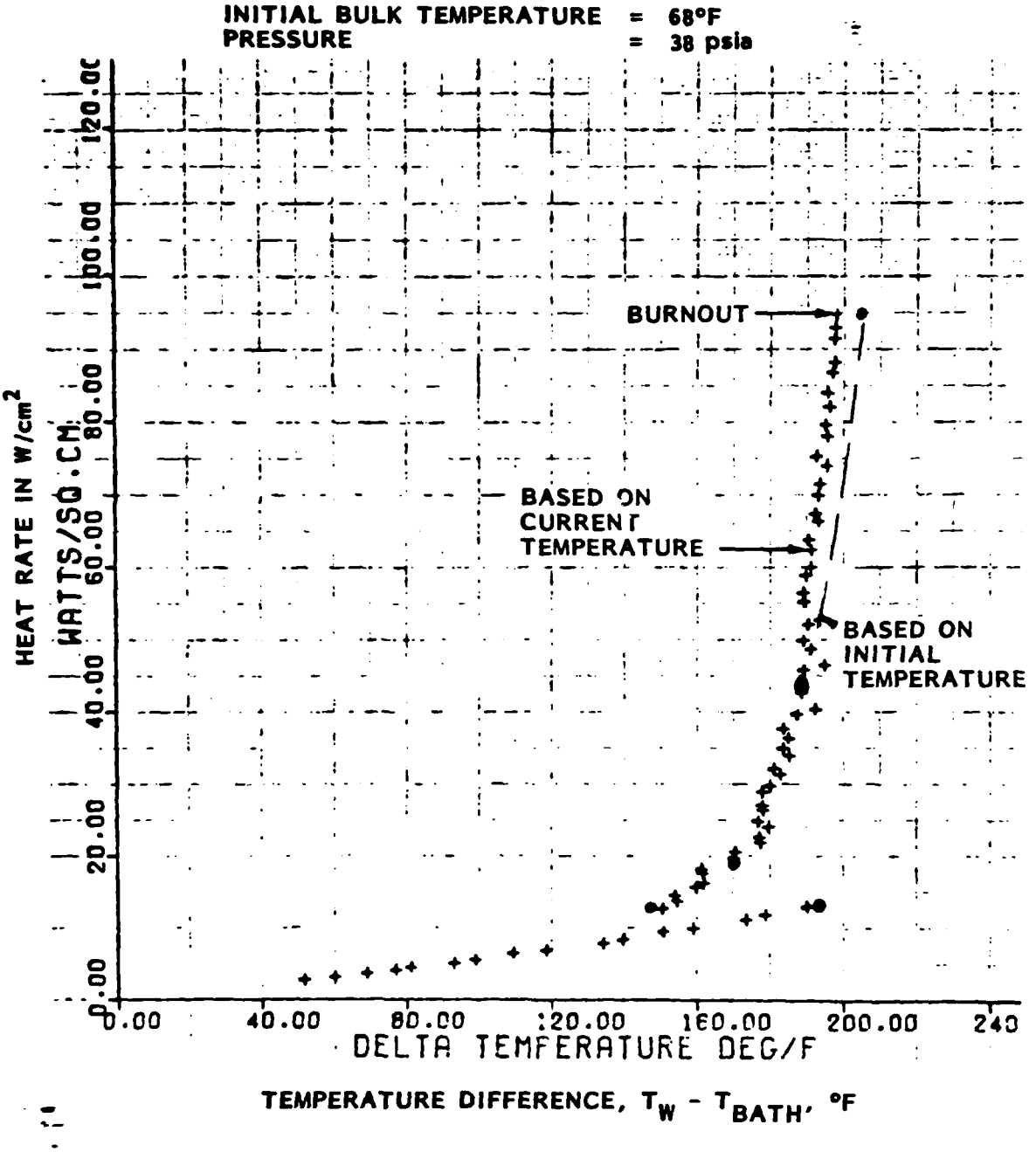

Fig. 4-2 Isopropyl Alcohol With Aluminum Ribbon

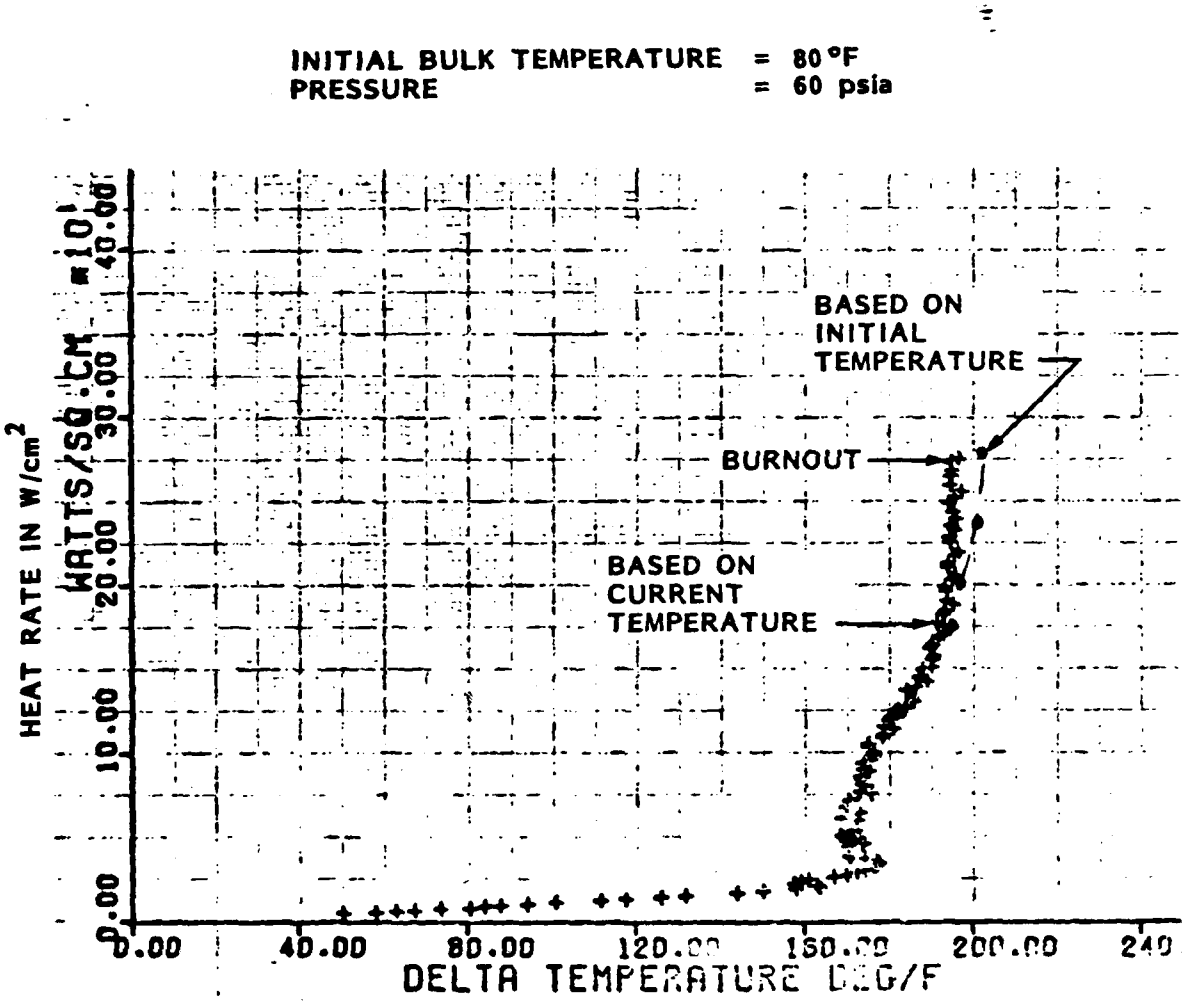

TEMPERATURE DIFFERENCE, $T_W - T_{BATH}$, °F

Fig. 4-3 Monomethylhydrazine With Aluminum Ribbon, Nominal Conditions

(U) over the initial bath temperature). The onset of boiling occurred at a flux of about 30 to 40 W/cm^2 and a ribbon temperature of about 250°F (ΔT = 180°F). The ribbon actually cools slightly (approximately 10°F) after boiling onset, due to the increased heat transfer, but then increases as the heat flux is increased up to burnout. The measured burnout heat flux was within the error bands of the pre-test predictions (which were 320 ± 100 W/cm^2), although slightly on the low side. The transition to nucleate boiling from free convection occurred at somewhat higher heat flux than anticipated (predicted to be about 10 W/cm^2), although there was significant uncertainty in this predicted value.

(U) The second test on MMH employed a platinum ribbon rather than an aluminum ribbon; otherwise the test conditions and test procedures were essentially identical (a slightly higher initial temperature). The results of the tests were also nearly identical. Burnout occurred at a slightly higher ribbon temperature (286°F vs. 285°F) and slightly higher heat flux (300 vs. 280 W/cm^2) than with aluminum. Thus the characteristics of MMH appear to be nearly independent of ribbon material, at least for these conditions.

(U) The third test on MMH examined the effects of initial bath temperature on nucleate boiling and burnout heat flux. As indicated in Section 2, when the bath temperature is increased, the fluid is closer to boiling (at constant pressure). Thus the onset of boiling occurs at lower heat fluxes, and the critical heat flux is also reduced. For this test, the initial bath temperature was raised to 252°F, which is just below the saturation temperature of 275°F at 60 psia. The onset of boiling occurred rapidly, and the burnout condition was reached at a critical heat flux of only 132 W/cm^2 (vs. about 300 W/cm^2 for room temperature). The results are shown in Fig. 4-4. This test allows a determination of the dependency of CHF on initial propellant temperature, or the coefficient K_2 in Eq. (6) of Section 2 (see the following discussion). It should be noted that this test was run with a platinum ribbon rather than aluminum due to a temporary shortage of aluminum. However, based on the first two tests on MMH, the effect of different ribbon material is believed to be negligible.

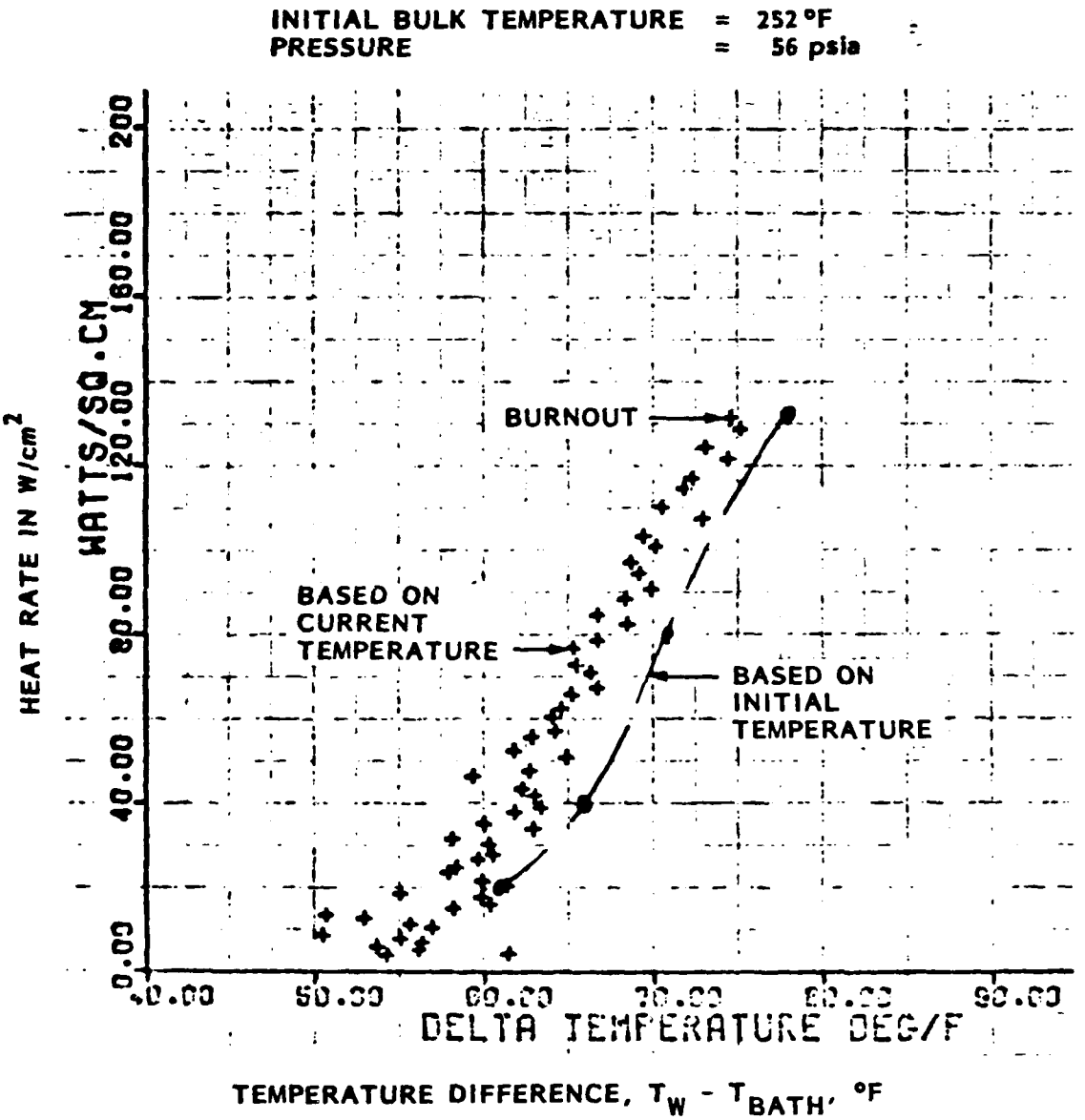

Fig. 4-4 Monomethylhydrazine With Platinum Ribbon, Near Saturation Temperature

(U) The last test on MMH, using an aluminum ribbon, was conducted in one pass; i.e., the heat rate was not cycled but was reached in one continuous increase of heat flux up to burnout. This test was performed to determine if there were any "aging" effects due to the cycling of the ribbon, such as might be caused by a build-up of residue or deposits on the ribbon surface by reactions with the propellant. As indicated in Table 4-1, the CHF for this one-pass test was essentially the same as for the normal cyclic technique.

(U) Mixed Oxides of Nitrogen. The tests on MMH were followed by tests on MON, as shown in Table 4-1. For the nominal conditions of 60 psia and fluid bulk temperature at room temperature (in this case 50 to 55°F), the measured burnout heat flux for MON is about 100 to 120 W/cm^2. This is about one-third of the value for MMH (280 to 300 W/cm^2). It is somewhat lower than the pre-test predicted values (using assumed coefficients), which was 160 W/cm^2, with a ± 30 percent uncertainty band (112 to 208 W/cm^2). The MMH results were also less than estimated, but only by about 10 percent.

(U) The MON data exhibit somewhat more scatter than that for MMH, which was reasonably well behaved. For the normal procedure, where the aluminum ribbon is cycled several times before burnout is reached, burnout occurred at 118 W/cm^2 (Fig. 4-5). When burnout was reached in a single pass, the maximum heat flux was 95 W/cm^2, or about 20 percent lower (for MMH, the single-pass results were about 7 percent higher). For the same fluid conditions with a platinum ribbon, the burnout heat flux was 98 W/cm^2.

(U) The other two tests on MON are of particular interest. The third test on MON as shown in Table 4-1 was run with the fluid at a higher bulk temperature. The objective of this test was to determine the dependence of burnout heat flux and boiling characteristics on fluid bulk temperature at a given pressure. The nominal procedure is to heat the fluid to just below the saturation temperature, as was done with MMH. For MON, the saturation temperature is about 130°F at 60 psia. However, for a fluid mixture such as MON (10 percent NO, 90

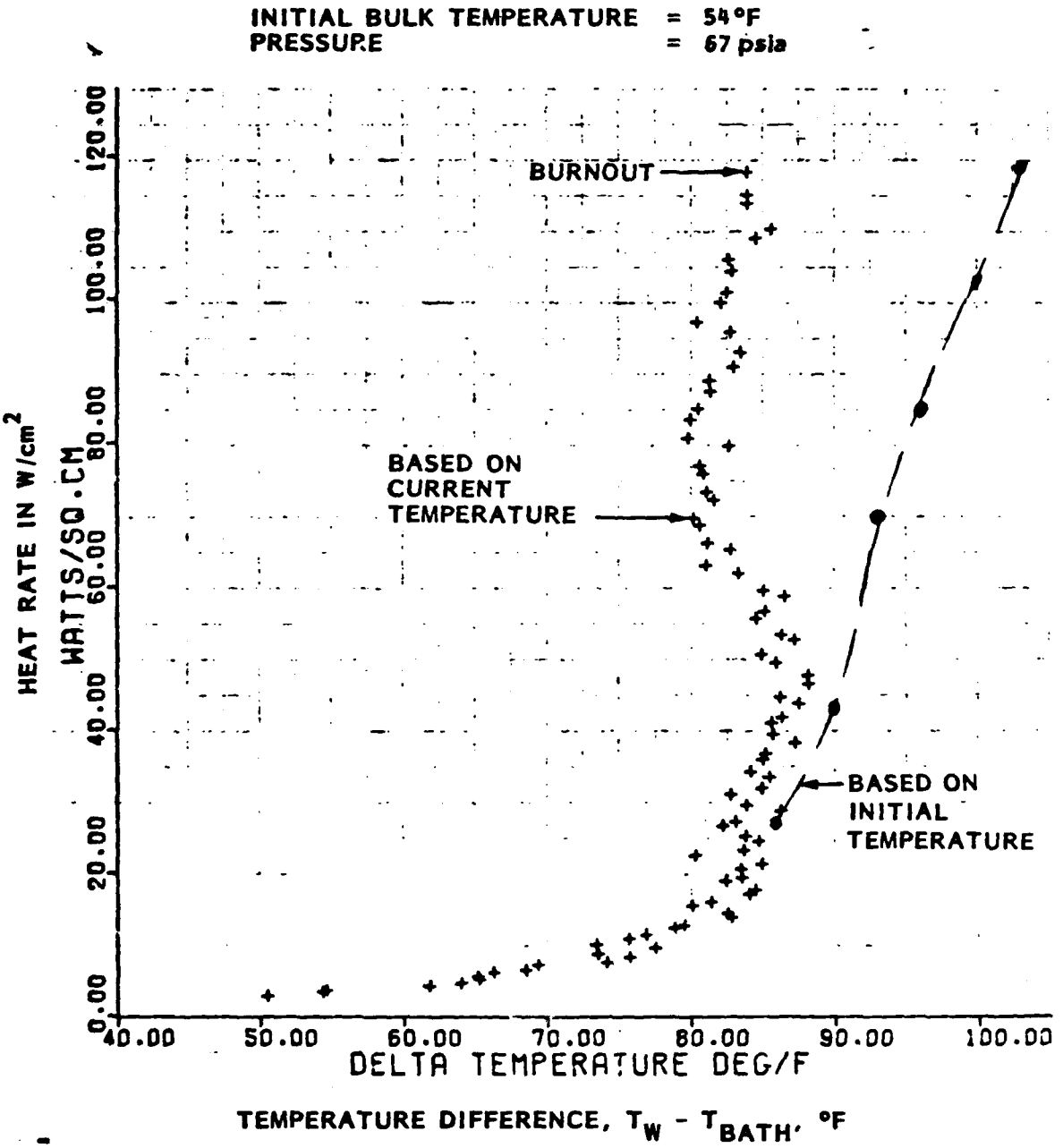

Fig. 4-5 Mixed Oxides of Nitrogen (90-10) With Aluminum Ribbon, Nominal Conditions

(U) percent N_2O_4), the two fluids do not vaporize at the same temperature. For MON, the NO begins to vaporize first. In fact, in the first few tests, an increase in pressure was observed during the tests as the ribbon and bath were heated. This was attributed to vaporization of the NO. Therefore it was decided to not test at saturation temperature but at an intermediate temperature (92°F) where the initial NO content in the fluid was still about 10 percent. The interesting result is that the measured burnout heat flux was only slightly less than at 50 to 55°F (i.e., 110 W/cm^2 measured). This indicates that there is little or no dependency on fluid bulk temperature, at least in the range of 50 to 90°F. It is unlikely that this trend would hold as the temperature was raised to the saturation temperature. Unfortunately, funding limitations did not permit any further MON testing.

(U) The last test on MON with an aluminum ribbon shown in Table 4-1 was designed to investigate rate effects. The rate at which the ribbon temperature was increased (i.e., heat rate) was varied systematically, as shown in Fig. 4-6. A maximum heat rate of 50 W/cm^2 was used; this rate is well above the onset of boiling, but about half that at burnout for the nominal heat rate profile. The time at which this maximum rate was reached was decreased by 50 percent in each subsequent run. Starting at 200 seconds, runs of 100, 50, 25, and 12 seconds were conducted. For the last run at 12 seconds, the burnout condition was actually observed at 49 W/cm^2, which is about half that for the slower rate. These results indicate that, for MON, a burnout heat flux of 50 W/cm^2 may be more appropriate for typical laser heat rates. No rate effects tests were conducted for MMH.

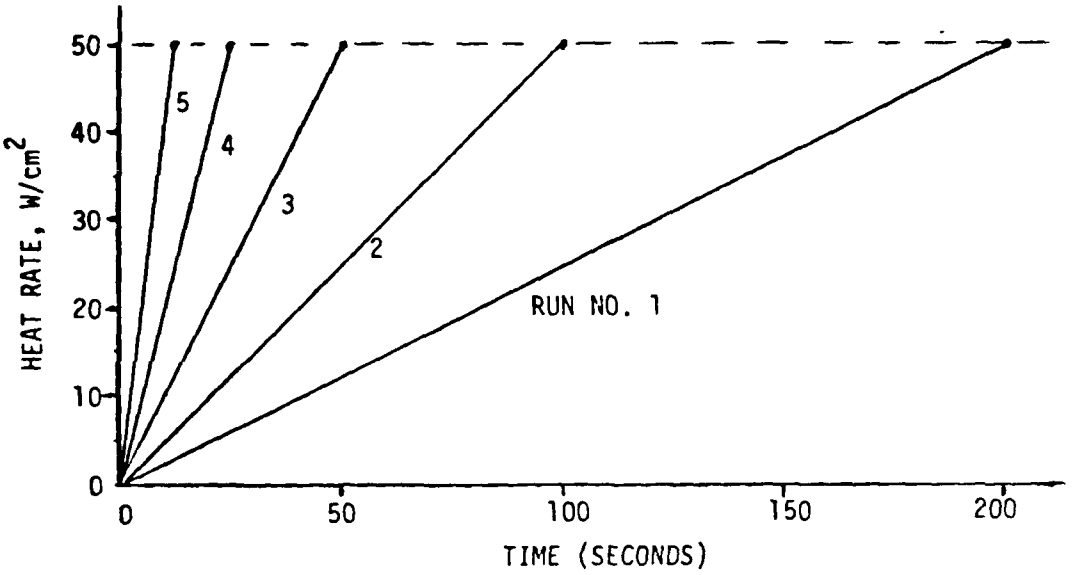

Fig. 4-6 Rate Effects on MON

4.2 ANALYTIC CORRELATION OF RESULTS

(U) The analytic models employed to predict the liquid heat transfer characteristics of propellants were presented in Section 2. Of interest in this study are the correct values for (1) the nucleate boiling heat transfer coefficient C_{SF} and the exponent r in Eq. (4); and (2) the critical heat flux (CHF) coefficients K_1 and K_2 of Eqs. (5) and (6), respectively. The data presented in the previous section (Sec. 4.1) are used to derive these coefficients.

(U) The procedure for data reduction is shown in Fig. 4-7. This procedure is relatively straightforward. The surface coefficient C_{SF} and exponent r are determined from Eq. (4) for each run. The propellant properties used in the determination of the dimensionless parameters are shown in Appendix B.

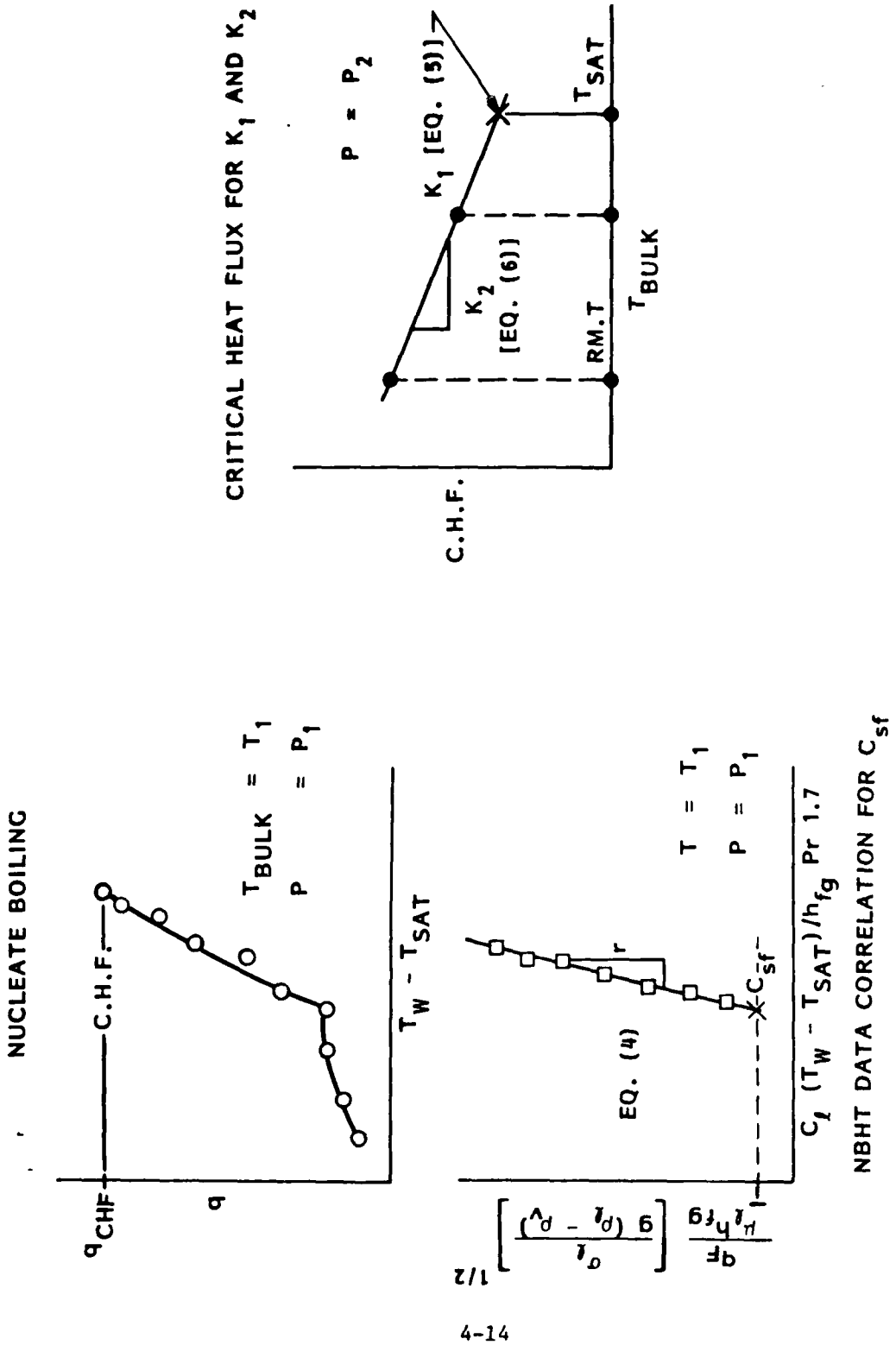

Fig. 4-7 Data Reduction Procedure

(U) For each run, the computed value of the dimensionless parameter groups (omitting C_{SF} and r) corresponding to each experimental data point in the NBHT regime was plotted on log-log paper. A least-squares curve fit to these points was constructed. Intercept of this line with the ordinate=unity line established C_{SF} . The exponent r also is similarly obtained from the same least-squares fit line. To determine the coefficients for the CHF, the coefficient K_2 is first determined from two runs at different initial bulk temperatures for a constant pressure. This allows a determination of CHF at the saturation temperature, and thus an evaluation of the coefficient K_1 .

(U) A summary of the coefficients derived from the data for the conditions tested are shown in Table 4-2. For the propellants, the values shown in Table 4-2 for C_{SF} and r are for the tests on aluminum ribbons in which burnout was reached in one pass, which are most representative of the actual case. In general, the scatter of C_{SF} data for MMH was somewhat greater than for MON (the reverse of the case for CHF). The NBHT data for surface coefficients are applicable for surfaces which could be characterized as smooth to very smoooth (a bit short of polished).

(U) The critical heat flux (CHF) was determined for all liquids for the conditions of interest (see Table 4-1). For the propellants, the nominal conditions are room temperature and a pressure of about 60 psia. In order to determine the correlation coefficients K_1 and K_2 , it is necessary to conduct tests at various initial liquid bulk temperatures for a given initial pressure. Such tests were only performed for the propellants (thus there are no coefficients for water or alcohol). MMH demonstrated a strong dependency of CHF on initial propellant temperature, whereas MON did not; thus the coefficient K_2 is much larger for MMH.

Table 4-2

LIQUID HEAT TRANSFER COEFFICIENTS DERIVED FROM TEST DATA

Liquid/Ribbon	C_{SF} (Eq. 4)	r (Eq. 4)	K_1 (Eq. 5)	K_2 (Eq. 6)	Comments
RECOMMENDED VALUES					
MMH/Aluminum	0.0093	0.27	0.19	3.2	One Pass
MON (90 - 10)/Aluminum	0.003	0.53	0.27	0.85	One Pass
TEST PROCEDURE VALIDATION (FOR REFERENCE)					
Water/Platinum	0.0131	0.28	----	----	Test System Verification
Water/Platinum	0.013	0.33	0.18	5.3	Recommended by Rohsenow (Ref. 10, Sec. 13)

Section 5
CONCLUSIONS AND RECOMMENDATIONS

5.1 MAJOR CONCLUSIONS

As shown in Table 4-1, the primary quantity of interest in this study, the "burnout" heat flux (also called the critical heat flux, or CHF) has been accurately established experimentally for MMH and MON propellants at nominal wall heating rates (approximately corresponding to 300 sec total heating time). Under these conditions, the CHF for MMH is about 290 W/cm^2 and for MON is about 110 W/cm^2 in the pressure and temperature ranges of prime interest. These values were found to be accurate and repeatable to within a few percent using the LMSC test facility and techniques developed in this program and agree well with LMSC's earlier, analytic, quantitative pretest predictions.

Sufficient CHF data were obtained to establish the coefficient of each of the correlation relations for (1) saturated liquid; and (2) subcooled liquid for a wide range of pressure, temperature, and gravitational (acceleration) vector conditions for the two propellants. Recommended coefficients, obtained from test data, are presented in Table 4-2 for the propellants.

The nucleate boiling heat transfer (NBHT) regime leading to CHF and ranking just below CHF in importance for applications of interest, also was experimentally investigated for MMH and MON in this study. The surface coefficient and exponent of the NBHT correlation relation were established from test data corresponding to smooth aluminum wall for the two propellants; recommended values are given in Table 4-2. These recommended values are empirically deduced from NBHT test data taken in a single run all the way to CHF onset and prompt consequent thin aluminum test ribbon destruction (melt down). Surface coefficient and exponent values deduced from successive sets of NBHT runs on the same

ribbon, but terminated before CHF onset to save the ribbon, generally produced different surface coefficient and exponent values for the propellants than the recommended ones of Table 4-2, which are based on one-pass tests. Differences were caused by metal/propellant reactions and consequent surface film deposit produced in the multiple-run, elevated-temperature tests. This condition was much more pronounced for MMH because of the much higher temperature range and CHF onset value compared to that for MON.

Before the propellant heat transfer data summarized above was obtained, the experimental test facility was first validated for CHF and NBHT data by performing tests in these regimes on water/platinum, whose results are widely documented, in close agreement, and are considered the "standard" for NBHT and CHF data techniques. For water/platinum at STP in the LMSC test facility, CHF was 605 and 610 W/cm^2 in two separate runs; 610 W/cm^2 is the standard reference value. Deduced surface coefficient and exponent also are in good agreement with the reference value for each (see Table 4-2). Based on these results, the LMSC test facility is considered to have produced valid, accurate, new data on the propellants tested in this program.

The final test series in this program, which was designed to explore the importance of heating rate effects on CHF for the propellants, produced results which demonstrate that CHF for MON is significantly heating-rate dependent. This is also expected to be true for MMH, though tests of this type were only conducted on MON because of funding limitations. The CHF for MON earlier had been established to be about 110 W/cm^2 for an approximately 250 sec (nominal) run time. As depicted in Fig. 4-6, a set of linear-heating-rate tests on MON up to a maximum rate of 50 W/cm^2 was conducted, beginning with a run time of 200 sec. In each successive run, the time to maximum (50 W/cm^2) was halved. On the fifth run, a CHF of 49 W/cm^2 was achieved after 12 sec of linearly increasing heating rate. This heating time corresponds to the approximate time scale of particular interest, and strongly suggests that baseline CHF (300 sec, nominal) values for the propellants established in this test program are very

conservative on the high side, if much shorter heating time is of primary interest. Nominal heating times in this program were set by a number of factors: (1) conditions required for test facility validation; (2) preventing premature ribbon destruction (it was relatively expensive to prepare the facility for another test after such an event); and (3) test equipment limitations (e.g., ribbon thickness, power supply capacity, etc.).

Rate effects on the propellants could be performed with relatively simple, inexpensive modifications to the existing test facility installed at LMSC's Santa Cruz Test Facility. The principal change required is a higher capacity power supply, which also would permit a thicker test ribbon and enable additional testing flexibility and efficiency.

5.2 RECOMMENDATIONS FOR FURTHER WORK

The program reported here was very modest in scope and funding, and required significant analytical, hardware/facility, and test technique development and validation effort before propellant data could be obtained. While the recommended propellant heat transfer data are considered valid for the primary purposes of this study, it would be desirable to have additional replicated runs on the tests conducted to provide greater reliability in deduced heat transfer values. Also, the test matrix only permitted one or two values of bulk liquid temperature or pressure for each propellant; extrapolation to quite different other conditions could be made with higher confidence with additional test data at other values of these parameters.

Further exploration of rate effects on the propellants clearly is an area that justifies further attention because of the likely substantial impact it would have in systems applications of the results reported here. Sufficient data was taken on MON at the end of this program to establish that rate effects for timescales of primary interest will be quite significant.

No NBHT data on the effect of wall surface roughness was taken in this program. All test ribbons had surface condition which can be characterized as "smooth", suppressing onset of nucleate boiling and thus providing only one bounding extreme of the range of possible NBHT characteristic conditions. If rate effects were to be explored using a larger power supply, the thicker test ribbons that would then be permissible also would allow systematic variation of surface roughness condition.

The validated, existing test facility for obtaining heat transfer characteristics of hazardous propellants has been used up to this point only for two such propellants: MMH and MON 90-10. Other hazardous propellants or mix ratios of interest now could be easily and inexpensively tested to establish their corresponding characteristics.

Finally, this test facility would be ideal for efficiently developing non-hazardous, "simulation" liquids having the same NBHT and CHF characteristics as propellants of interest. The simulation liquids then confidently could be used in place of the hazardous propellants in large-scale, liquid-backed component tests, thus avoiding the undesirable secondary response effects of hazardous liquids, but retaining important heat transfer characteristics.

Section 6
REFERENCES

1. Lockheed Missiles & Space Co., Inc., Laser Vulnerability and Effects Program, Final Report (U), LMSC-L050041, 25 Jan 1980 (SECRET).

2. ------, Novel Kill Mechanisms Program, Laser Lethality Technology Task (U), Final Report, LMSC-L034224, Jun 1978 (SECRET).

3. Aerojet-General Corporation, "Performance and Properties of Liquid Propellants," AJEC-8160-6S, 1961.

4. S. F. Bizjak and D. F. Stai, "Temperature-Entropy Diagram of Monomethyl Hydrazine," AIAA Journal, Vol. 2, No. 5, May 1964, pp. 954-956.

5. D. F. Stai, F. Bizjak, S. E. Stephanon, "Thermodynamic Properties of Nitrogen Tetroxide," J. of Spacecraft, Vol. 2, No. 5, Sep-Oct 1965, pp. 742-745.

6. J. M. Robinson, "Post Boost Propulsion System Propellant Characteristics Report," BSD-TR-67-168, April 1967.

7. W. M. Rohsenow, "A Method of Correlating Heat Transfer Data for Surface Boiling of Liquids," Trans ASME, Vol. 74 (1952), pp. 969-975.

8. N. Zuber, M. Tribus, J. W. Westwater, "The Hydrodynamic Crisis in Pool Boiling of Saturated and Subcooled Liquids," Proceedings of the International Conference on Developments in Heat Transfer, Am. Soc. of Mech. Engr., New York (1962), pp. 230-236.

9. W. M. Rohsenow, "Boiling Heat Transfer," Developments in Heat Transfer (W. M. Rohsenow, ed.), pp. 169-260, The M.I.T. Press, Cambridge, Mass., 1964.

10. W. M. Rohsenow, "Boiling," Handbook of Heat Transfer (W. M. Rohsenow, J. P. Hartnett, eds.,), McGraw-Hill Book Co., New York, 1973.

11. R. M. Milton and C. F. Gottzman, "Liquified Natural Gas: High Efficiency Reboilers and Condensers,: Chem. Eng. Progress, Vol. 74 (1952), pp. 56-61.

12. H. Kato, et. al., "On the Turbulent Heat Transfer by Free Convection from a Vertical Plate," J. of Heat and Mass Transfer, Vol. II, pp. 1117-1125, 1968.

13. R. W. Conrad, E. L. Roy, and D. W. Mangum, "Interim Report on the Effects of Heat-Sinks on the Thermal Response of Metals," DRDMI-HA-0180-R, 14 May 1979, Army High Energy Laser Laboratory, Redstone Arsenal, Alabama.

14. R. W. Conrad, E. L. Roy, and D. W. Mangum, "Quarterly Report on the Effects of Heat-Sinks on the Thermal Response of Metals," DRSMI-HA (R&D) -0679-R, 14 July 1979, Army High Energy Laser Laboratory, Redstone Arsenal, Alabama.

Appendix A
SUMMARY OF DATA

This Appendix presents a summary of typical data for the tests. An overall summary was presented in Table 4-1 of the burnout heat flux results. Representative data that was obtained on each run is shown in Figs. A-1 through A-6. The plots shown are the actual data from the plots obtained from the computer. The figures show, respectively:

Fig.	Data-Time Variation of:
A-1	Current
A-2	Voltage
A-3	Heat Rate
A-4	Ribbon Temperature
A-5	Ribbon Temperature (Detail at Burnout)
A-6	Heat Transfer Coefficient

The other data that was typically plotted for each run was the heat rate as a function of the difference between wall temperature and bath temperature, which is the primary result for each test (as discussed subsequently and in Section 4).

The data shown is for the first of the series of tests on MMH, and aluminum ribbon at nominal conditions (room temperature, 60 psia). As discussed in Section 4, the general procedure was to determine the onset of boiling in the initial runs of a series on a given ribbon for given conditions. Once this was established, the subsequent runs were configured to reach the onset or boiling relatively quickly. This is evident in Fig. A-1, where the current level of 20 amps (about 10 watts / cm^2) is reached very quickly (current was the central variable used in the tests). Once this level was reached, the

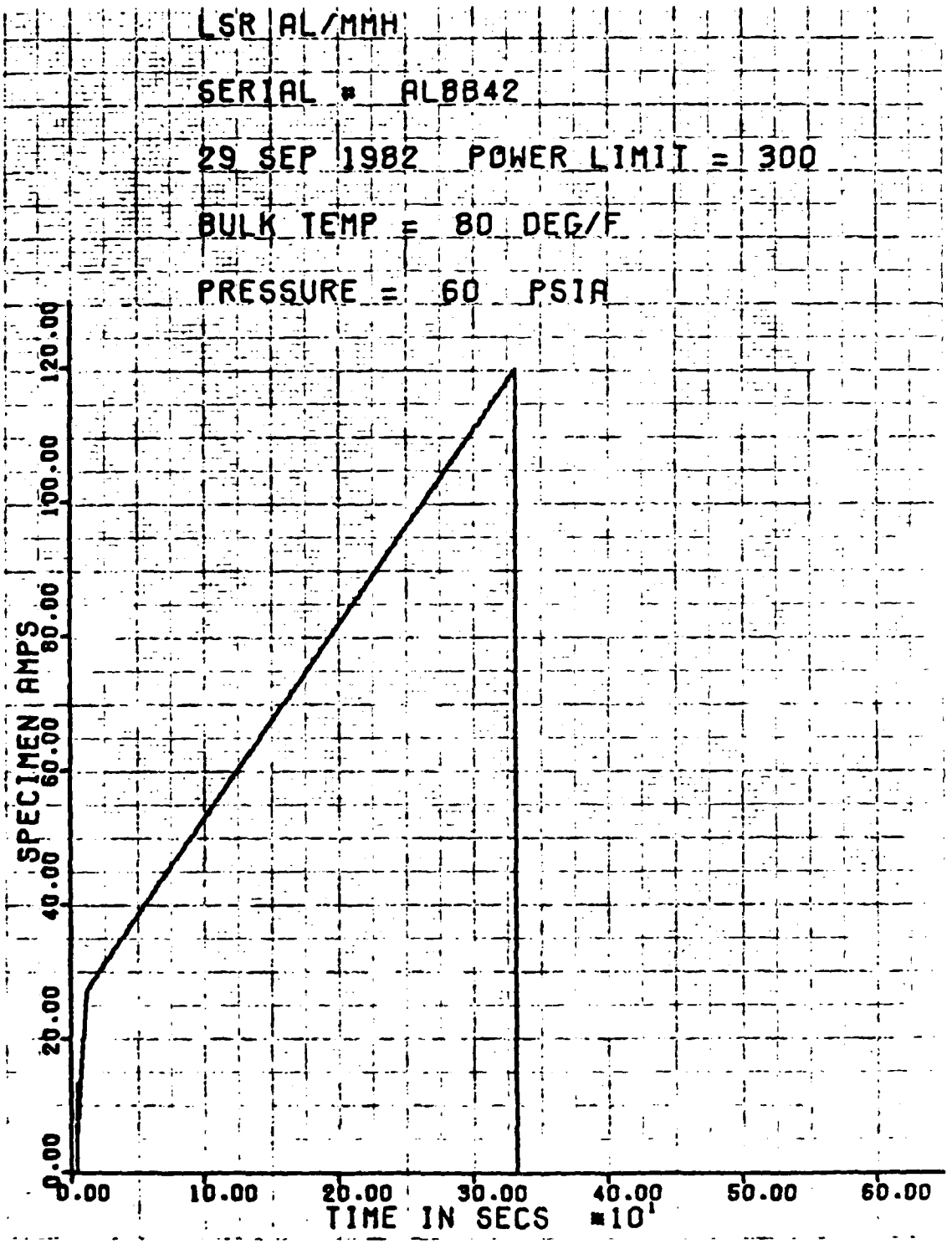

Fig. A-1 Typical Current History

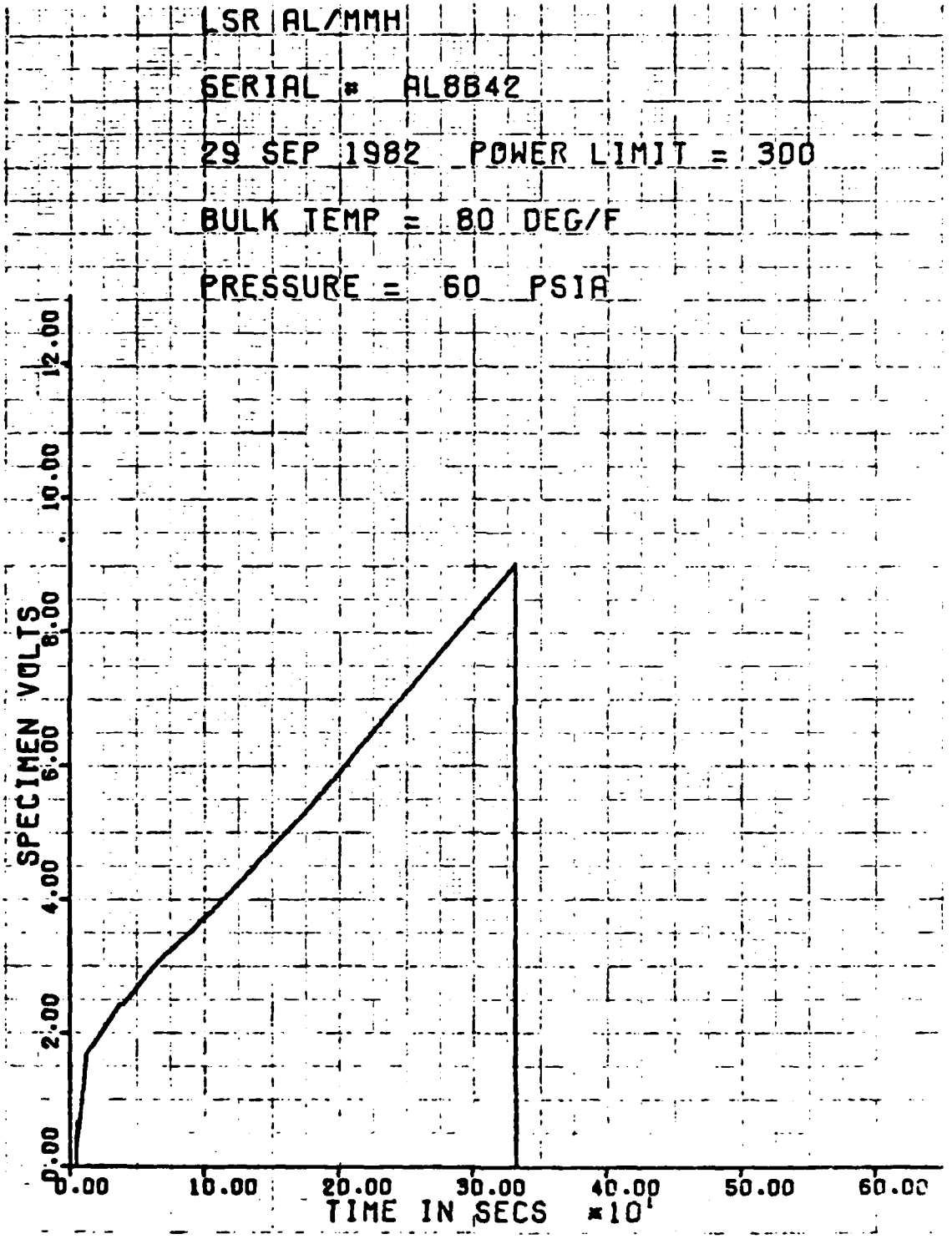

Fig. A-2 Typical Voltage History

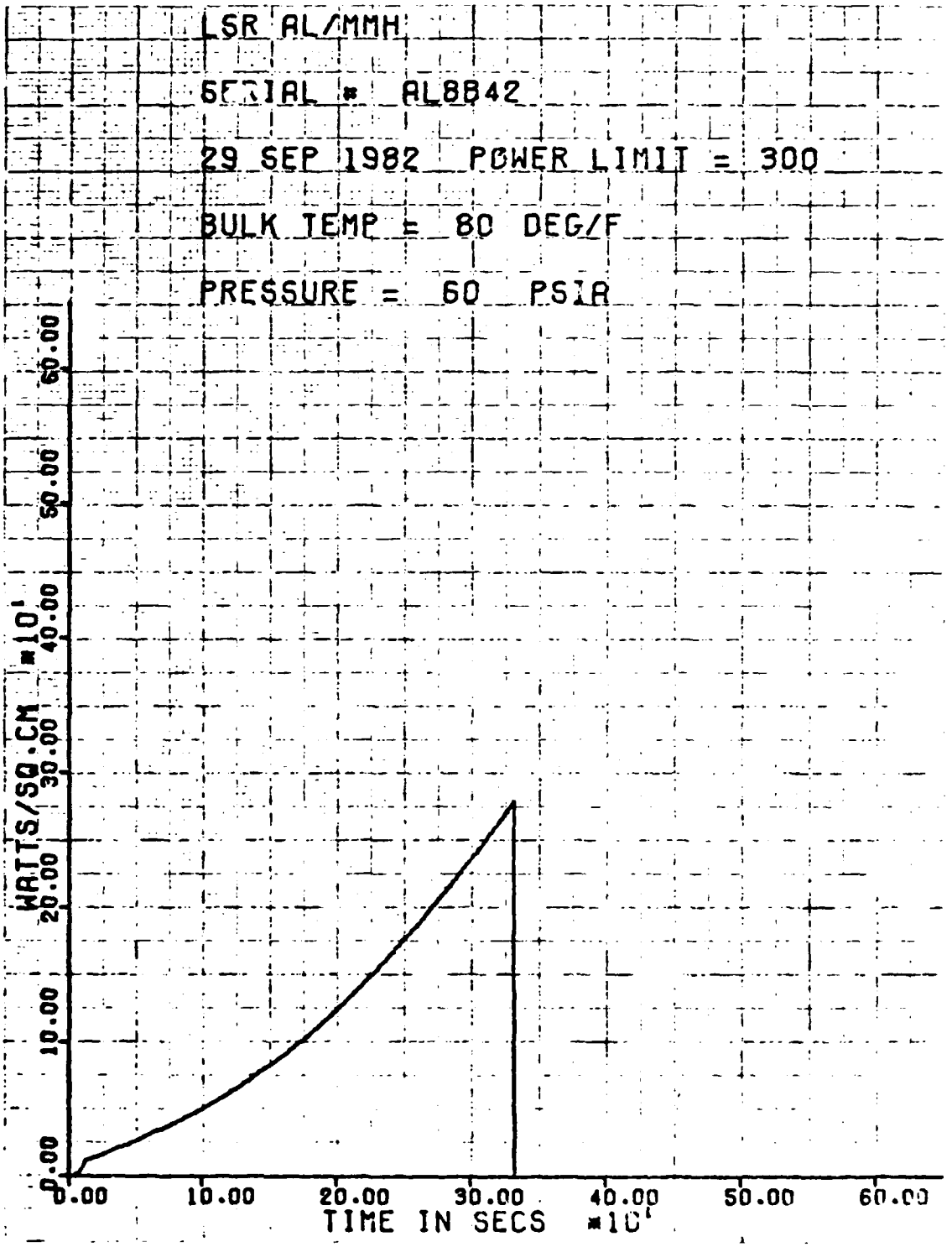

Fig. A-3 Typical Heat Rate History

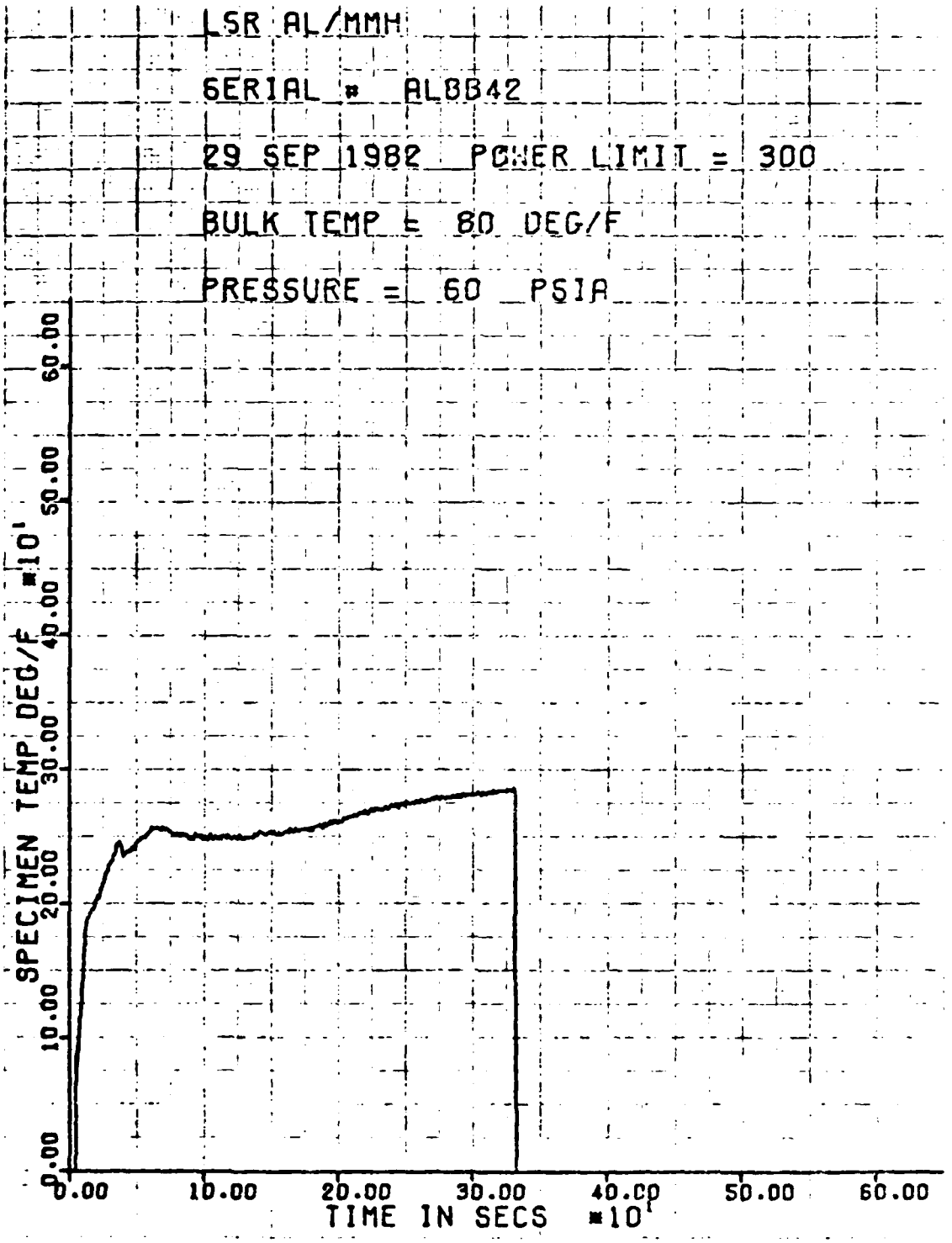

Fig. A-4 Typical Temperature History

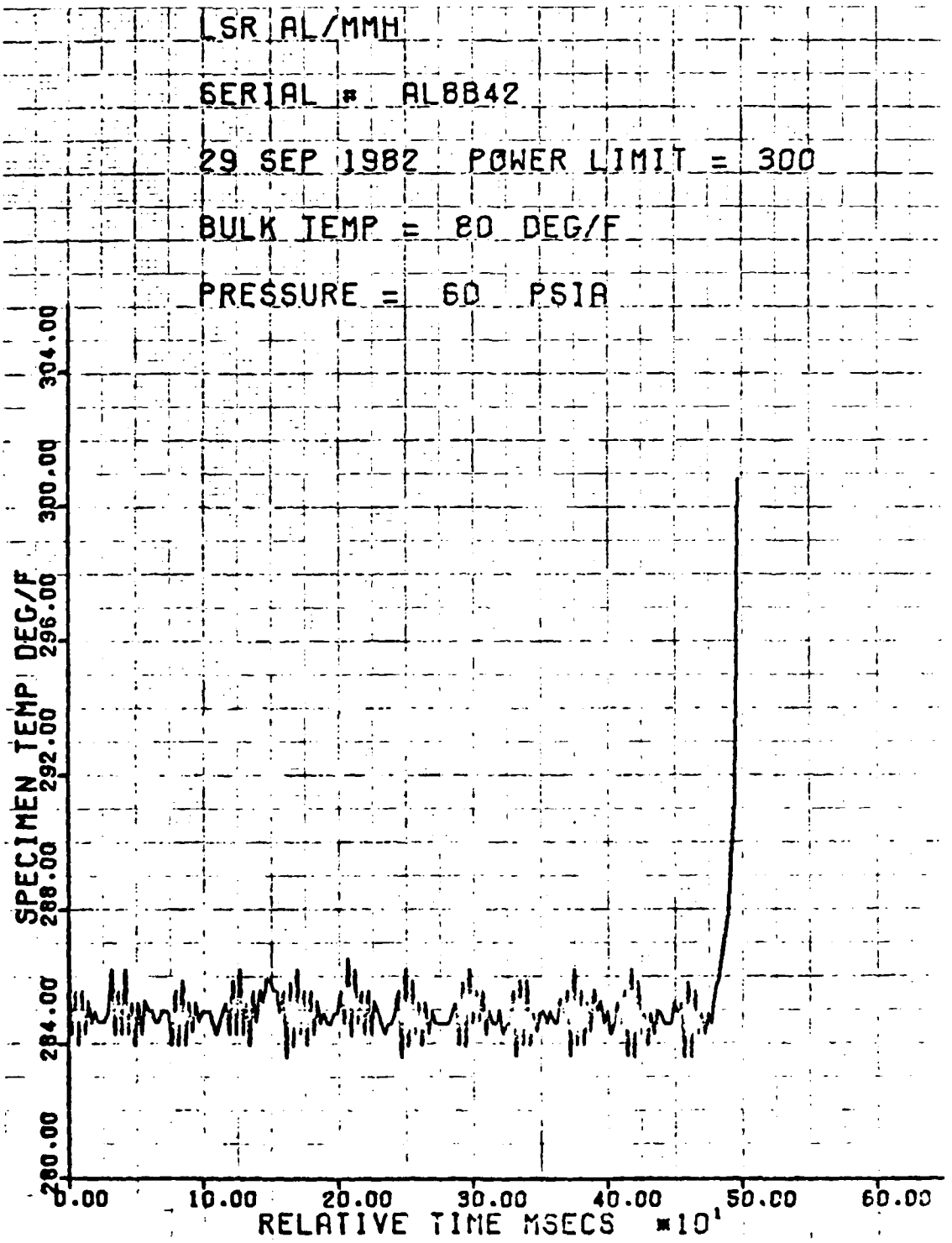

Fig. A-5 Typical Temperature History at Burnout

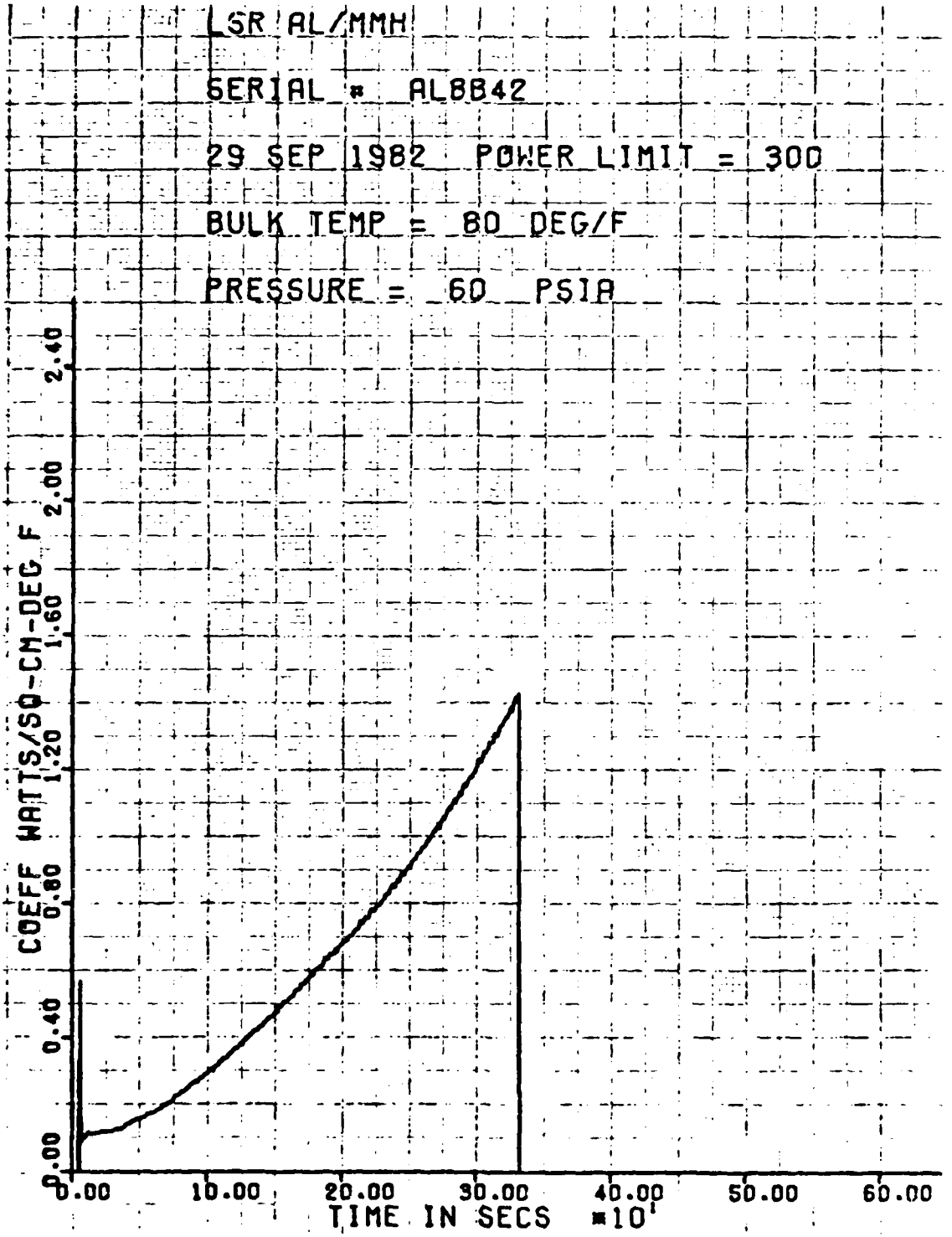

Fig. A-6 Typical Heat Transfer Coefficient at Burnout

current was increased at a slower, linear rate, such that it would produce a predetermined maximum heat flux at a given time. The resultant voltage, which is measured, is shown in Fig. A-2. The corresponding heat flux is shown in Fig. A-3. The specimen (ribbon) wall temperature, which is determined from the measured resistance of the ribbon and the calibration curve (Fig. 3-9), is shown in Fig. A-4. Figure A-5 shows a detail of the temperature history just before burnout, indicating how quickly the ribbon temperature rises once burnout is reached. The last figure, Fig. A-6, is the average heat transfer coefficient history, which is simply the heat rate divided by the wall-to-bath temperature difference. This parameter provides a relatively simple means of determining the relative behavior of fluids as a function of test parameters.

HEAT FLUX RESULTS

As indicated previously, and discussed in Section 4, the primary results of the tests are the relationship of heat flux to wall-to-bath temperature difference. Several of these results were shown in Figs. 4-1 to 4-5. These results for each of the thirteen tests conducted in this program are shown in Figs. A-7 to A-19. The curves shown are for the last run of the series of runs for a given set of conditions, the run in which burnout, or the critical heat flux (CHF), is reached. The end conditions for these tests were shown in Table 4-1. As discussed previously, two curves are shown; one based on the current, real-time bath temperature, and one based on the initial bath temperature. In general, bath temperature rise was important for water and MON, and essentially insignificant for alcohol and MMH.

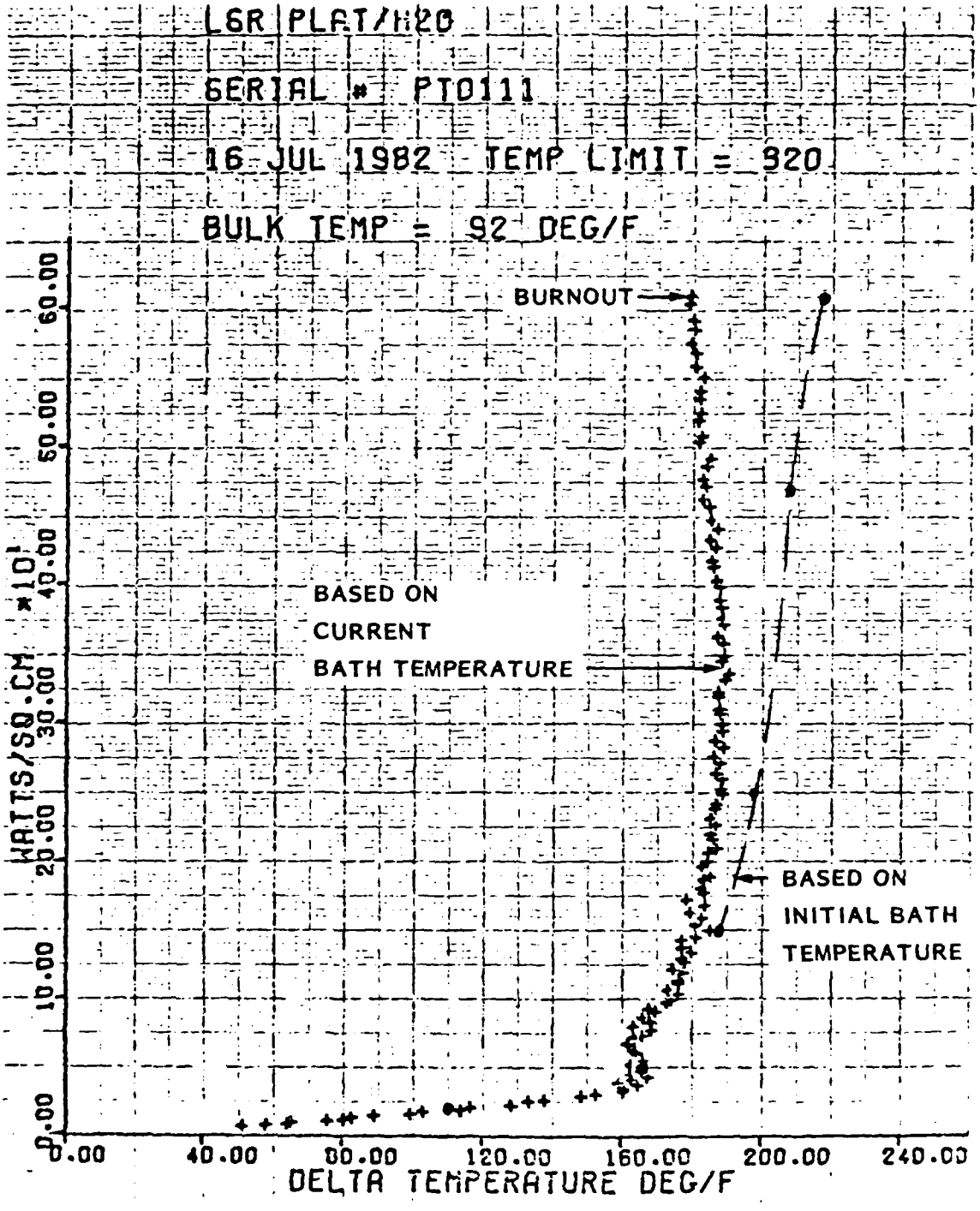

Fig. A-7 Water/Platinum, Standard Conditions, Run 1

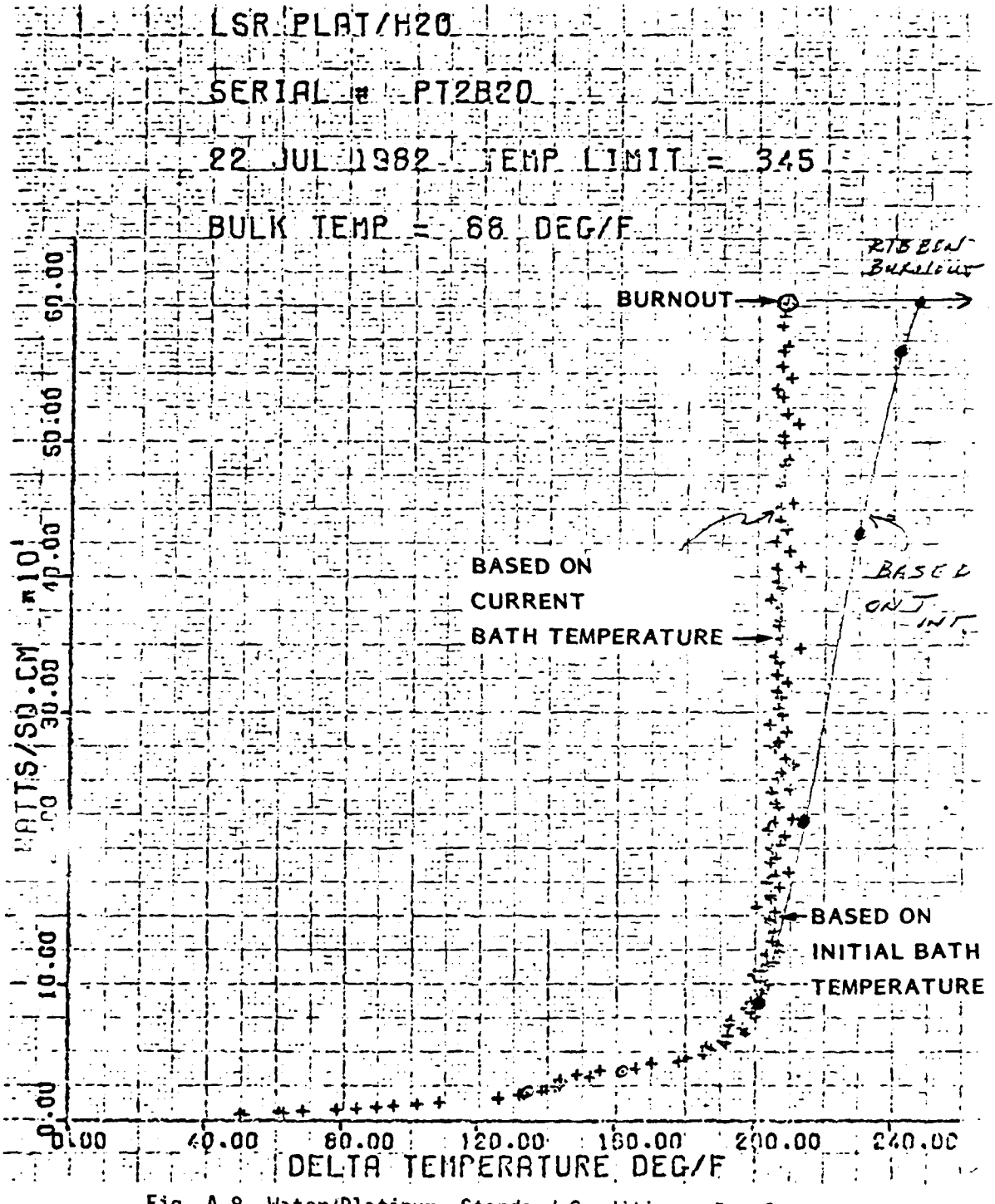

Fig. A-8 Water/Platinum, Standard Conditions, Run 2

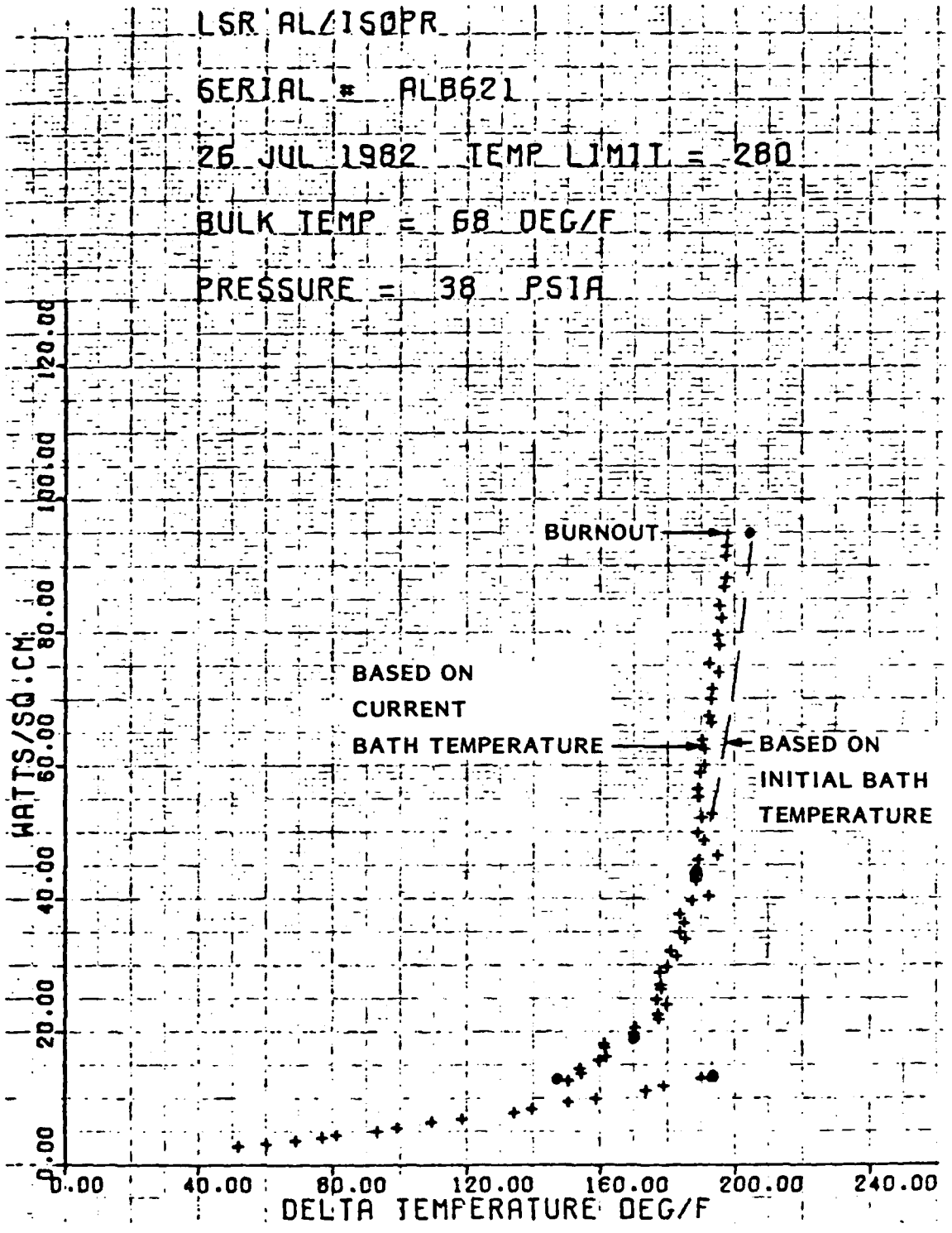

Fig. A-9 Isopropyl Alcohol/Aluminum, Run 1

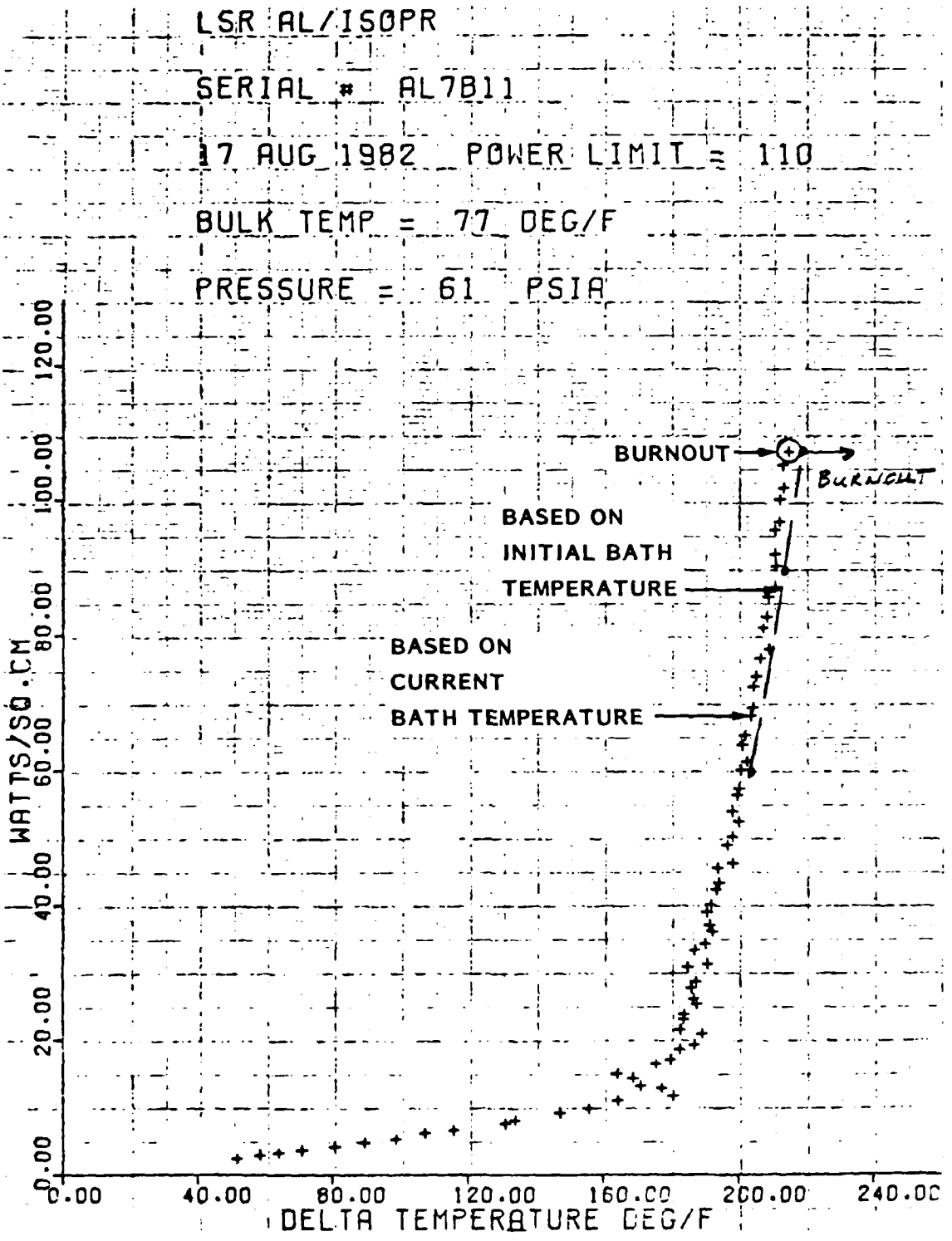

Fig. A-10 Isopropyl Alcohol/Aluminum, Run 2

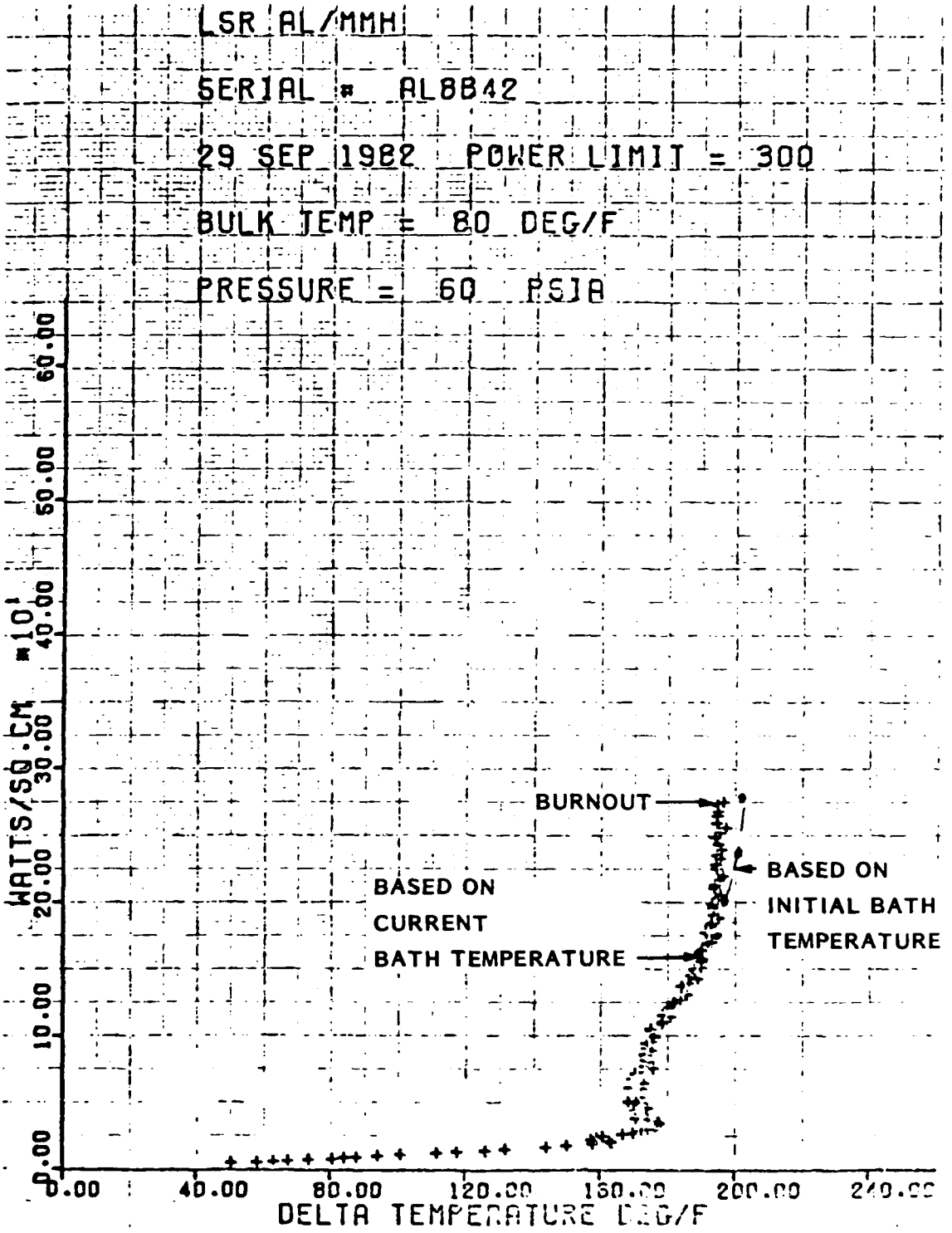

Fig. A-11 Monomethylhydrazine/Aluminum, Nominal Conditions

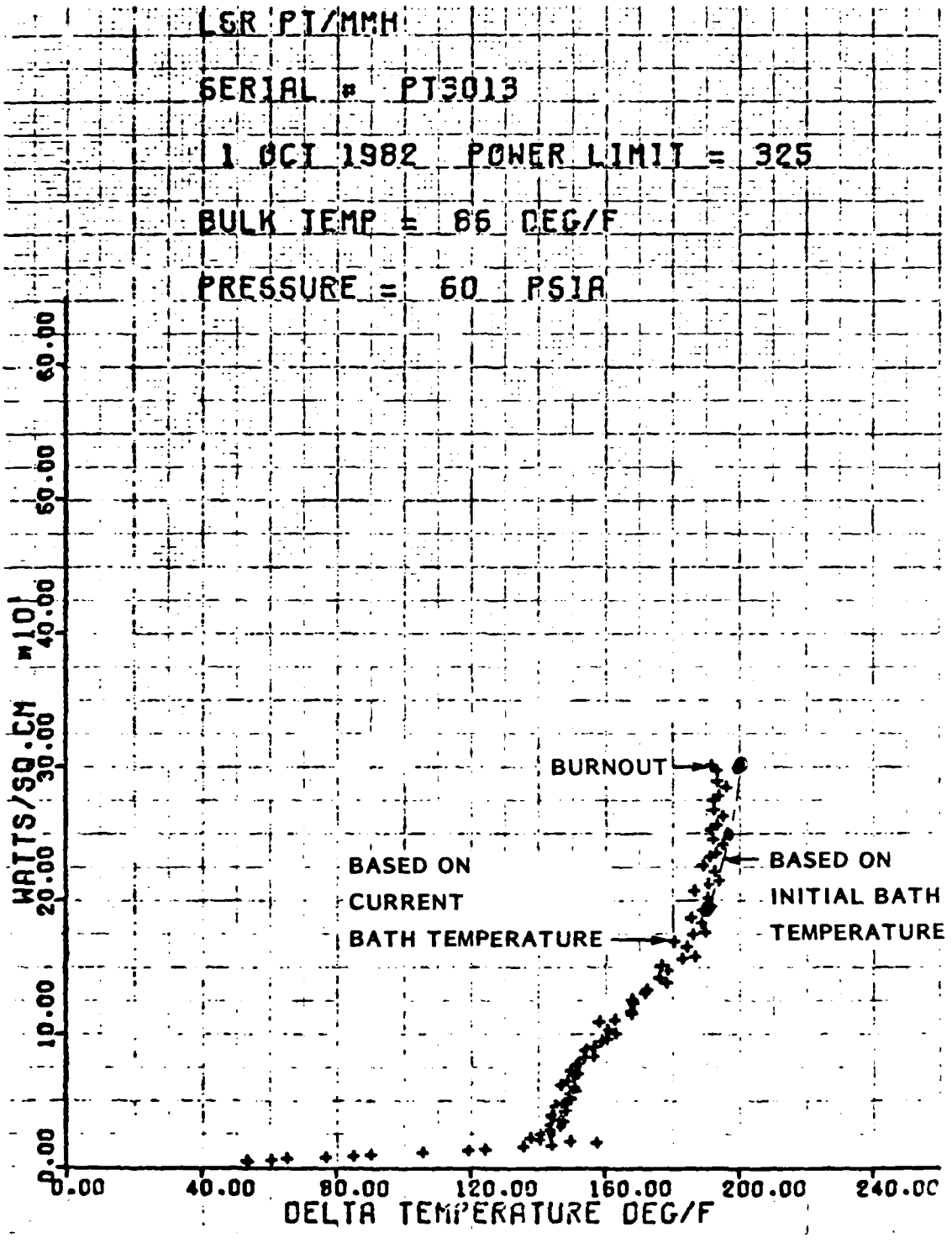

Fig. A-12 Monomethylhydrazine/Platinum, Nominal Conditions

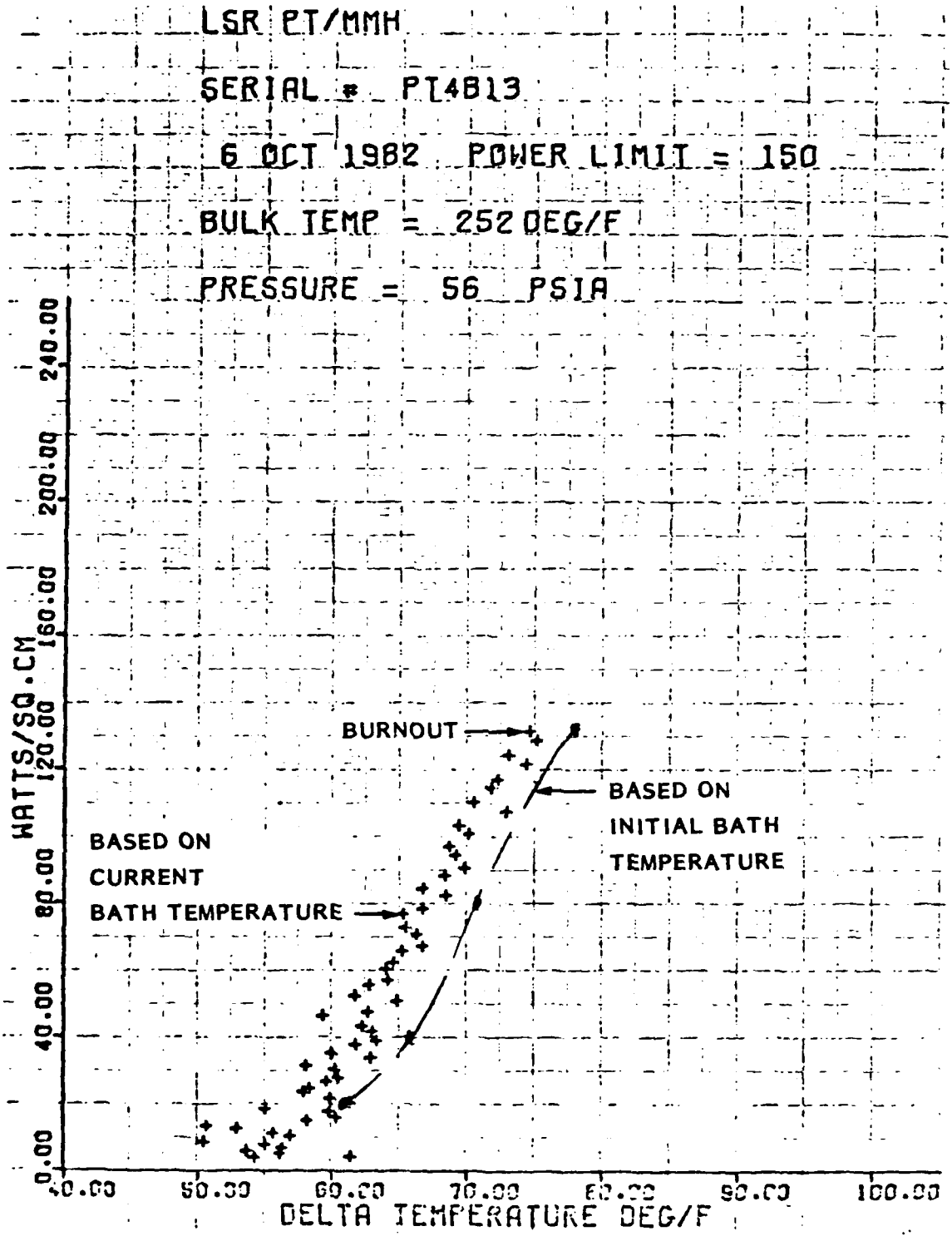

Fig. A-13 Monomethylhydrazine/Platinum, Bulk Temperature Near Saturation

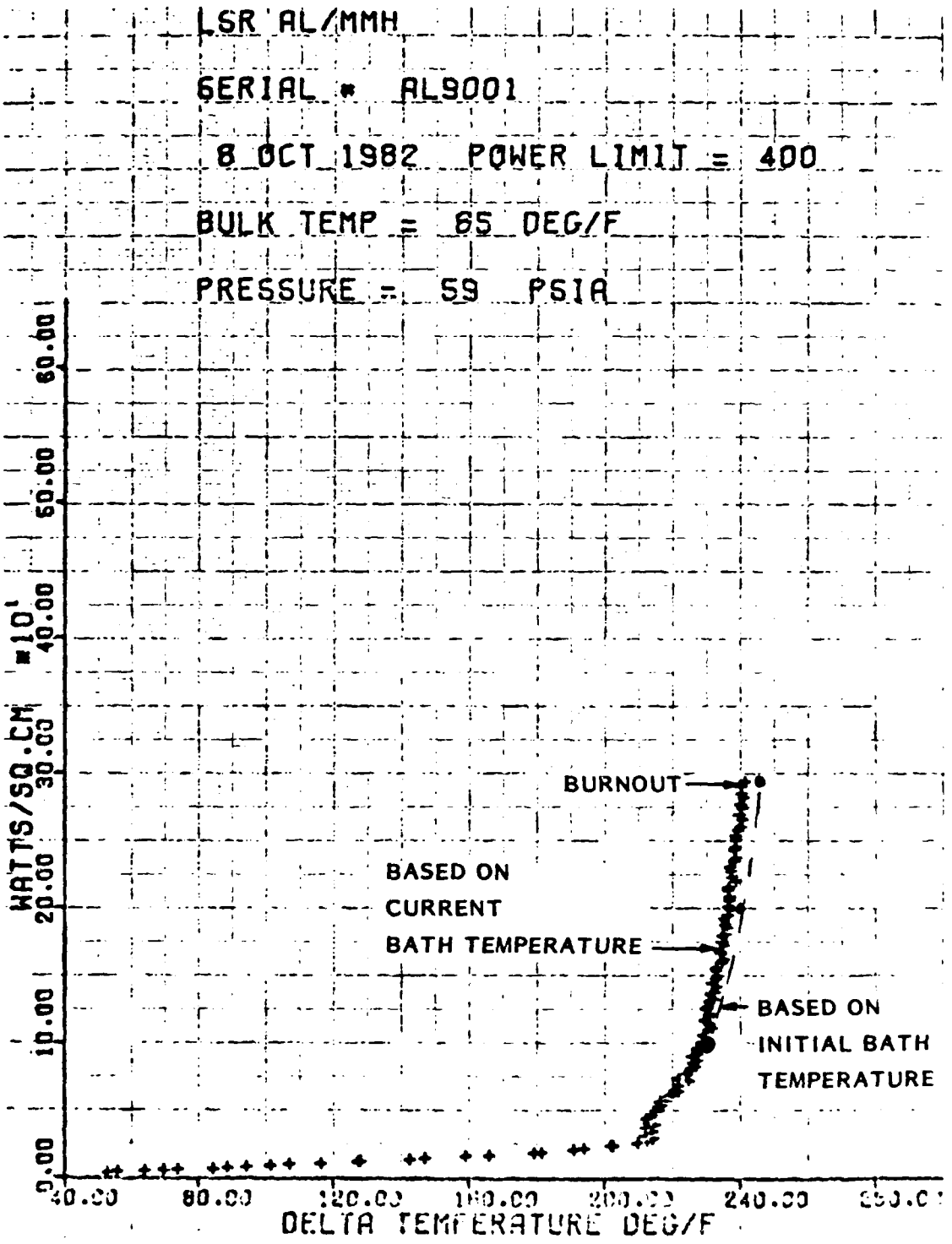

Fig. A-14 Monomethylhydrazine/Aluminum, Nominal Conditions, Single Pass

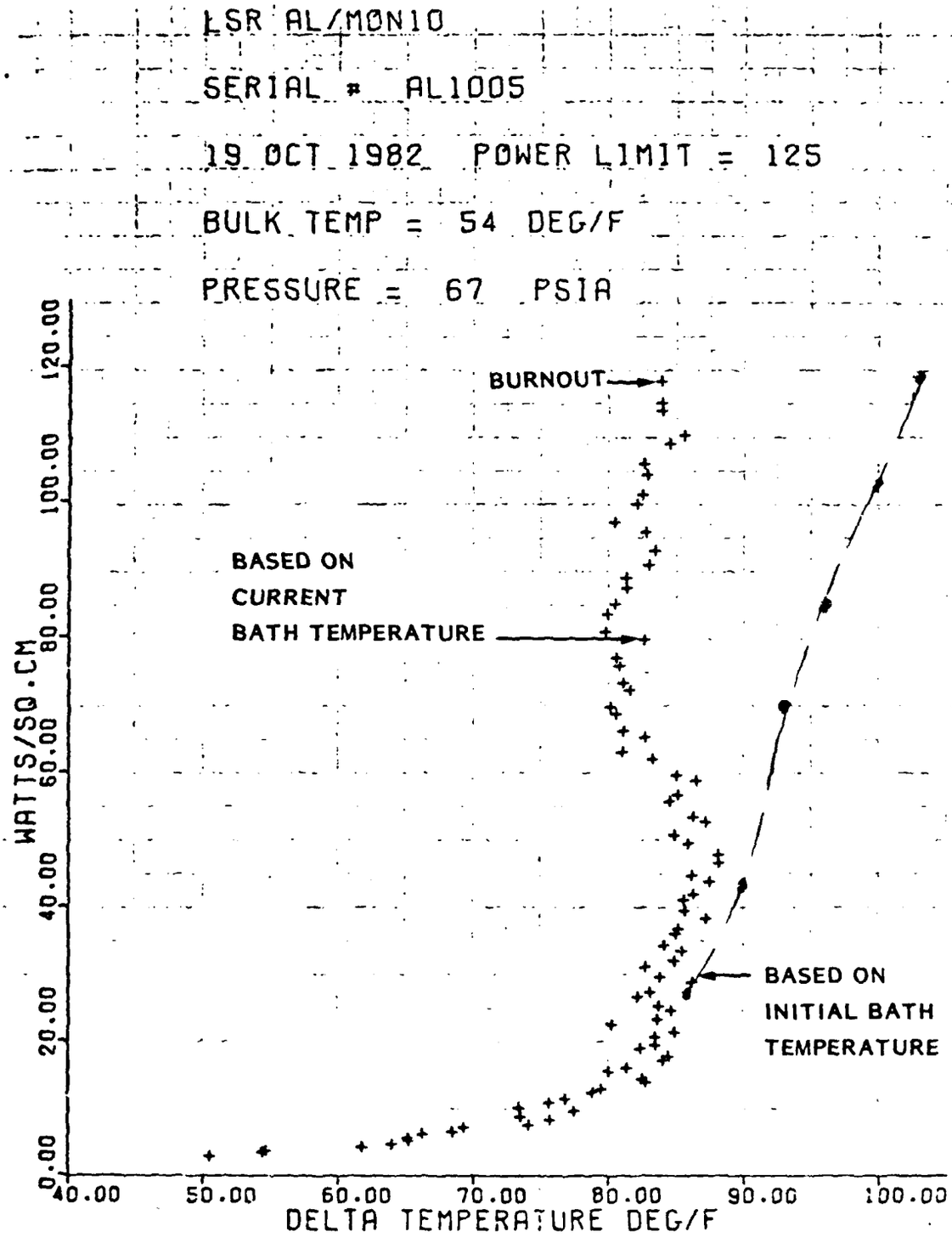

Fig. A-15 Mixed Oxides of Nitrogen/Aluminum, Nominal Conditions

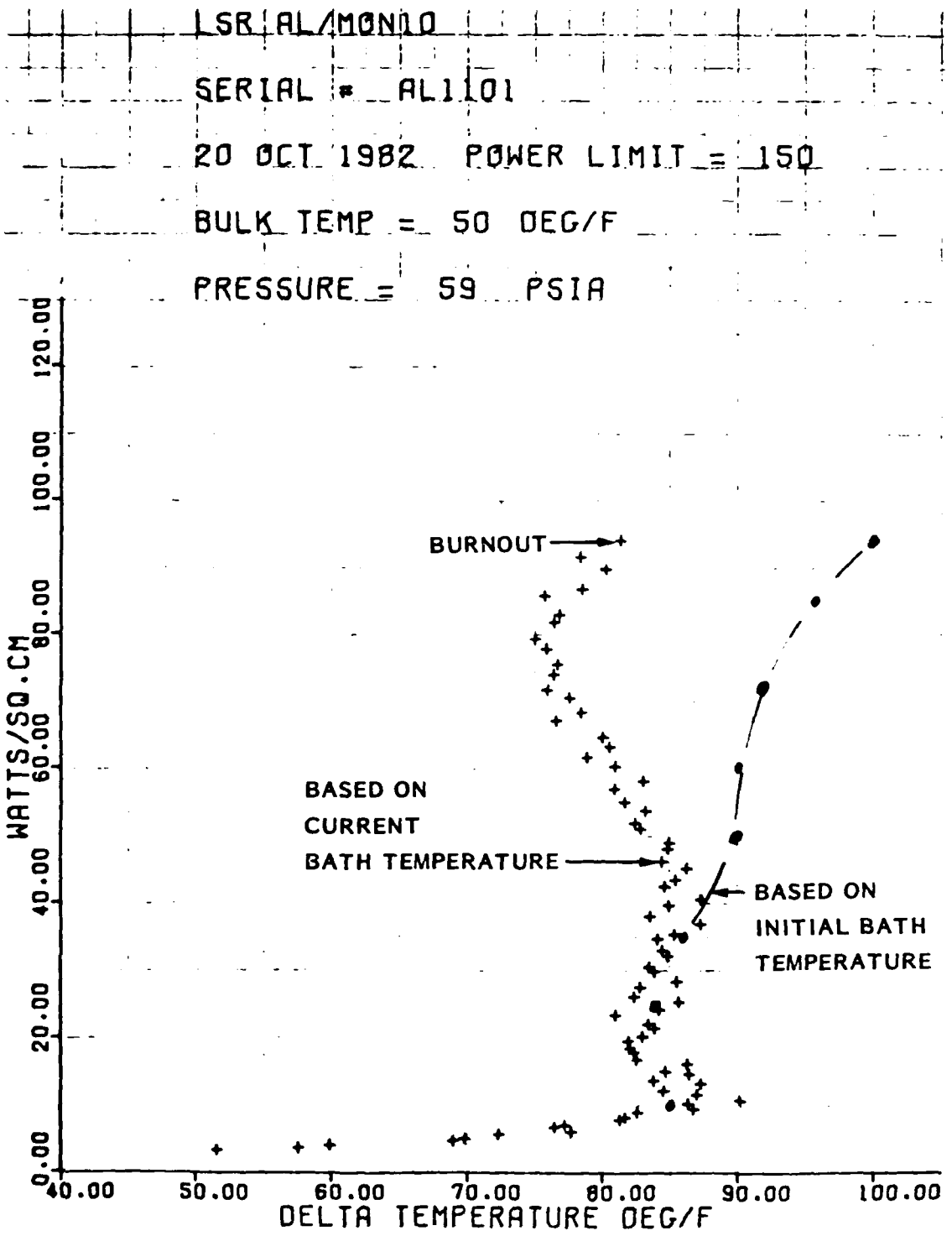

Fig. A-16 Mixed Oxides of Nitrogen/Aluminum, Nominal Conditions, Single Pass

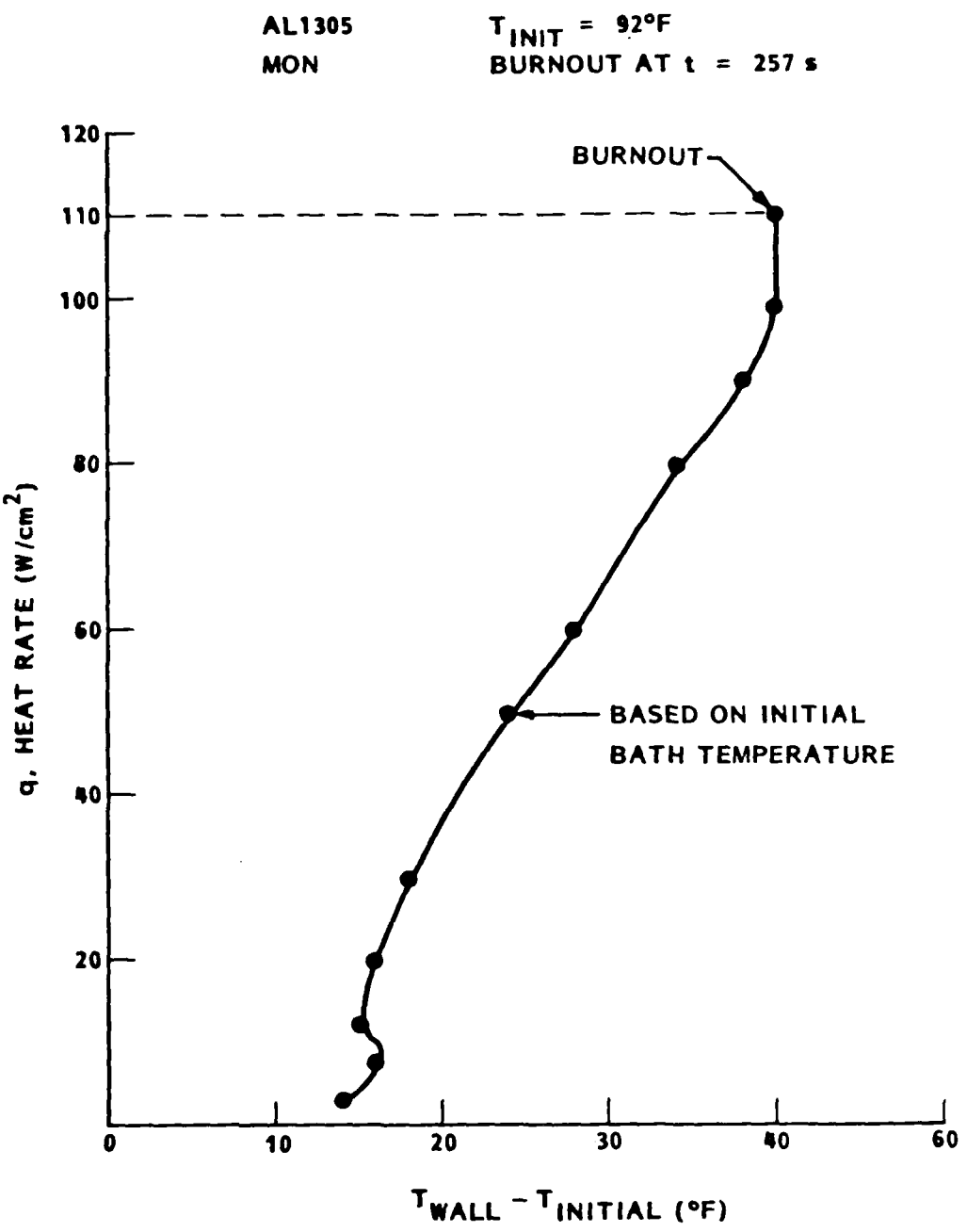

Fig. A-17 Mixed Oxides of Nitrogen/Aluminum, Higher Bulk Temperature

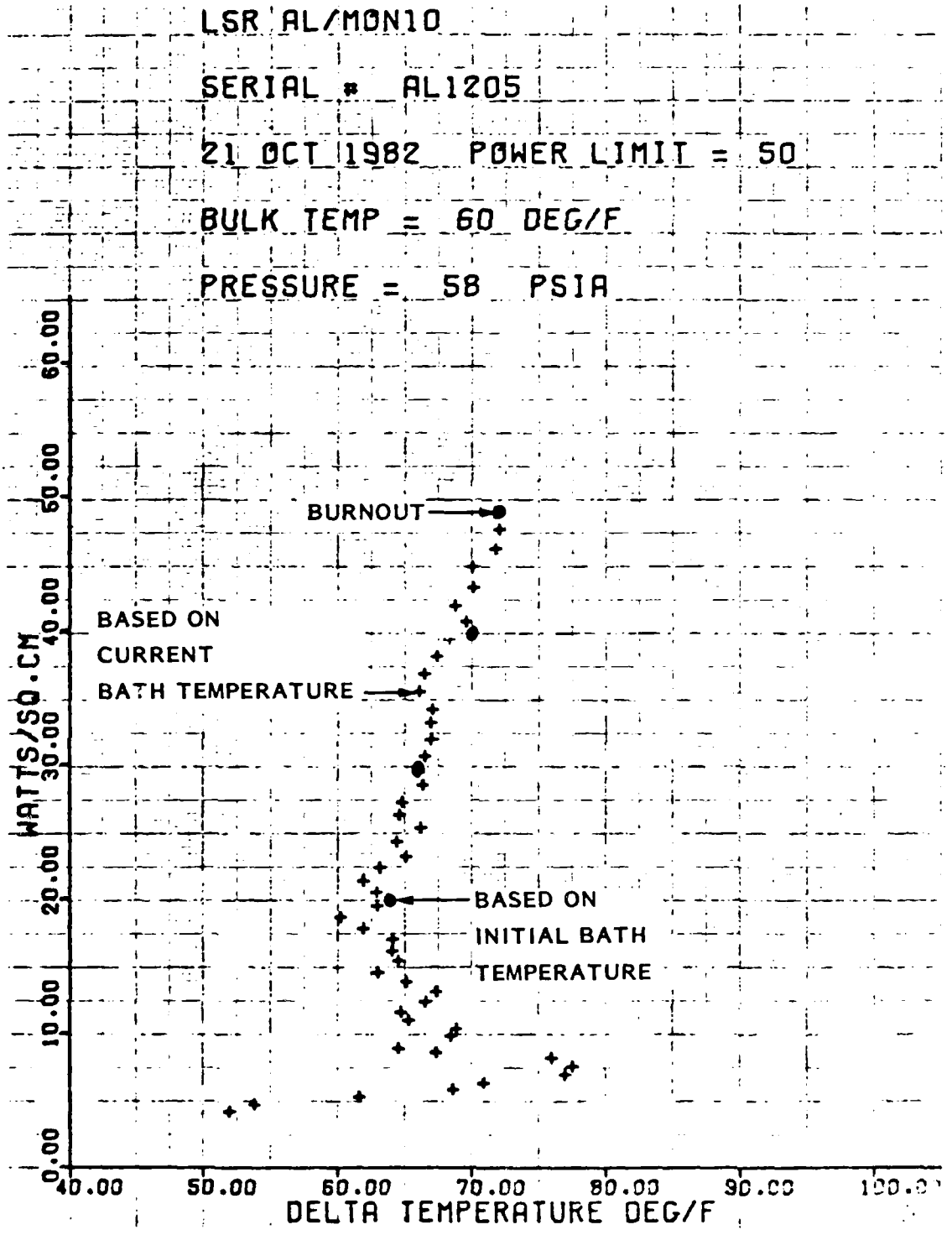

Fig. A-18 Mixed Oxides of Nitrogen/Aluminum, Nominal Conditions, Rate Effects

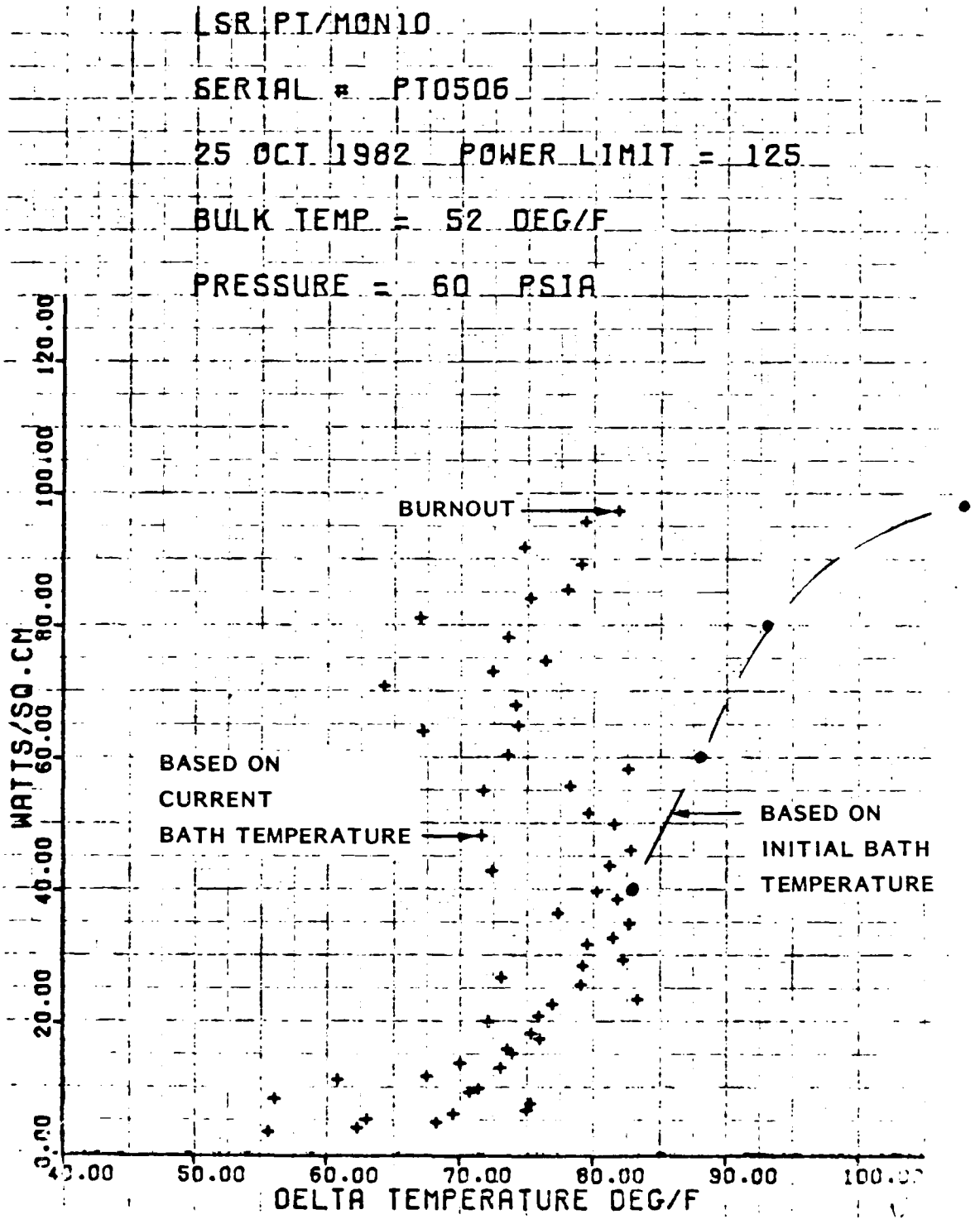

Fig. A-19 Mixed Oxides of Nitrogen/Platinum, Nominal Conditions

Appendix B
LIQUID PROPELLANT PROPERTIES

The propellant properties required to evaluate the correlation equations are presented in Tables B-1 and B-2 and in the figures indicated below.

Property	MMH Figure	MON Figure
liquid density	B-1	B-7
saturated vapor pressure	B-2	B-8
surface tension	B-3	B-9
specific heat	B-4	B-10
viscosity	B-5	B-11
thermal conductivity	B-6	B-12

The property data presented in the above figures were obtained from References B-1 to B-3. Wherever possible, the data from the different sources are compared with each other. In all cases where comparisons were made, there was good agreement in property data values. In many cases the property data reported in References B-1 to B-3 are identical since the data were obtained from the same prime source.

The spread in property data values reported in the literature is sufficiently small that the resulting uncertainty in NBHT and CHF is negligible. The reported data are based on experimental measurements and theoretical calculations performed by independent groups. The good agreement in property data values attests to the accuracy of the data.

REFERENCES

B-1. Constantine, M. T., "Engineering Property Determination on Rocket Propellants," AFRPL-TR-70-147, November 1970.

Table B-1 PHYSICAL PROPERTIES OF MONOMETHYLHYDRAZINE AT 25C° (77F°) (Page 1 of 3)

Property	Value	
	Metric	English
General Identification		
Identification	Monomethylhydrazine, MMH	
Molecular Formula	$CH_3N_2H_3$	
Molecular Weight	46.072	
Freezing Point	-52.37 C	-62.27 F
Triple Point	—	—
Normal Boiling Point	87.95 C*	190.3 F*
Critical Properties		
Temperature	312 C	593.6 F
Pressure	81.3 atm	1195 psia
Density	0.29 g/ml	18.1 lb/cu ft
Phase Properties		
Density		
Solid		
Liquid	0.8711 g/cc	54.386 lb/cu ft
Gas		
Thermal Expansion $\left(\frac{1}{V}\left(\frac{\partial V}{\partial T}\right)_p\right)$	1.062×10^{-3}/C**	5.90×10^{-4}/F**
Compressibility		
Adiabatic	4.846×10^{-5} atm^{-1}	3.297×10^{-6} psi^{-1}
Isothermal	3.90×10^{-5} atm^{-1}**	2.65×10^{-6} psi^{-1}**
Vapor Pressure	0.065 atm	0.955 psia

*Calculated from vapor pressure equation
**Calculated data

Table B-1 PHYSICAL PROPERTIES OF MONOMETHYLHYDRAZINE AT 25C° (77F°) (Page 2 of 3)

Property	Value	
	Metric	English
Phase Properties (Continued)		
Surface Tension	33.82 dynes/cm	2.317×10^{-3} lb/ft
Thermodynamic Properties		
Heats of		
Formation (Liquid)	+12.95 Kcal/mole	+505.9 Btu/lb
Fusion	2490.5 cal/mole at MP	97.30 Btu/lb at MP
Vaporization	9648 cal/mole	376.9 Btu/lb
Combustion (Gross)	311.711 kcal/mole	12178.3 Btu/lb
Heat Capacity		
Solid	0.3893 cal/g-C at MP	0.3893 Btu/lb-F at MP
Liquid	0.700 cal/g-C	0.700 Btu/lb-F
Gas		
Cp Cv	—	—
Entropy	—	—
Enthalpy	—	—
Transport Properties		
Viscosity		
Liquid	0.776 centipoise	5.21×10^{-4} lb_m/ft-sec
Gas		

Table B-1 PHYSICAL PROPERTIES OF MONOMETHYLHYDRAZINE AT 25C° (77F°) (Page 3 of 3)

Property	Value	
	Metric	English
Transport Properties (Continued)		
Thermal Conductivity		
Liquid	5.903×10^{-4} cal/cm-sec-C	0.1428 Btu/hr-ft-F
Gas		
Sonic Velocity		
Liquid	1548.9 m/sec	5081.8 ft/sec
Gas		
Electromagnetic Properties		
Index of Refraction		
Dipole Moment	1.68 ±0.14 Debyes	
Dielectric Constant		
Liquid	19.2 at 15.6 C (60 F) 17.3 at 32.2 C (90 F)	
Gas		
Electrical Conductivity	4.1×10^{-5} ohm^{-1} cm^{-1} at 23 C (73.4 F)	
Magnetic Susceptibility		

General Description

Appearance: Clear, colorless, hygroscopic liquid
Odor: Ammoniacal odor characteristic of relatively low molecular weight amines
Toxicity: Threshold Limit Value (TLV) = 0.5 ppm

Table B-2 PHYSICAL PROPERTIES OF MIXED OXIDES OF NITROGEN (MON) AT 25C° (77F°)

Property	Value		Value		Value	
	Metric	English	Metric	English	Metric	English
General Identification						
Identification	MON 90-10		MON 75-25		MON 70-30	
Nominal Composition	90 w/o N_2O_4-10 w/o NO		75 w/o N_2O_4-25 w/o NO		70 w/o N_2O_4-30 w/o NO	
Molecular Weight*	87.344 g/g-mole	87.344 lb/lb-mole	81.182 g/g-mole	81.182 lb/lb-mole	79.327 g/g-mole	79.327 lb/lb-mole
Freezing Point	-21 C	-9.4 F	-54 C	-65.2 F	-81 C	-113.8 F
Normal Boiling Point**	9.7 C	49.4 F	-9.0 C	15.9 F	-16.1 C	3.0 F
Critical Properties						
Temperature						
Pressure						
Density						
Phase Properties						
Density						
Liquid	1.408 g/cc	87.89 lb/cu ft	1.379 g/cc	86.07 lb/cu ft	1.371 g/cc	85.56 lb/cu ft
Gas						
Thermal Expansion (cubic)						
Compressibility						
Adiabatic			6.736×10^{-5} atm^{-1}	4.583×10^{-6} psi^{-1}		
Isothermal						
Vapor Pressure	2.074 atm	30.48 psia	5.096 atm	74.89 psia	7.229 atm	106.2 psia
Surface Tension†	--	—	26.55 dynes/cm	1.819×10^{-3} lb/ft	—	—
Thermodynamic Properties						
Heats of						
Formation (Liquid)††	-0.278 Kcal/100g	-5.00 Btu/lb	+6.93 Kcal/100g	+124.7 Btu/lb	+9.54 Kcal/100g	+168.1 Btu/lb
Fusion						
Vaporization						
Heat Capacity						
Liquid			0.434 cal/g-C	0.434 Btu/lb-F		
Gas						
Entropy						
Enthalpy						
Transport Properties						
Viscosity						
Liquid	0.358 centipoise	2.40×10^{-4} lb/ft-sec	0.413 centipoise	2.78×10^{-4} lb/ft-sec	0.456 centipoise	3.06×10^{-4} lb/ft-sec
Gas						
Thermal Conductivity						
Liquid						
Gas						
Sonic Velocity						
Liquid			1044.3 m/sec	3426.4 ft/sec		
Gas						
Electromagnetic Properties	No electromagnetic properties have been reported for any solutions of NO in N_2O_4					
Index of Refraction						
Dipole Moment						
Dielectric Constant						
Electrical Conductivity						

*Based on NO present as N_2O_4
**Calculated from vapor pressure equation.
†Although additional values were determined in Ref.C-9, they were not included because of their questionable accuracy.
††Calculated Value.

GENERAL DESCRIPTION

Description: The mixed oxides of nitrogen (MON) designates a series of solutions of NO in N_2O_4. The NO reacts with the N_2O_4 as it dissolves to form N_2O_3, which is soluble in N_2O_4.

Odor: Irritating and acid-like due to the NO .

Toxicity: Threshold Limit Value (TLV) = 5 ppm (9mg/cu m) as NO .

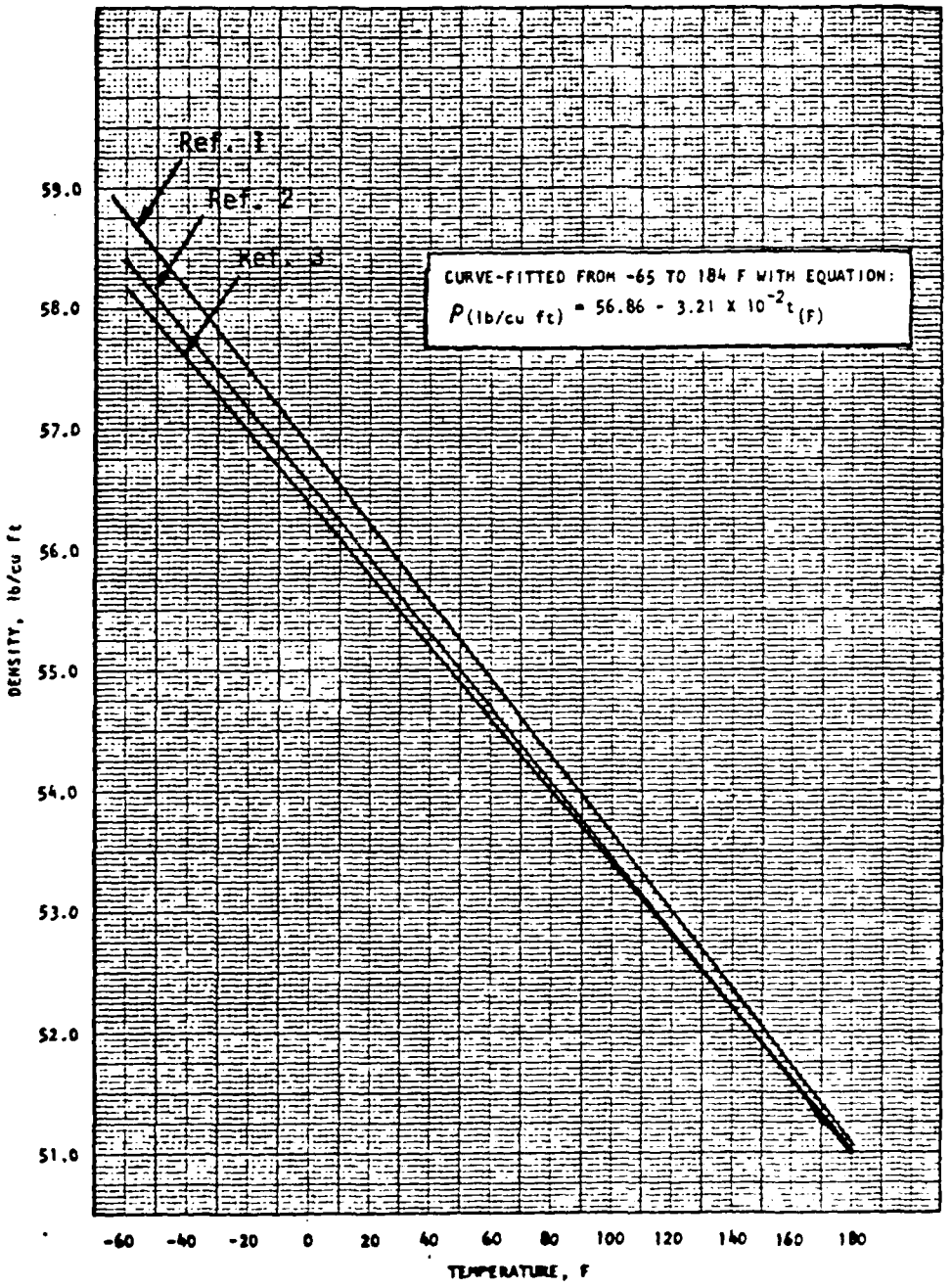

Fig. B-1 Density of Liquid Monomethylhydrazine

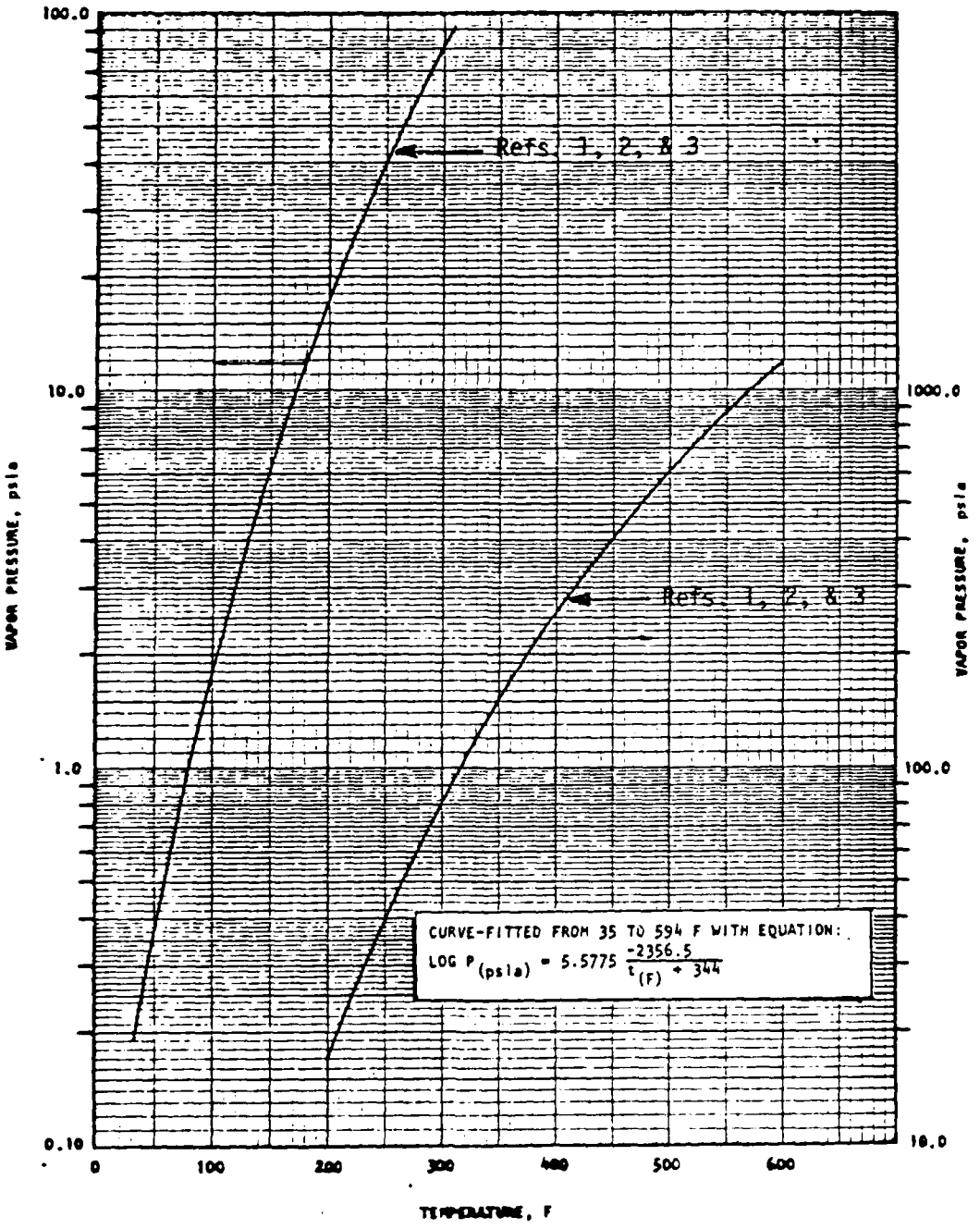

Fig. B-2 Vapor Pressure of Monomethylhydrazine

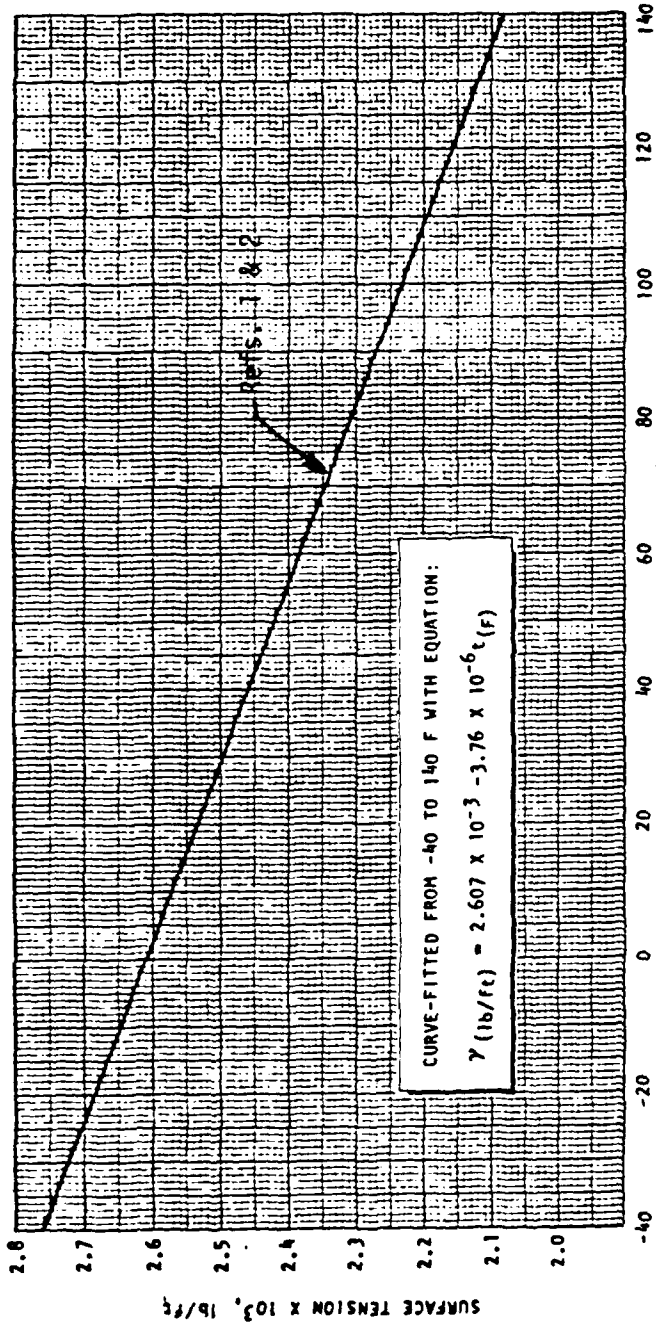

Fig. B-3 Surface Tension of Monomethylhydrazine

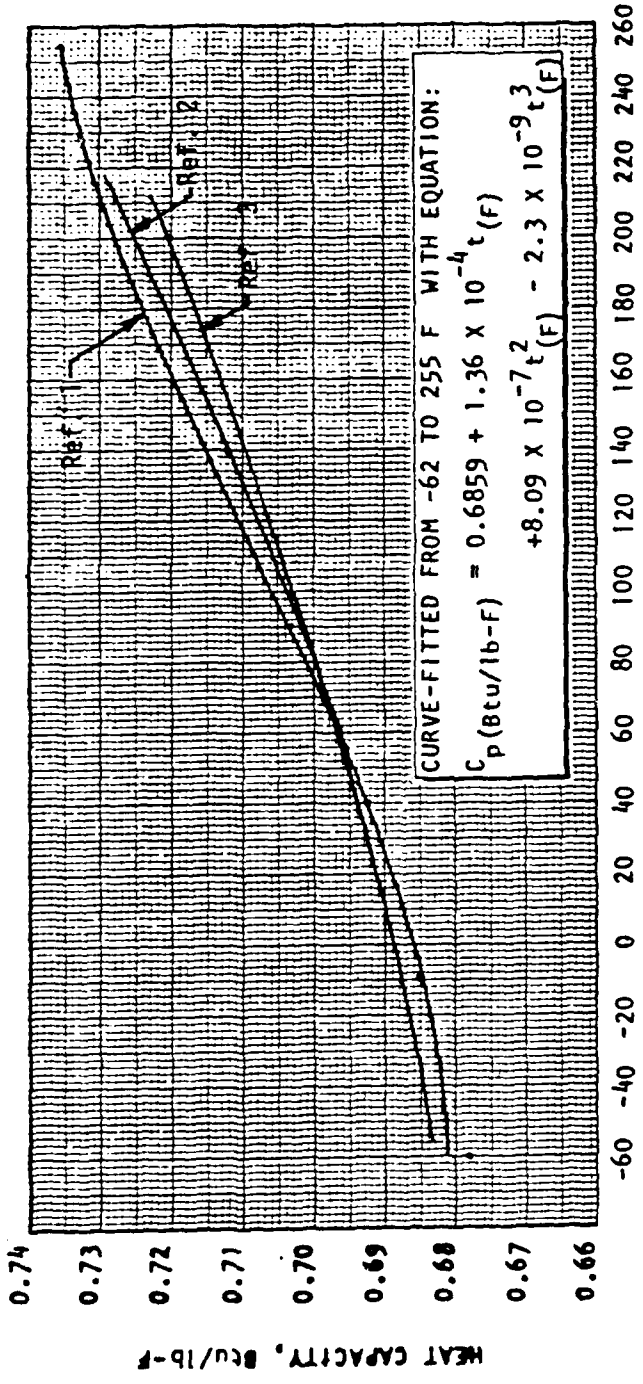

Fig. B-4 Heat Capacity of Liquid Monomethylhydrazine

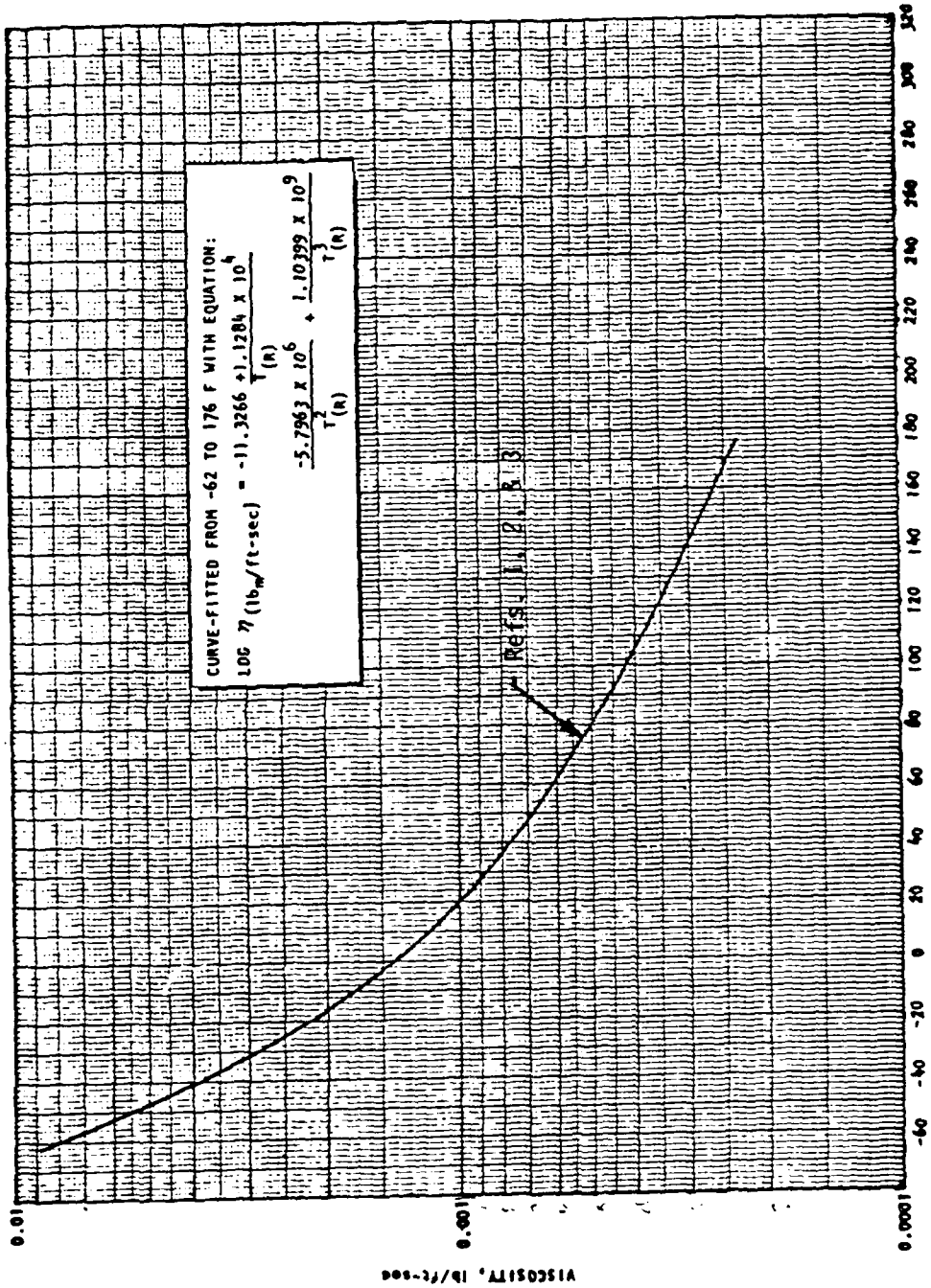

Fig. B-5 Viscosity of Liquid Monomethylhydrazine

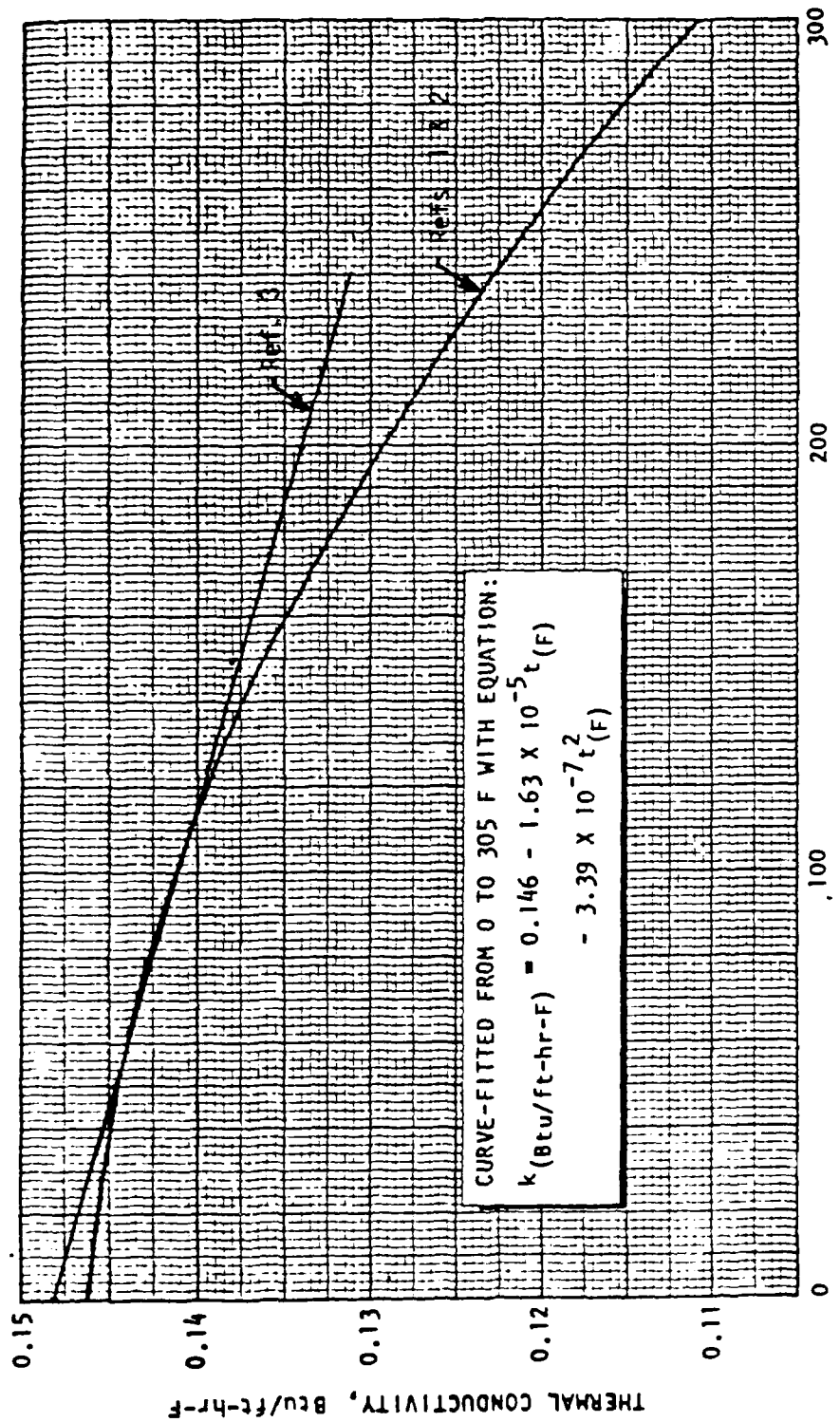

Fig. B-6 Thermal Conductivity of Liquid Monomethylhydrazine

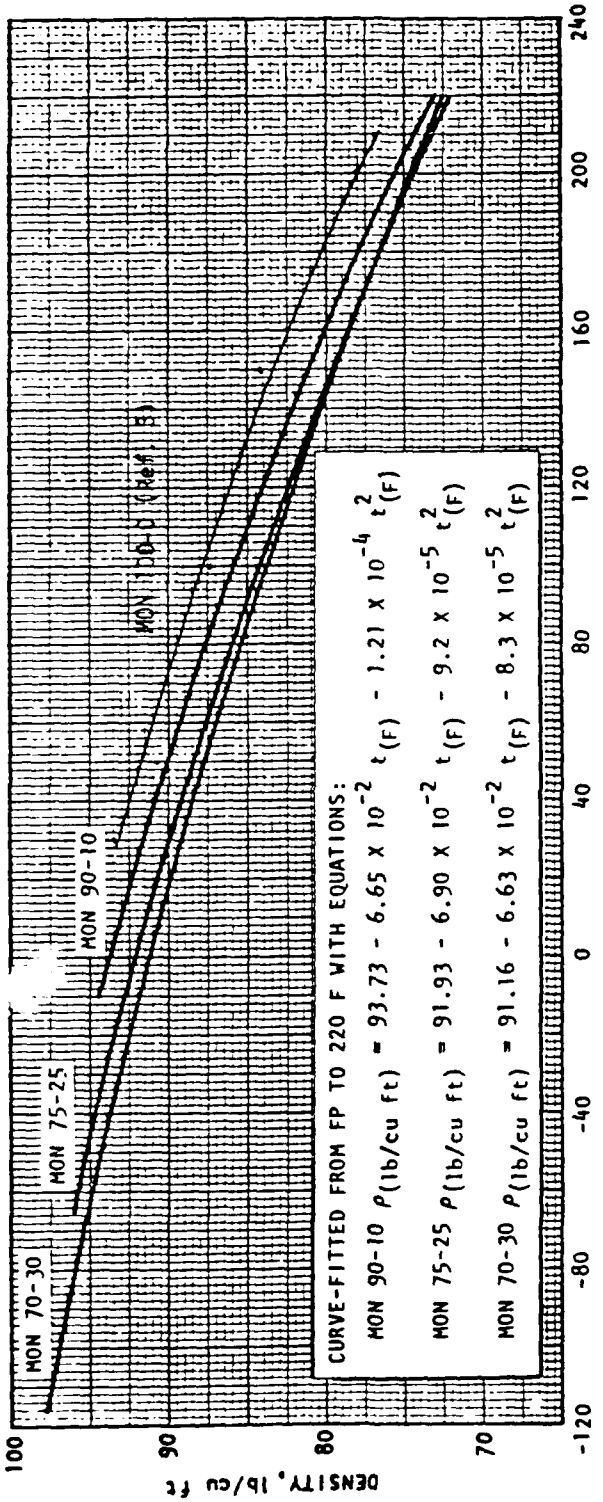

Fig. B-7 Density of the Mixed Oxides of Nitrogen

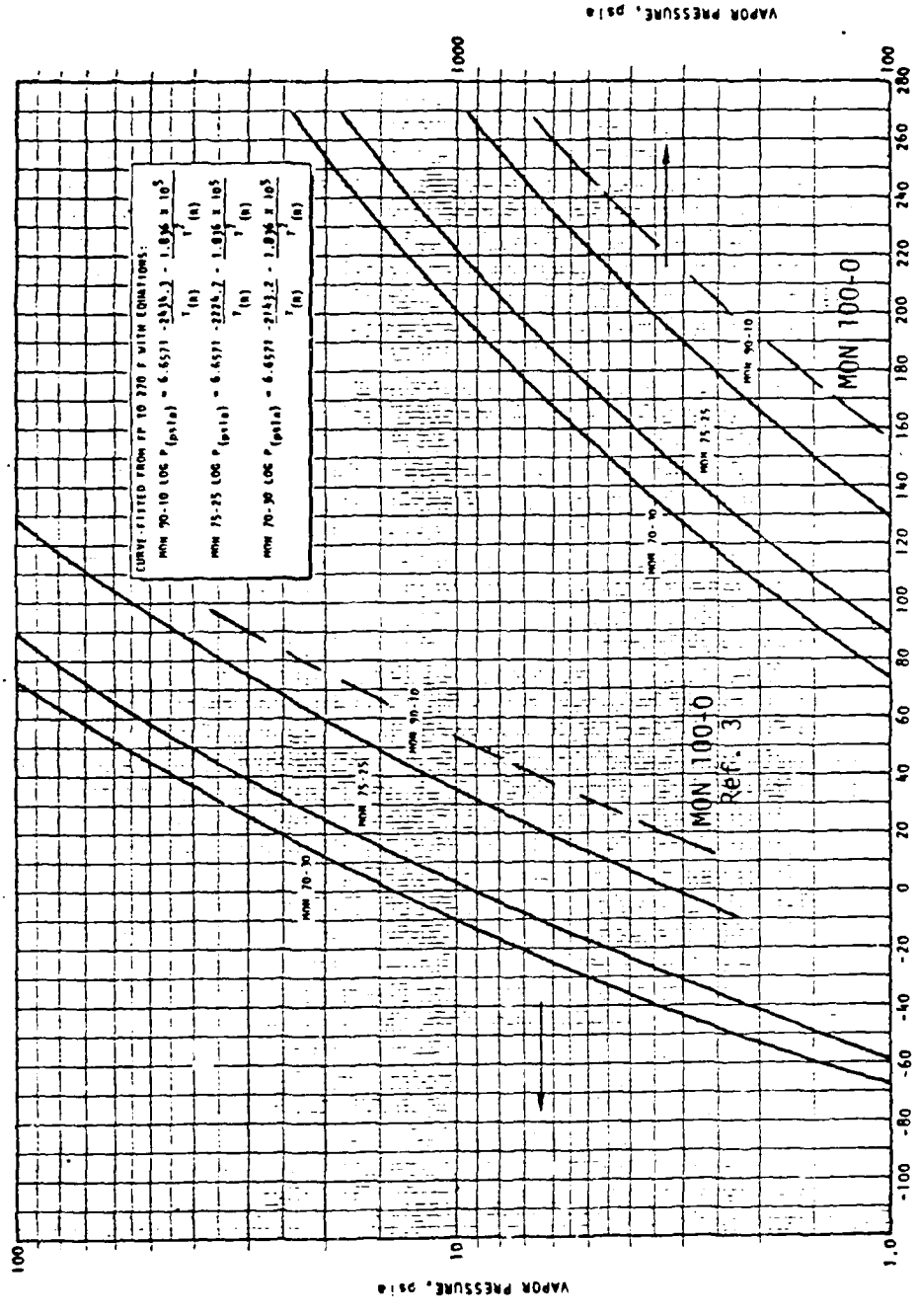

Fig. B-8 Vapor Pressure of the Mixed Oxides of Nitrogen

AD A134 584 LASER EFFECTS AND VULNERABILITY PROGRAM LIQUID PROPELLANT CHARACTERIZATION(U) LOCKHEED MISSILES AND SPACE CO INC PALO ALTO CA PALO ALTO RESEARCH LAB 2/2

UNCLASSIFIED JUN 83 LMSC/D878096 DASG60-81-C-0104 F/G 20/5 NL

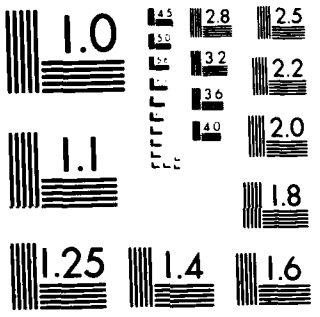

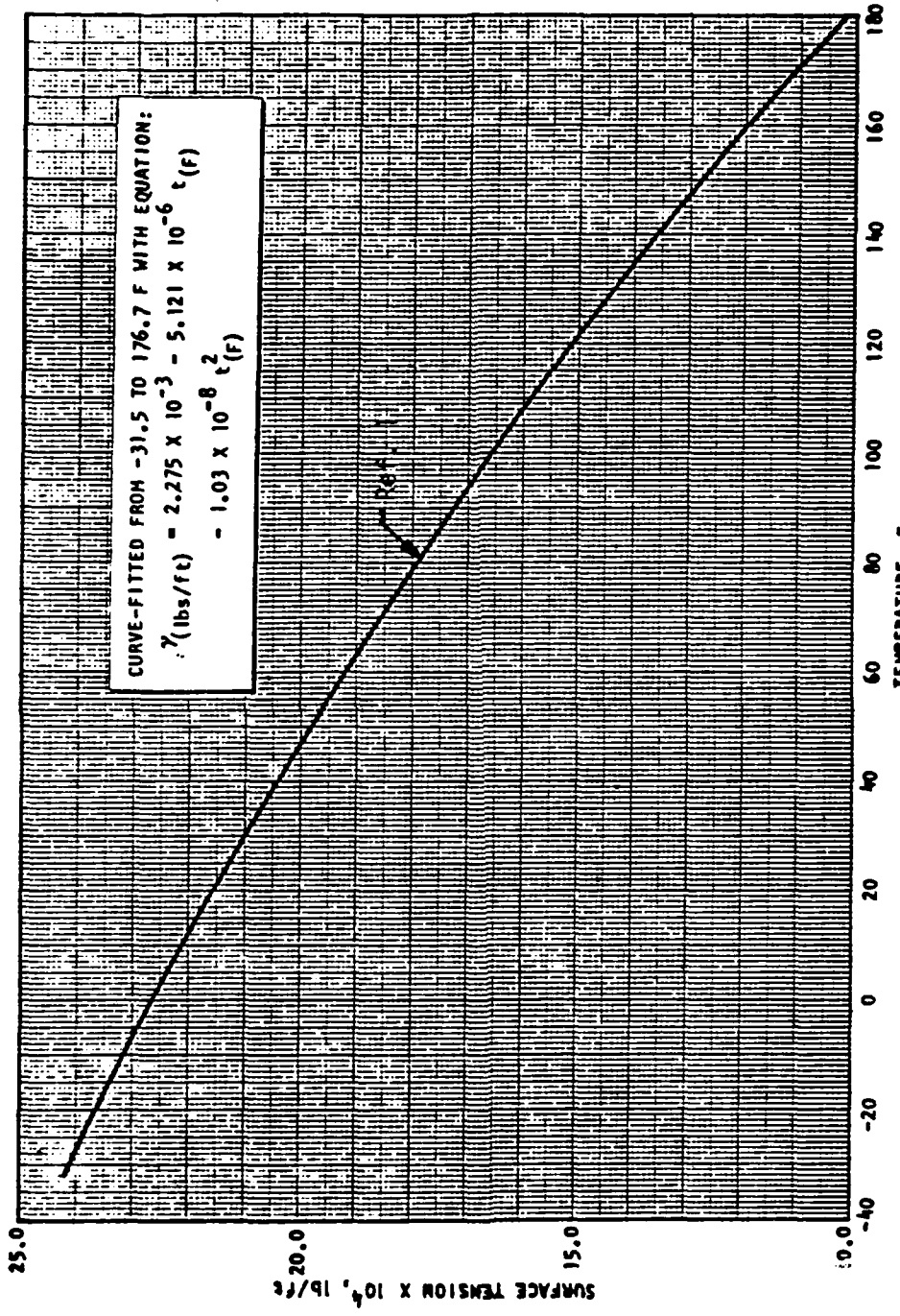

Fig. B-9 Surface Tension of Saturated Liquid MON-25

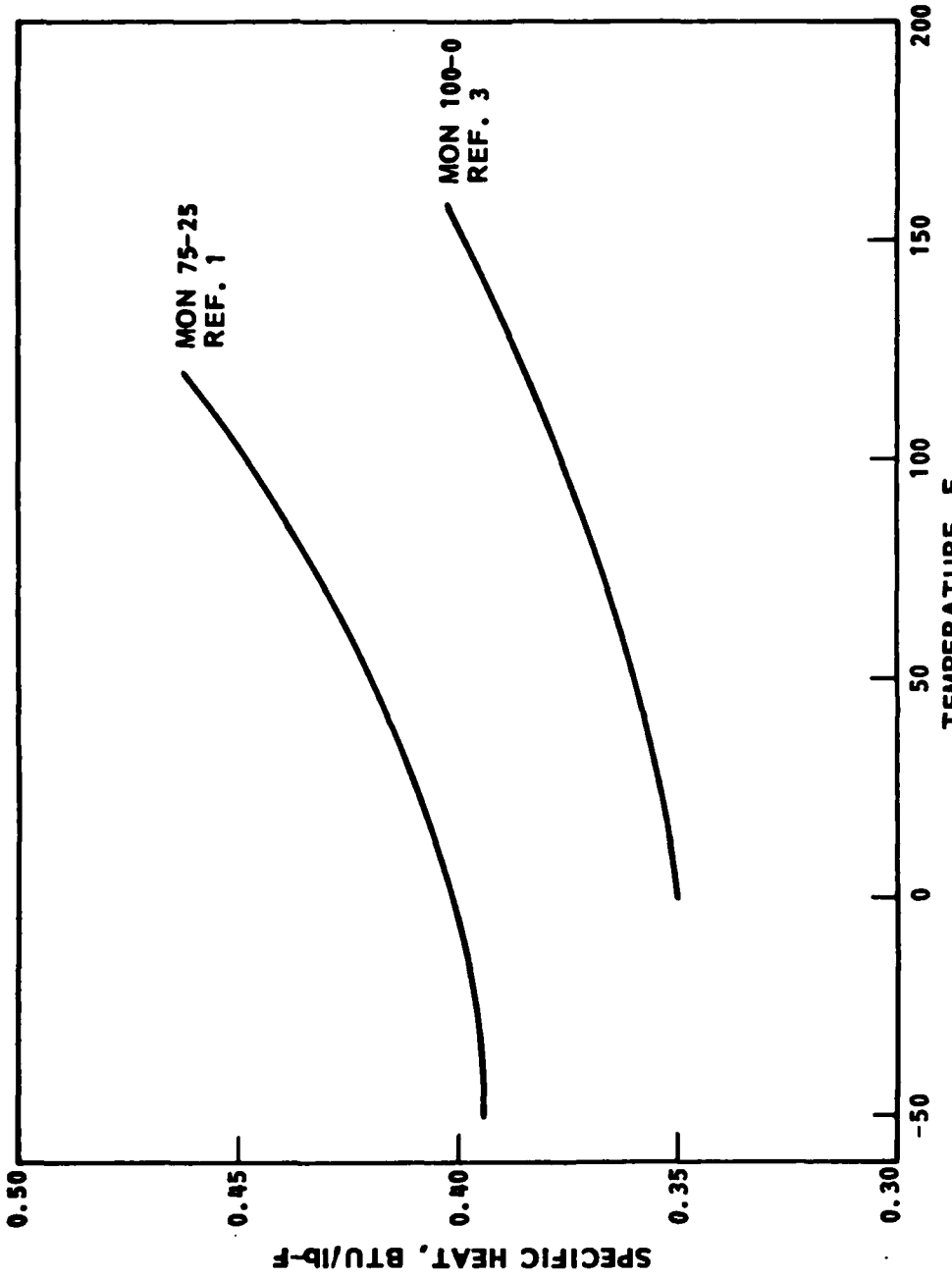

Fig. B-10 Specific Heat of Saturated Liquid MON

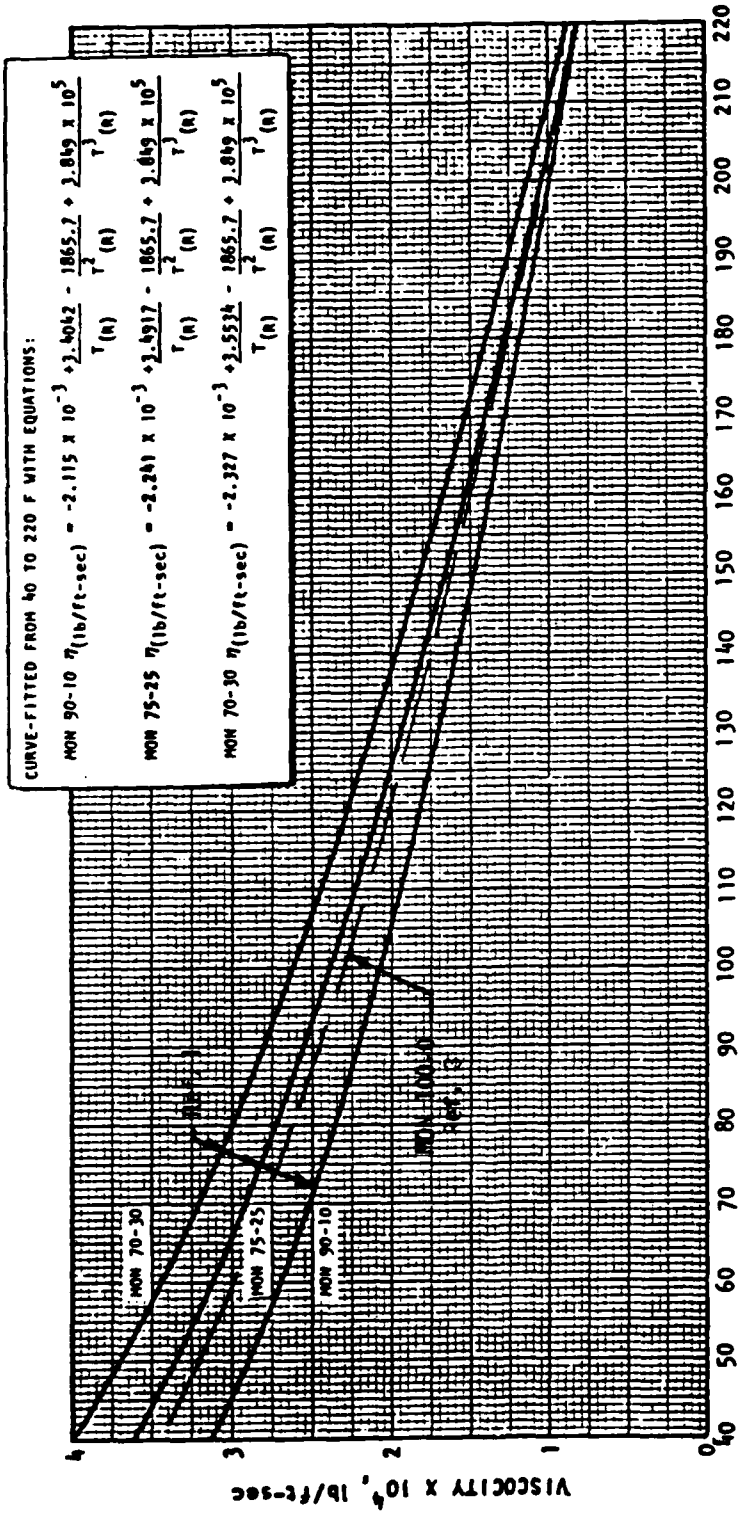

Fig. B-11 Viscosity of the Mixed Oxides of Nitrogen

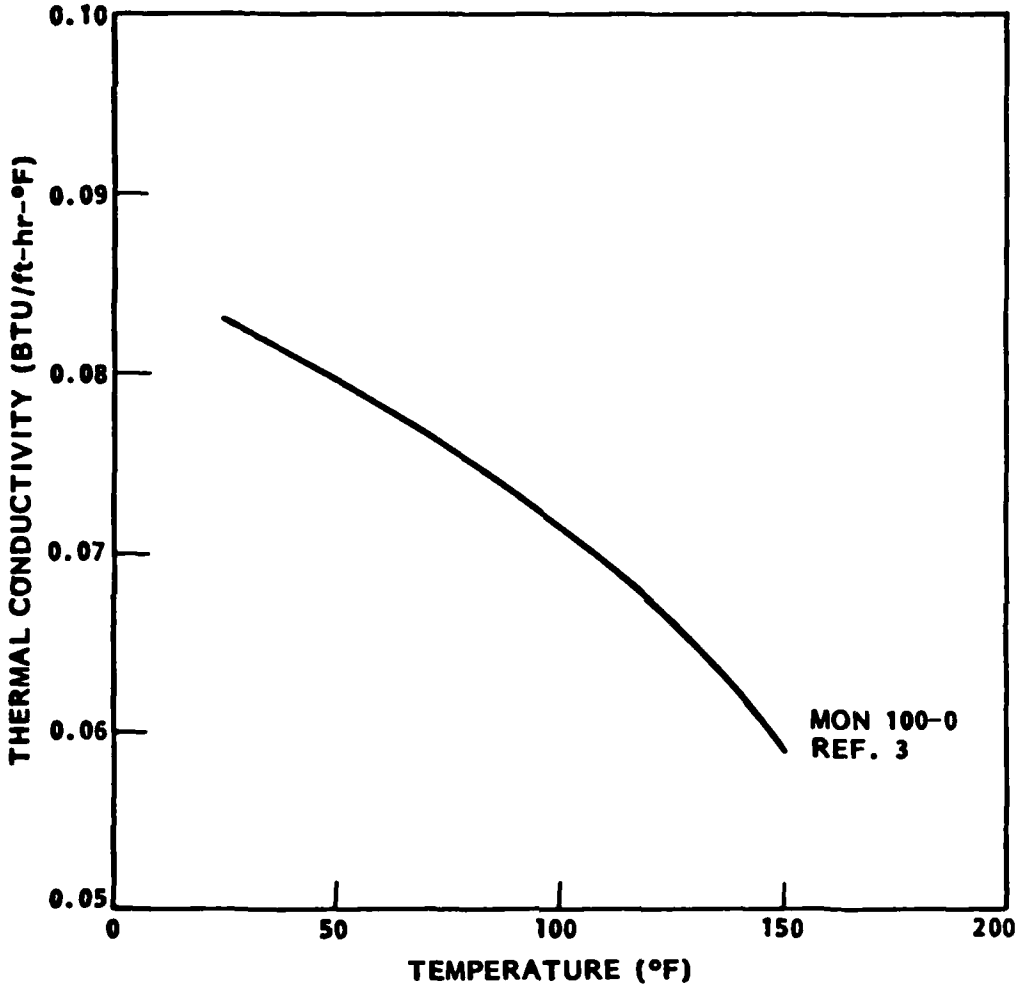

Fig. B-12 Thermal Conductivity of N_2O_4 (MON 100-0)

B-2. Marsh, W. R. and Knox, B.P., "WSAF Propellant Handbooks Hydrazine Fuels," Vol. I., AFRPL-TR-69-149, March 1970.

B-3. Performance and Properties of Liquid Propellants, AJEC8160-65, June 1961.

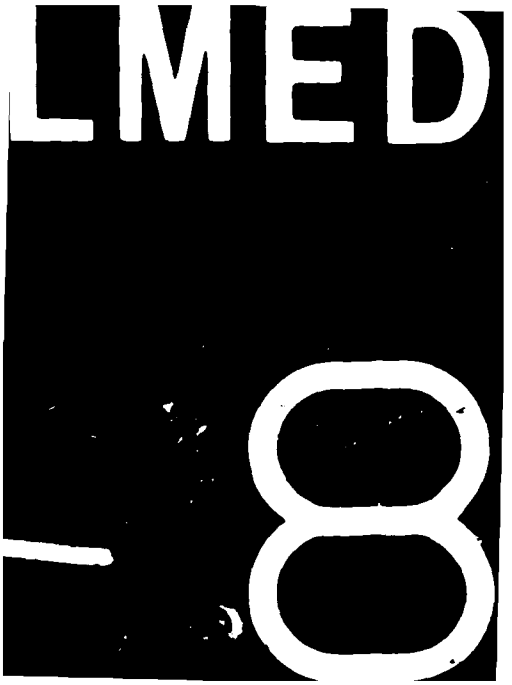
LMED
8